SOUTHERN APPALACHIAN COLD AIR DAMMING (CAD): A CLIMATOLOGY AND SIMULATION OF CASE STUDIES

by

JARED ALLEN RACKLEY

(Under the Direction of John A. Knox)

ABSTRACT

Topography is known to affect synoptic and mesoscale weather patterns throughout the world. One such effect, cold air damming (CAD), occurs when a shallow, surface-based layer of relatively cold air becomes entrenched against the windward side of a mountain range. In this thesis, a 30-year climatology (1981 – 2010) of cold air damming events in the southern Appalachians is conducted using hourly surface observations and North American Regional Reanalysis (NARR) data. The period is analyzed both statistically and spatially, revealing the surprisingly high frequency with which CAD affects as far south and west as Florida and Alabama. Using high resolution numerical modeling, case studies of wedge front convection (WFC) and CAD erosion are also conducted to better understand the role of CAD on convection and on the convective environment.

INDEX WORDS: Cold air damming, wedge front convection, numerical modeling, climatology

SOUTHERN APPALACHIAN COLD AIR DAMMING (CAD): A CLIMATOLOGY AND SIMULATION OF CASE STUDIES

by

JARED ALLEN RACKLEY

B.S., The University of Georgia, 2013

A Thesis Submitted to the Graduate Faculty of The University of Georgia in Partial Fulfillment of the Requirements for the Degree

MASTER OF SCIENCE

ATHENS, GEORGIA

2015

SOUTHERN APPALACHIAN COLD AIR DAMMING (CAD): A CLIMATOLOGY AND SIMULATION OF CASE STUDIES

by

JARED ALLEN RACKLEY

Major Professor:	John A. Knox
Committee:	Thomas L. Mote
	J. Marshall Shepherd

Electronic Version Approved:

Suzanne Barbour
Dean of the Graduate School
The University of Georgia
December 2015

ACKNOWLEDGEMENTS

First and foremost, I would like to recognize my Lord and Savior, Jesus Christ, for providing me with the daily strength and motivation needed to successfully complete this Master's thesis. I would also like to thank my major professor, Dr. John Knox, for his invaluable assistance and time, and my committee members, Dr. Marshall Shepherd and Dr. Tom Mote, for their helpful feedback in the construction of this thesis. It has been a privilege to continue my academic education in atmospheric science under your guidance and instruction. Finally, I would like to thank friends and family who have encouraged me along this journey and contributed to my professional development.

TABLE OF CONTENTS

Page

LIST OF TABLES

Page

LIST OF FIGURES

Page

CHAPTER 1

INTRODUCTION AND LITERATURE REVIEW

1.1 Overview

Topography is known to impact synoptic and mesoscale weather patterns throughout the world. One such common effect, cold air damming (CAD), occurs when a shallow, surface-based layer of relatively cold air becomes entrenched against the windward side of a mountain range [Richwien 1980]. The shallow dome of cold and stable air that becomes established during a CAD event is often identified by the characteristic "U"- or "wedge"- shaped inverted ridge that appears in the sea level pressure field and is typically only present below the 850 hPa pressure level [Baker 1970, Bell and Bosart 1988]. The appearance of this inverted ridge along the southern Appalachians has given rise to the use of the term "wedge" as a colloquial name for CAD by operational forecasters in the region. Though the phenomenon of CAD has been well known by forecasters throughout the last century, studies were not conducted until the late 1960s [Baker 1970] and it was a full decade later that the term "damming" began to be used [Richwien 1980]. While CAD is known to occur in many different mountainous regions worldwide [e.g., the Front Range of the Colorado Rockies [Dunn 1987], the Andes Mountains [Garreaud and Wallace 1998; Lupo et al. 2001], the central Mountain Range of Taiwan [Chien and Kuo 2006], and even the Antarctic Peninsula [Schwerdtfeger 1975]], this study will focus entirely on cold air damming that occurs along the southern Appalachians in the southeastern U.S.

The structure of this thesis is outlined as follows. In the second chapter, an objective 30-year climatology of Appalachian cold air damming is evaluated from 1980-2010 in order to

update and expand previous climatologies. Additionally, a new algorithm will be presented in order to determine the previously unstudied frequency and spatial pattern of CAD cold dome impacts in the southern extent of the damming region. Results will include southern damming region site-specific CAD frequency statistics never before quantified. In the third chapter, the effects of the cold air dome on convection and the convective environment, specifically in a high instability, low shear ambient environment, will be assessed using the WRF-ARW with modified terrain. The fourth chapter includes an analysis of an unforecast precipitation event, previously believed to be related to CAD erosion. Finally, a concluding discussion of the results of these studies and their use to forecasters is provided in the fifth chapter.

1.2 Project Motivation

Though forecast accuracy and knowledge of CAD events have improved substantially over the past four decades that CAD has been a topic of scientific study, uncertainty remains. While Bell and Bosart [1988] conducted a relatively long climatology of CAD events using the older, non-objective classification scheme, and Bailey et al. [2003] conducted a shorter 12-year climatology using objective and expanded classifications, a long-term climatology using the updated scheme has not been performed. Furthermore, while surface conditions (e.g., cloud cover, temperature, and sea level pressure) have been observed to be relatively homogeneous within the cold dome, previous literature largely ignores the varying degree of effects that CAD can have on conditions along its southernmost extent, namely the central Georgia and sometimes eastern Alabama region. While cold domes have been observed to penetrate as far to the southwest as Birmingham, AL weaker cold air domes may only extend into the northeast Georgia region. The extent to which the damming protrudes to the southwest can have significant impacts on sensible weather (and forecasts) in this southern region. At this time

however, no studies have analyzed this variation in CAD spatial extent from a climatological perspective.

Site-specific CAD impacts have been studied in previous literature. Bailey et al. [2003] utilized impacts at Greensboro, NC (GSO) to stratify cases into low- and high-impact events. However, a climatology of site-specific impacts throughout the entire damming region has never been attempted. Sites along the southern extent of the damming region (i.e., central Georgia into eastern Alabama) are of particular interest as impacts may vary significantly with strength and spatial extent of the cold air dome.

As discussed previously, Baker [2009] and Baker and Lackmann [2009] conducted a study to analyze the effects of the wedge front on convection. Their convective simulations analyzed a CAD event in a relatively moderate surface-based convective available potential energy (SBCAPE) and strong deep-layer shear environment. However, no studies have yet analyzed the potentially differing effects of the wedge front on convection within a higher convective available potential energy (CAPE), lower deep-layer shear environment. Analysis of wedge-front convection (WFC) within a high SBCAPE or substantial most-unstable CAPE (MUCAPE) and weak 0-6 km shear environment was suggested as needed future work by Baker [2009].

Finally, CAD erosion remains a topic of interest due primarily to the fact that models often have significant trouble with the timing and duration of erosion processes. CAD erosion is problematic because multiple different mechanisms and scenarios of erosion can take place within differing CAD event types. While erosion mechanisms and scenarios were researched by Stanton [2003] and composite climatologies were performed by both Stanton [2003] and Green

[2006], few case studies of CAD erosion exist in the literature. Stanton [2003] noted that more case studies of erosion events are needed to gain better understanding of erosion events.

1.3 Background

Cold air damming can best be described as the effects of "orographically modified geostrophic balance" [Bell and Bosart 1988] when statically stable flow encounters a mountain barrier. In the southeastern U.S., CAD generally occurs when a strong surface anticyclonic system (typically 1030 hPa central pressure or higher), referred to as the "parent high" [Bailey et al. 2003], is situated to the north of the Appalachians (most favorably north of 40° N). As air parcels within the geostrophic flow about the parent high approach the Appalachians to the east, the parcels' westward momentum is decreased and convergence occurs near the Appalachian barrier. This decrease in the magnitude of the flow velocity weakens the northward-directed component of the Coriolis force and the flow turns to the south and accelerates in response to the now-unbalanced pressure gradient force. As the ageostrophic northerly flow accelerates, the Coriolis force strengthens once again and acts to deflect the flow in a toward-barrier direction. This causes both an accumulation of mass and orographic ascent along the eastern Appalachian slopes. The mass accumulation and adiabatic cooling due to the orographic ascent cause a hydrostatic pressure increase. The resulting pressure gradient force acting in the away-from-barrier direction is kept in near balance by the toward-barrier Coriolis force. Through this, a strong northerly flow is established and maintained.

These processes allow an adjustment of the original geostrophic flow into a locally modified geostrophic balance in the presence of the orographic barrier [Bell and Bosart 1988]. The newly forced low-level mountain-parallel jet helps to maintain a shallow cold dome through cold air advection. This advection increases the static stability within the dome, enhances the

temperature inversion at the top of the dome, and causes enhanced hydrostatic pressure rises, further strengthening the high pressure ridge [Xu et al. 1996]. With the mountain-parallel jet in place, the cold dome can extend as far to the south as central Georgia and persist for several days before eroding [e.g., Forbes et al. 1987].

CAD events are entirely dependent upon blocking of flow by the Appalachian Mountains. This is directly related to the static stability of the upstream air mass, which can be assessed through consideration of the dimensionless Froude number (*Fr*) [Manins and Sawford 1982]:

$$Fr = \frac{U}{NH} \tag{1.1}$$

where *U* is the flow speed normal to the barrier, *H* is the height of the barrier, and *N* is the Brunt–Väisälä frequency (a measure of static stability):

$$N = \left(g\theta^{-1}\frac{\partial\theta}{\partial z}\right)^{\frac{1}{2}}. \tag{1.2}$$

The square of the Froude number is the ratio of the kinetic energy of the flow to the potential energy required for the flow to surmount the barrier. At large Froude numbers, flow is generally able to ascend the mountain barrier without significant deflection. However, if the Froude number is low, flow is blocked by the barrier and a CAD event is made possible if other factors are present [Keeter et al. 1995; Bell and Bosart 1998]. Previous studies [e.g., Forbes et al. 1987; Bell and Bosart 1988] found that Appalachian CAD events typically occur with Froude numbers of 0.3 to 0.4.

Diabatic processes can also play an important, though usually secondary, role in cold air dome maintenance. Scenarios do exist where these processes can play a dominant role in CAD initiation, but these will be discussed in detail later. Fritsch et al. [1992] found that clouds and precipitation can have a significant role in strengthening the cold air dome through evaporational

cooling. Evaporational cooling of precipitation falling through the cold, dry surface layer will act to increase the static stability of the layer by strengthening the temperature inversion across the top of the dome. Bell and Bosart [1988] suggested that evaporation contributed 20 – 30% of local cooling during a CAD event in March 1985. Increased cloud cover over the damming region, referred to as solar sheltering, can limit incident solar radiation from reaching the surface, thus keeping temperatures in the region cooler and increasing the temperature gradient along the cold dome periphery [Fritsch et al. 1992; Bailey et al. 2003]. Fritsch et al. [1992] estimated that the combined effects of solar sheltering and evaporational cooling during a precipitating CAD event caused an approximately 2 hPa rise in sea level pressure within the ridge.

The horizontal extent (width) of a cold air dome can be assessed by the Rossby radius of deformation (L_r), or the e-folding distance away from the blocking barrier [Xu and Gao 1995]:

$$L_r = \frac{\sqrt{g'H}}{f}, \text{ where } g' = \frac{g\Delta\theta}{\theta_0}. \quad (1.3)$$

Here, g is the gravitational acceleration, $\Delta\theta$ is the change in potential temperature from the warmer ambient atmosphere to the cold air within the dome, θ_0 is the absolute potential temperature of the warm air, H is the height of the barrier, and f is the Coriolis parameter. Xu and Gao [1995] calculated values of L_r around 250km to 300km for several case studies. It has also been found that the Laplacian ($\nabla^2 x$) of sea level pressure or potential temperature in the mountain-normal direction provides a good quantitative measure of the strength of a pressure ridge or the intensity of a cold air dome, respectively [Bell and Bosart 1988].

The structural integrity of a CAD dome strongly depends on the strength of the inversion separating the cold dome from the ambient environment. Erosion of a CAD dome can occur under many different scenarios [Bailey et al. 2003; Stanton 2003; Lackmann and Stanton 2004]. Stanton [2003] identified five processes responsible for CAD erosion: (i.) differential thermal

advection, (ii.) solar heating, (iii.) lower-tropospheric divergence, and (iv.) shear-induced mixing (entrainment) across the top of the cold dome. A fifth mechanism, the advance of a coastal/warm front, relates to several of these processes. Case studies have shown that some instances of CAD demise involve erosion from the surface upward through surface heating (e.g., the progression of a coastal front inland or surface divergence). Other cases involve the erosion of the dome from the top to the surface, such as the reduction of potential temperature differences across the inversion through cold air advection aloft [Stanton 2003; Green 2006].

Regardless of the scenario, when the cold air dome is eroded, the inversion is eradicated and mixing with the environment takes place [Lackmann and Stanton 2004]. Lackmann and Stanton [2004] note that the bulk Richardson number (eq. 1.4), evaluated across the inversion, provides a means of monitoring the strength of the inversion layer:

$$Ri_B = \frac{\frac{g\Delta\theta_v}{\theta_v}}{\frac{(\Delta u)^2+(\Delta v)^2}{\Delta z}} \quad . \tag{1.4}$$

The numerator in (4) is proportional to the strength of the capping inversion, while the denominator is the strength of the wind shear across the inversion layer. A small Richardson number (e.g., large shear or a weak inversion) indicates a greater chance of entrainment and turbulent mixing across the inversion layer that will ultimately be responsible for erosion of the CAD dome [Lackmann and Stanton 2004].

A comprehensive climatology of CAD was first conducted by Bell and Bosart [1988] by means of a 50-year monthly climatology spanning the 20-year period from 1899 to 1918 and the 30-year period from 1950 to 1979. Their results show that October to April account for 67% of all damming events and 68% of all damming days. The number of CAD events was found to be greatest in March, followed closely by December. Indeed, they found that while events along the Appalachians occurred 2-3 times a month during the cool season (October through March), 3-5

events per month were likely to occur during March and December. The summer months were found to have fewer events than the winter months, with July having the lowest annual number of events. Furthermore, the climatology showed that winter months were five times more likely to experience a strong CAD event than July.

A subjective classification scheme for CAD events was researched and developed by operational forecasters in the 1990s [Hartfield et al., 1996, unpublished; Keeter et al. 1995; Kramer 1997; Hartfield 1998]. These were based on the strength and position of the parent high and whether or not precipitation was falling within the damming region (i.e., the relative role of synoptic forcing versus the influence of diabatic processes in the establishment and maintenance of the cold air dome). The idealized CAD development described previously, in which strong synoptic scale features at the surface and aloft play the largest role, is referred to as "classical" CAD. Other contributing surface-based processes, such as evaporative cooling from precipitation and solar sheltering, are secondary to synoptic forcing in cold dome onset and maintenance in the classical model.

The alternate extreme, "in situ CAD," occurs when precipitation plays the dominate role in cold dome establishment. In these cases, cool, dry air must already be in place at the surface in the damming region. Here, the surface high is not favorably located, and thus, cold air cannot be advected into the region. Precipitation falling into this dry air causes evaporative cooling which produces a hydrostatic pressure rise. The result is an adjustment in the surface wind flow to a north-northeast direction which can then advect cold air into the region, initiating CAD.

Some CAD events develop with the nearly equal influence from both synoptic forcing and diabatic processes. These typically occur when the parent high is progressive or is in a favorable location but is weaker than needed for classical CAD. A weak damming event can be

initiated by the synoptic forcing, but will require evaporative cooling from precipitation falling into the region to cool temperatures, enhance static stability, and thereby strengthen the CAD event [Fritsch et al. 1992]. This type of CAD event, where both synoptic-scale forcing and diabatic processes are important to CAD establishment, is termed "hybrid" CAD.

Bailey et al. [2003] expanded these three classifications and set objective definitions for them, adding subcategories as appropriate. This expansion was necessary in order to capture some events that did not fit into the original classification scheme. They identified and defined a total of six classifications based on the original qualifiers of CAD intensity and influence of diabatic processes. In order to include weaker CAD events that were not significantly influenced by evaporational cooling, an additional classification of "weak dry" (WKDR) was created. Further, the "classical" category was split into "dry onset" (CDRY) and "diabatically enhanced" (CDEN) events depending on the role of precipitation at CAD onset. Hybrid (HYBR) and in situ (INST) classifications remained similar to their original definitions. Bailey et al. [2003] then created a sixth "unclassificable" (UNKN) category for events that deviated from the other specifications. These cases included those that were in situ-like, but did not have precipitation at CAD onset.

Through examination of many CAD cases, Bailey et al. [2003] defined the six new classifications of the CAD spectrum using NCEP North American Regional Reanalysis (NARR) data and hourly surface observations from ten stations chosen for their location within or proximity to the damming region: Richmond, VA (RIC); Charleston, WV (CRW); Lynchburg, VA (LYH); Norfolk, VA (ORF); Bristol, TN (TRI); Greensboro, NC (GSO); Wilmington, NC (ILM); Knoxville, TN (TYS); Greenville-Spartanburg, SC (GSP); and Charleston, SC (CHS). Bailey et al. [2003] defined the categories as follows:

1. Classical diabatically enhanced (CDEN) – At the 6-h analysis time closest to CAD onset, the parent high in the NCEP sea level pressure analysis must be centered north of 40°N between 100° and 65°W with a central pressure greater than or equal to 1030 mb. This criterion ensures that the anticyclone is strong and favorably positioned. The duration of the event must exceed 24-h so as to eliminate progressive highs. Precipitation is reported at the central stations in lines A, B, or C within 6-h of onset.
2. Classical dry onset (CDRY) – The same criteria as for CDEN except that no precipitation is reported at any of the center stations within 6-h of onset. Again, the parent high is strong and located in a favorable position for CAD, but diabatic processes play a negligible role in CAD initiation.
3. Hybrid (HYBR) – Precipitation is reported at one or more of the center stations in lines A-C within 6-h of onset. The parent high must exhibit a central pressure of less than 1030 mb and be centered between 100° and 65°W if north of 40°N at onset. If the parent high center is located south of 40°N, the high must be centered between 100° and 70°W and the central pressure is not considered. These criteria ensure that the parent high is either weak or is not optimally positioned for CAD, and that diabatic processes are capable of contributing to CAD onset.
4. Weak dry (WKDR) – The central sea level pressure in the parent high is less than 1030 mb, with the high centered between 100° and 65°W and north of 40°N, or south of 40°N and between 100° and 70°W at onset. There is no precipitation reported within 6-h of onset. These criteria are consistent with weak synoptic forcing and a lack of diabatic contribution.

5. In situ (INST) – Precipitation must be reported within 6 h of onset. If the parent high is south of 40°N, then the parent high must be centered east of 70°W. If the parent high is north of 40°N, then the parent high must be east of 65°W. These criteria represent cases where the high is unable to provide significant synoptic support to damming but had passed the region previously, leaving in place dry air at low levels.
6. Unclassifiable (UNKN) – All cases that do not fit one of the above categories. Some of these cases include those that fit the description of INST except that no precipitation fell at onset of the event. Others include events where a strong arctic high (>1050 mb) was centered west of 100°W but was large enough to affect most of Canada and provide support for Appalachian CAD. Other cases featured a cyclone to the southwest of the damming region.

Bailey et al. [2003] conducted an updated, objective climatology using the new classification scheme and CAD algorithm for a 12-year period from 1984-1995. Unlike Bell and Bosart [1988], Bailey et al. [2003] found that the peak in damming events was during the month of September, not March. This difference is due to the CAD algorithm's ability to capture weaker CAD events than the methods used by Bell and Bosart [1988]. However, when Bailey et al. [2003] used a linear ranking method to pull out only the 200 strongest events, they found that these results more closely matched those of Bell and Bosart [1988]. The frequency of strong events was shown to be greatest during February and March, while June, July, and August were characterized by a larger number of weak events.

Using the updated climatology and CAD classification scheme, Bailey et al. [2003] noted that different CAD erosion mechanisms were not exclusive to certain CAD types. Indeed, several distinctive erosion scenarios were seen to occur within each CAD type. Using composites for

classical CAD scenarios, Stanton [2003] classified these scenarios according to the synoptic pattern in place at the erosion time. Stanton [2003] defined these scenarios as follows:

1. Coastal Low – A low pressure system is present or forms between 79°W and 60°W and between 25°N and 40°N during the time period from 24 hours before demise time to 6 hours after demise time.
2. Northwestern (NW) Low – A low-pressure system moves from the west to northwest of the CAD region. The system is centered between 100°W and 70°W and between 40°N and 60°N. Any cold front associated with the low pressure system, determined by the shape of isobars and the gradient of potential temperature, must remain to the west of the Appalachian Mountains through 6 hours after demise time.
3. Cold-frontal Passage – This scenario is similar to the NW Low scenario; however, the cold front passes the spine of the Appalachian Mountains no later than 6 hours after demise time.
4. Residual Cold Pool – Evaluation of the RUC analyses shows no major change in synoptic features over the eastern United States. The high-pressure system may simply become ill-defined and/or move to the east or southeast.
5. Southwestern (SW) Low – A low-pressure system approaches the CAD region from the south or southwest. Unlike the Coastal Low scenario, the low-pressure system is west of 79°W 24 hours before demise. After this time, the system is centered between 100°W and 60°W and between 25°N and 40°N.

The frequent presence of a shallow cold air dome along the eastern slopes of the southern Appalachians is a well-known challenge to operational forecasters in the southern U.S. [Baker 1970; Bell and Bosart 1988; Hartfield 1998]. CAD events can have a significant impact on the

region's sensible weather, including temperature, sky cover, and precipitation. While modern mesoscale numerical models have significantly improved forecasting capabilities of CAD events in the past two decades, the models still have a tendency to underestimate CAD impacts and duration, often eroding the cold air domes prematurely [Forbes et al 1987; Stauffer and Warner 1987; Bell and Bosart 1988; Keeter 1995; Kramer 1997; Stanton 2003; Green 2006].

The relative coldness of the dome is a result of cold air advection parallel to the mountain barrier, orographic ascent, and evaporative cooling and sub-cloud sheltering from insolation when sufficient moisture and lift are present [Bailey et al. 2003]. Bell and Bosart [1988] found that temperature differences could exceed 20°C between the air within the dome and the ambient air along the surrounding coast. Differences of this magnitude can have huge implications for temperature forecasts in the region. The decreased visibility and low cloud ceilings often associated with CAD can also affect aviation as pilots are forced to use instrument flight rules.

Perhaps the most difficult aspect of CAD facing operational forecasters is precipitation forecasting. Because of CAD's prevalence in the winter months in a region with climatological temperatures generally above freezing, damming events can have a significant effect on precipitation type. Precipitation falling through the cold air dome may reach the surface as freezing rain, ice pellets, or occasional snow where rain would have otherwise been the dominant type. The warm air "nose" present above the cold air dome sets up a vertical temperature profile that can be conducive for freezing rain when surface temperatures are below freezing. Appalachian ice storms are well documented [e.g., Forbes et al. 1987] and can have major impacts on society. Indeed, climatologies show a pronounced increase in the frequency of freezing rain occurrences along the eastern Appalachians that can be mostly attributed to CAD [Changnon and Karl 2003].

Beyond precipitation type, isentropic lift or "overrunning" of warmer air above the dome can lead to unforecast or higher amounts of precipitation than anticipated. Furthermore, while stability within the dome inhibits convective activity and higher convective precipitation amounts, local frontogenesis and convergence along the dome periphery (wedge front) serves as a lifting mechanism and can act to enhance convective development [Baker and Lackmann 2009; Baker 2009]. Baker and Lackmann [2009] identified multiple cases of active wedge front convection (WFC) occurring along the cold dome periphery. Using high resolution Weather Research and Forecasting (WRF) model simulations, they found that pre-squall-line convection near the wedge front included discrete cell structures and cell splits with increased longevity that would otherwise have been more linear in form without the presence of CAD. This convection developed in an area of increased low-level storm relative helicity (SRH), a measure of the potential for cyclonic updraft rotation, along the wedge front. However, it was found that the frequency of moderately strong updraft rotation was notably lower in the presence of CAD than without a cold dome present, likely due to decreased moisture and instability [Baker and Lackmann 2009]. Baker [2009] speculated that differences in ambient CAPE and shear environments have a greater influence on the role of the wedge front on convective development than anticipated. It was hypothesized that the influence of the CAD cold dome on convection would be maximized in an ambient atmosphere with high SBCAPE, substantial MUCAP), and weak 0-6 km shear.

CHAPTER 2

A CLIMATOLOGY OF SOUTHERN APPALACHIAN COLD AIR DAMMING[1]

[1] Rackley, J.A. and J.A. Knox. Submitted to *Weather and Forecasting*

Abstract

A 30-year climatology (1981 – 2010) of cold air damming (CAD) events in the southern Appalachians was conducted using hourly surface observations and North American Regional Reanalysis (NARR) data. Analysis of the spatial distribution and frequency of these events reveals that some part of the Southeast is affected by CAD on fifty days out of each year, and even the northern Florida Panhandle and much of Alabama experience CAD conditions on about thirty days annually. Spatially, different CAD types tend to exhibit one of two patterns in the southernmost extent of the cold air dome: a more southerly dome with a ridge axis oriented from north-northeast to south-southwest or a more westerly dome with a ridge axis in a northeast to west-southwest orientation. These patterns may be the result of both splitting around the region of higher terrain in east-central Alabama and Coriolis forcing in stronger CAD types with higher wind speeds. Analysis of the frequency of CAD by type on a month-by-month and year-by-year basis confirms previous work that CAD is much more frequent during the cold season versus the warm season, with CAD occurring on 6.8 days per month during December and only 1.3 days per month during July. Analysis was also stratified by CAD type, revealing that weak-dry events were the most common. Classical type events with stronger and more favorably positioned parent highs exhibited the longest average duration, nearly 45 hours, while other CAD types averaged approximately half as long.

Key words: Cold air damming, Appalachians, Climatology

2.1 Introduction

Topography is known to affect synoptic and mesoscale weather patterns throughout the world. One such effect, cold air damming (CAD), occurs when a shallow, surface-based layer of relatively cold air becomes entrenched against the windward side of a mountain range [Richwien 1980]. The shallow dome of cold and stable air that becomes established during a CAD event is often identified by the characteristic "U"- or "wedge"- shaped inverted ridge that appears in the sea level pressure field and is typically only present below the 850 hPa pressure level [Baker 1970; Bell and Bosart 1988; Lackmann 2011]. CAD can also be observed in the near-surface temperature field, where the difference in temperature between the damming region and coast can exceed 20°C during strong CAD events [Bell and Bosart 1988].

Cold air damming can best be described as the effects of "orographically modified geostrophic balance" [Bell and Bosart 1988] when statically stable flow encounters a mountain barrier. In the southeastern U.S., CAD generally occurs when a strong surface anticyclonic system (typically 1030 hPa central pressure or higher), referred to as the "parent high" [Bailey et al. 2003], is situated to the north of the Appalachians (most favorably north of 40° N). As air parcels within the geostrophic flow about the parent high approach the Appalachians from the east, the parcels' westward momentum is decreased and convergence occurs near the Appalachian barrier [Smith 1982]. This weakens the northward-directed component of the Coriolis force and the flow turns to the south and accelerates in response to the now-unbalanced pressure gradient force. As the ageostrophic northerly flow accelerates, the Coriolis force strengthens once again and acts to deflect the flow in a toward-barrier direction, causing both an accumulation of mass and orographic ascent along the eastern Appalachian slopes. The mass accumulation and adiabatic cooling due to the orographic ascent cause a hydrostatic pressure

increase. Geostrophic adjustment occurs when the resulting pressure gradient force acting in the away-from-barrier direction is kept in near balance by the toward-barrier Coriolis force, creating and maintaining a strong northerly flow [Baker 1970; Richwien 1980; Bell and Bosart 1988; Xu 1990; Xu and Gao 1995]. The cold advection favored in this flow results in increased static stability and enhanced hydrostatic pressure rises [Xu et al. 1996]. Diabatic processes (i.e. clouds and precipitation) can also play an important, though usually secondary, role in cold air dome maintenance through evaporational cooling and solar sheltering [Forbes et al. 1987; Bell and Bosart 1988; Lee et al. 1992; Fritsch et al. 1992; Langmaid and Riordan 1998; Bailey et al. 2003].

Though forecast accuracy and knowledge of CAD events have improved substantially over the past four decades, CAD remains a well-known challenge to operational forecasters in the southeastern U.S. [Baker 1970; Bell and Bosart 1988; Hartfield 1998]. CAD events can have a significant impact on the region's sensible weather, including temperature, sky cover, and precipitation. In particular, CAD is known to affect precipitation type during the cold season [e.g. Forbes et al. 1987; Keeter et al. 1995] and trigger convection along the cold dome periphery, or "wedge front," during the warm season [Bosart et al. 1972; Ballentine 1980; Garreaud and Wallace 1997; Baker 2009]. While modern mesoscale numerical models have significantly improved forecasting capabilities of CAD events in the past two decades, the models still have a tendency to underestimate CAD impacts and duration, often eroding the cold air domes prematurely [Forbes et al 1987; Stauffer and Warner 1987; Bell and Bosart 1988; Keeter et al. 1995; Kramer 1997; Stanton 2003; Lackmann and Stanton 2004; Green 2006]. Even today's rapidly updating, high-resolution mesoscale models (e.g. the High Resolution Rapid

Refresh) show a tendency to underestimate effects of solar sheltering and erode the cold air dome too quickly [Grumm 2015].

Bell and Bosart [1988] conducted a relatively long climatology of CAD events using a non-objective classification scheme, and Bailey et al. [2003] conducted a shorter 12-year climatology using objective and expanded classifications. However, a long-term climatology using the objective scheme has not been performed. Furthermore, while surface conditions (e.g., cloud cover, temperature, and sea level pressure) have been observed to be relatively homogeneous within the cold dome, previous literature largely ignores the varying degree of effects that CAD can have on conditions along its southernmost extent, namely central Georgia and even sometimes eastern Alabama. While cold domes have been observed to penetrate as far to the southwest as Birmingham, AL, weaker cold air domes may only extend into northeastern Georgia. The extent to which CAD protrudes to the southwest can have significant impacts in this region.

The primary objectives of this study are to, 1) update the previous CAD literature with an extended objective climatology, 2) determine the previously unstudied frequency and spatial pattern of CAD impacts in the southern extent of the damming region, and 3) determine station-to-station CAD frequency variations from the CAD climatology as a whole.

2.2 Data and Methodology

An updated and extended objective climatology of CAD was constructed using the Bailey et al. [2003; hereafter, B03] objective CAD-identification algorithm. To identify a full spectrum of CAD events objectively, the CAD-detection algorithm was adapted and run for the 30-yr period 1981 to 2010. This algorithm was designed to identify the characteristic inverted pressure ridge, cold air dome, and ageostrophic northeasterly flow associated with CAD events using

hourly surface observations and Laplacians ($\nabla^2 x$) of sea level pressure (P_{SLP}) and potential temperature (θ) in the mountain-normal direction. Following B03, Laplacians were evaluated using Python scripting for three mountain-normal lines of surface observations and a single mountain parallel line that represents northeasterly flow. Each line contains surface observations from three stations within the damming region, with the center station representing the core of the damming region, and the stations on either side approximately perpendicular to the Appalachian Mountains. Line A consists of the following stations: Charleston, WV (CRW); Lynchburg, VA (LYH); and Norfolk, VA (ORF). Line B includes: Bristol, TN (TRI); Greensboro, NC (GSO); and Wilmington, NC (ILM). Knoxville, TN (TYS); Greenville-Spartanburg, SC (GSP); and Charleston, SC (CHS) make up line C. Laplacians are calculated along these lines using

$$\nabla^2 x = \frac{\frac{x_3 - x_2}{d_{2-3}} - \frac{x_2 - x_1}{d_{1-2}}}{\frac{1}{2}\left(d_{2-3} + d_{1-2}\right)} \tag{2.1}$$

where x is either the sea level pressure or the potential temperature and subscripts are stations from west to east along the mountain-normal line. In (1), d represents the distance between stations. Negative values of ($\nabla^2 SLP$) are associated with a higher pressure at the center station, while positive values of ($\nabla^2 \theta$) are associated with colder potential temperatures at the center station.

Temporal and numerical thresholds for CAD detection were applied to computed values. These CAD detection criteria are summarized as follows:

- The mountain-normal Laplacian of sea level pressure must be negative and exceed in magnitude one standard deviation of the average of all the negative mountain-normal Laplacian values in the dataset.

- The mountain-normal Laplacian for potential temperature must be greater than zero.
- Sea level pressure must be greater at the center station relative to the end stations.
- The difference in the pressure along line D must be greater than 1.5 mb between either GSP and GSO or GSO and RIC, with higher values to the northeast.
- All requirements must be met for at least six consecutive hours on at least one of the mountain-normal lines (A–C).

As with previous CAD climatologies, vertical atmospheric soundings were not used, despite their usefulness in identifying CAD presence and strength, due to their limited spatial and temporal resolution. Utilization of the B03 algorithm allows for objective detection, classification, and comparison with respect to previous studies.

While this study does not stray from the original B03 algorithm implementation, the data sources used for hourly observations used in this work differ from those used in B03. Hourly surface station observations were retrieved from the National Climatic Data Center (NCDC) Climate Data Online (CDO) database, while the previous study utilized the older Solar and Meteorological Surface Observation Network (SAMSON) archives. This study also chooses to linearly interpolate missing data for gaps of up to six hours versus the 3 hour limit used in B03, as this helped to eliminate falsely detected CAD demise due to brief data gaps.

To maintain consistency with previous studies and to check algorithm accuracy, identified events were compared to a subjectively identified list of 30 CAD events from 1 January 2001 through 31 May 2002. This list was also used by B03, in which 26 of the 30 events were correctly identified. This study, using the criteria above, correctly identified all 30 events during the period. Surface analyses within the first several hours of initiation were viewed for each detected event, and no inconsistences were observed. Still, it should be noted that the

algorithm missed several events when compared to subjectively identified CAD databases [e.g. Baker 2009].

In an effort to avoid over-counting a single CAD event that exhibits periods of weakening below algorithm thresholds, consecutive CAD events that are synoptically driven by the same parent high and separated by fewer than 18 hours were analyzed using reanalysis and surface data and combined into a single event as necessary. While this deviates from previous uses of the CAD detection algorithm, we believe that this serves as a more realistic representation of each CAD event. Detected CAD events were stratified into cases using the classification scheme outlined in B03. We summarize this scheme below for the reader.

The B03 classification scheme is a modification of that developed by operational NWS forecasters [Hartfield et al. 1996; Kramer 1997; Hartfield 1998]. Classification of each event was based on the strength and location of the parent high and whether or not precipitation was falling within 6 h of onset at the center station of the first line activated (Fig. 2.2). These criteria were determined using a combination of surface observations and North American Regional Reanalysis (NARR) data [Mesinger et al. 2006], and defined six CAD cases as discussed in B03:

1. Classical diabatically enhanced onset (CDEN) – At CAD onset, the parent high in the NCEP sea level pressure analysis must be centered north of 40°N between 100° and 65°W with a central pressure greater than or equal to 1030 mb. This ensures that the anticyclone is strong and favorably positioned. Precipitation must be reported at the central stations in lines A, B, or C within 6h of onset, and the total event duration must exceed 24h.
2. Classical dry onset (CDRY) – The same criteria as for CDEN except that no precipitation is reported within 6h of onset and diabatic processes play a negligible role.

3. Hybrid onset (HYBR) – Precipitation is reported at one or more of the center stations within 6h of onset. The parent high must exhibit a central pressure of less than 1030 mb and be centered between 100° and 65°W if north of 40°N at onset or between 100° and 70°W, and the central pressure is not considered if the high is south of 40°N. This ensures that the parent high is either weak or is not optimally positioned for CAD, and that diabatic processes are capable of contributing to onset.
4. Weak/dry onset (WKDR) – The central sea level pressure in the parent high is less than 1030 mb, with the high centered between 100° and 65°W and north of 40°N, or south of 40°N and between 100° and 70°W at onset. No precipitation is reported within 6h of onset. This is consistent with weak synoptic forcing and a lack of diabatic contribution.
5. In situ (INST) – Precipitation must be reported within 6h of onset. If the parent high is south of 40°N, then the parent high must be centered east of 70°W. If the parent high is north of 40°N, then the parent high must be east of 65°W. These criteria represent cases where the high is unable to provide significant synoptic support to damming but had passed the region previously, leaving in place dry air at low levels.
6. Unclassifiable (UNKN) – All cases that do not fit one of the above categories.

In order to quantify the previously unstudied variation in spatial extent and frequency of cold dome intrusion into the southeastern US (i.e. SC, GA, AL, and FL), a climatology of cold dome spatial extent was also conducted for the 30-yr period. An objective CAD spatial extent algorithm was developed to identify location of cold air advection within the dome. While the previously discussed B03 algorithm generally determines whether CAD is present or not within the core damming region (i.e. VA, NC, and SC), this algorithm attempts to determine whether CAD is present at specified stations across the southernmost damming region. For simplicity, the

algorithm relies on the assumption that northeasterly flow must be present and continuous from northeast to southwest within the cold air dome of a damming event. Hourly wind observations of speed and direction for 21 stations across SC, GA, AL, and FL (see Table 2.1) were utilized to identify this. Selected stations were required to have a complete record for the period 1981-2010, and effort was made to maintain an adequate spatial distribution across the study area with stations located both within and without the assumed damming region.

Compiled times of CAD events identified by the detection algorithm were used to initialize the algorithm in order to reject cases of northeasterly cold air advection unassociated with damming events. Threshold values for acceptable wind directions at each station were selected based on an examination of wind observations during several CAD cases. The algorithm uses an upstream-to-downstream hierarchical network, requiring that upstream (i.e. to the northeast) stations have flow within the specified threshold before downstream stations are checked for CAD. Upstream stations with missing data or calm conditions are considered to be within the dome if stations immediately downstream have flow within their specified thresholds. Upstream stations were also required to have greater or equal sea level pressure than their downstream counterparts. To reduce error in the algorithm caused by variable wind direction that occasionally occurs within the dome, times were analyzed in rolling 3 h segments, requiring that conditions for the station must fall within the specified threshold during at least one of the three hours.

Calculated frequency of CAD by station was mapped both in total and stratified by CAD type and season using a GIS. The spline interpolation method [Walter 2001] was chosen to map frequency of CAD dome spatial extent using a smooth surface true to the sampled data points.

For consistent comparison among CAD classes, map data was normalized by the total hours of CAD detected for each classification.

Hourly surface observations for each station were obtained from the NCDC Global Surface Hourly database (DS3505) and were utilized in both CAD detection and CAD spatial mapping. Data for the 10 surface stations used in the CAD detection algorithm were downloaded for the full 30-yr period from 1981 to 2010. Meteorological fields included temperature, station pressure, sea level pressure, altimeter reading, and hourly precipitation. Large portions of station pressure observations were found to be missing for various stations within the archive even while sea level pressure observations and altimeter readings were largely present. Therefore, for times in which altimeter readings were recorded while station pressure was absent, the altimeter readings were used to compute station pressure using

$$P_{stn} = P_a \times \left(\frac{\left(R_d - 0.0065 * h_m \right)}{R_d} \right)^{5.2561} \tag{2.2}$$

where P_{stn} is station pressure, P_a is the altimeter reading, R_d is the gas constant for dry air, and h_m is station height (Chu 1994). While this ensures the most complete dataset possible, it could account for inconsistencies between this study and previous studies utilizing different datasets. In addition, observations were linearly interpolated for cases with missing reports of six or fewer consecutive hours to reduce the effects of missing observations on CAD detection, temperature, sea level pressure, and station pressure.

The NCDC-NOMADS NARR-A online plotter was used to plot reanalysis of sea level pressure fields. NARR-A is available with 3-hr temporal frequency and grid-spacing of 32 x 32 km. Central sea level pressure and location of parent highs were manually recorded using the NARR-A online plotter.

2.3 Results

The CAD-detection algorithm was run using surface data for the 30-yr period from 1 January 1981 through 31 December 2010. Identified CAD frequency was analyzed by the number of hours, events, and affected days. All events included at least 6 CAD hours, while CDEN and CDRY event included at least 25 hours, as specified previously. CAD-affected days, hereafter referred to as "CAD days," were those that included one or more CAD hours. Frequency was also stratified by CAD type and the month of occurrence to demonstrate seasonal variation.

The algorithm identified 703 events, affecting a total of 1,504 days and encompassing 20,069 hours for the 30-yr period. CAD events were detected somewhere in the region by the algorithm on 13.7% of days during the period, or more than 7 weeks per year on average. This demonstrates the significant impact that CAD has on the Southeast.

Average monthly frequency for the strongest CAD events and the total CAD events and days is shown in Fig. 2.3 a-b. The results support previous studies in showing a more active cold season (defined as 15 October – 15 April) versus a less active warm season. December had the highest event frequency with 3.2 CAD events occurring per year. October and January followed closely with 2.9 and 2.6 events per year, respectively. June, July, and August had the lowest frequency of CAD events with 0.6, 0.6, and 0.8 events annually. For the 30-yr period, the summer months (JJA) had a total of 128 days of detected CAD. While summer months certainly see fewer CAD events, two summer events ranked in the top 4% of all events by strength, indicating that while summer events are few and generally weak, strong summer events are possible.

There is a significant departure from the B03 12-yr climatology for the month of August. B03 described August as having a frequency of just over 3 events per year, while this study finds an average of 0.8 events per year over the 30-yr period. This difference is likely the result of the longer period and this study's decision to combine closely consecutive events dynamically forced by the same parent high.

Following previous studies [Bailey 2001; B03], CAD strength was computed for each event using a linear combination of normalized measurements for event duration, sea level pressure and potential temperature Laplacians, and magnitude of the along-barrier pressure gradient. B03 found that the frequency of strongest cases more closely matched the Bell and Bosart [1988] 50-yr climatology. Indeed, monthly frequency for the strongest 350 events in our study (shown in Fig. 2.3a) closely matches results found by Bell and Bosart [1988], while the monthly frequency of all events shows a significant departure. Though the strongest 350 events showed a maximum during the winter months, results demonstrate that strong events are still present during the spring and fall seasons when the wedge front can trigger convection.

Output from the CAD detection algorithm was also analyzed by CAD hours per year, CAD events per year, and average CAD hours by month. Analysis of the average CAD hours by month was consistent with the event frequency by month. Very similar distributions for events per month, days per month, and hours per month indicate an approximately similar average length for individual CAD events across different months. Indeed, the average length of CAD events by month was clustered around 29 hours, with the exception of July and August. On average, July events had an average duration of only 19 hours, while August event durations averaged 24 hours. March events had the longest average duration at 31 hours. October had the highest average CAD hours at just over 87 per year, while the lowest month, July, saw only an

average of 12 CAD hours per year. An analysis of CAD event frequency and hour frequency by year showed significant variability from year to year (Fig. 2.4). The most active year in the period was 1994, with 79 days and 1124 hours recording CAD. The least active years were 2010 and 2006, with 28 CAD days (419 CAD hours) and 29 CAD days (365 CAD hours) respectively. The downward trend of 0.39 days per year, while intriguing and possibly related to slow (0.0-0.11°C/decade) upward trends in September-May temperatures across the United States during 1981-2010 [NCDC 2015; not shown], is not statistically significant at p=0.05.

Analysis was also stratified by CAD type (Table 2.2, Fig. 2.5). This revealed that Weak/Dry events were the most common, making up 31% of CAD events for the 30-yr period and an average of 7.2 per year. HYBR events followed closely with 29%. CDRY, CDEN, UNKN, and INST events were 17%, 11%, 7%, and 6%, respectively. CDEN, CDRY, and WKDR events show a large peak in frequency during the cold season and minima during the summer months. HYBR monthly frequency is less clear, though the highest average HYBR events per month occurred in March. INST and UNKN events deviated from this pattern significantly. INST monthly frequency shows a peak in April that continues through the summer months, while UNKN monthly frequency appears to be bimodal with a secondary peak in June. It should be noted that these two categories were weaker in nature and therefore tend to have lower impact of sensible weather.

Classical type events exhibited the longest per-event average duration for the 30-yr period (Table 2.2), in part due to classification constraints (i.e. classical types must be longer than 24 hours in duration). CDEN events ranged from 25 to 96 hours with an average of 44.3 hours long, and CDRY events ranged from 25 to 129 hours with an average of 45.2 hours. HYBR, WKDR, and INST events average approximately half as long, with 23.2, 22.0, and 22.0

hours per event, respectively, though their ranges (131, 134, and 123 hours respectively) include similar upper bounds to CDRY events. The upper bound of the CDEN event range was possibly lower due to strong, but faster moving parent highs. UNKN events recorded the shortest duration with an average of 19.9 hours per event and a range of only 6 to 71 hours. While WKDR events represented the highest percentage of total events by class for the period, analysis of the strongest 350 events (i.e. the strongest 50% of events), show HYBR and CDRY with the highest percentages, followed by CDEN (Table 2.2). These findings demonstrate that CDEN, CDRY, and HYBR events tend to be stronger than other CAD types, because their parent highs are stronger.

The spatial distribution of CAD events for the same 30-yr period demonstrates that large variability in the spatial extent of the cold air dome exists from event to event. Detected CAD hours are broken down site-by-site and stratified by type and season in Table 2.1. Unsurprisingly, Greer, SC, the northernmost site in the domain, experienced the highest number of detected CAD hours. However, because Greer is not the northernmost point of the damming region, the 19,003 CAD hours detected specifically at Greer for the 30-yr period by the spatial extent algorithm fall short of the total number of CAD algorithm detected hours for the entire domain by 1,066 hours. The most surprising result is the frequency with which the cold dome pushes into Alabama and parts of Florida (Fig. 2.6). On average, CAD was detected at Birmingham, AL, 252 hours (10.5 days) per year and 184 hours (7.7 days) per year at Tallahassee, FL. Even Mobile, AL, detected 173 hours (7.2 days) per year on average.

To verify the results from this algorithm, a case for which the algorithm analyzed the dome over southern Alabama and northern Florida was selected The Weather Prediction Center surface analysis for 0900 UTC 15 October 2009 (Fig. 2.7) shows a case in which the cold air

dome, enhanced by a coastal low off the east coast of Florida, pushes well into this region. The algorithm performed well in correctly identifying and rejecting CAD presence at each station for the duration of the event. However, the algorithm did exhibit a tendency to sporadically falsely reject CAD for single hours when several stations within the cold dome reported calm winds. This may lead to a slight *undercount* in per-station reported CAD hours, though the effect appears to be small. Thus, a new result of our climatology—that CAD is a real phenomenon all the way to the Gulf of Mexico—is robust.

Analysis of the overall spatial pattern for site-by-site CAD frequency shows two apparent lobes of the cold air dome, one extending to the west-northwest into Alabama, and the second extending to the southwest towards Tallahassee (Fig. 2.6). Comparing these patterns to regional elevation shows that the lobes tend to split around the region of higher terrain in east-central Alabama (e.g. Mt. Cheaha, elevation 734 m [2,407 feet]). Comparison of cold-season versus warm-season events (not shown) show that cold-season events slightly favored the west-northwesterly track into Alabama over the more southwesterly track into Florida. Warm-season events seem to favor both tracks equally, though the warm season pattern over north Central Alabama indicates that a higher percentage of warm-season events pushes into that region than cold-season events.

A comparison of spatial extent and frequency by CAD type is shown in Figure 2.8 a-f. CDEN, CDRY, and HYBR events all tend to slightly favor the west-northwesterly track into Alabama over the push into Florida. As these three classifications represent stronger synoptic forcing, the turn to the west-northwest is possibly due to the strengthened effect of the Coriolis force and reduced blocking effect (i.e. higher Froude number) as stronger wind speeds are advected into the area. Both INST and UNKN patterns show a displacement of the core of

highest frequency CAD to the northeast and seem to favor a southwesterly track. This is possibly due to the weak nature of these events as a result of little synoptic forcing.

2.4 Conclusions

This work objectively classifies cold air damming along the southern Appalachians and maps its spatial extent within the southernmost damming region (i.e. SC, GA, AL, and FL) for a 30-yr period. While climatologies of cold air damming have been constructed in the past, this study is the first to both objectively classify events and do so over a long period. In addition mapping and analysis of the spatial extent of the cold dome across the southernmost damming region has not been performed previously. The purposes of this research are to assess the application of the B03 objective detection and classification schemes to longer time periods and to assess the frequency and extent to which the cold dome pushes into its southern reaches.

On average, CAD was detected by the algorithm on more than 50 days, or more than 7 weeks, per year. Fifty days per year is non-trivial for a phenomenon with the potential to significantly impact forecasts of sensible weather. As found in previous studies, detected CAD is much more frequent during the cold season than in the warm season. This can increase the potential for difficult winter weather forecasts with the threat of dangerous icy precipitation. However, the results also demonstrate that strong CAD events can occur during the spring and summer months when the cold dome periphery is likely to trigger or enhance convection.

Maps of cold dome spatial extent reveal the surprisingly high frequency with which the cold dome pushes into portions of Florida and Alabama. Forecasters with CAD experience know that CAD can push as far west as Birmingham or as far south as Tallahassee; this study provides a quantitative measure of that assessment. The maps also indicate two potential trajectories once the dome pushes into central Georgia. A west-northwesterly path turns towards Anniston, AL,

and north of the Birmingham, AL area. Its counterpart, the southwesterly trajectory, continues pushing into southwest Georgia and Florida. Cold-season events seemed to favor the west-northwesterly track, as did the stronger CAD categories. These findings may provide forecasters with a quick estimate of where and how far the cold dome will push given the synoptic conditions. Future work utilizing the Weather Research and Forecasting (WRF) mesoscale model [Rackley 2015] will attempt to shed further light on why and how these two different trajectories form.

2.5 References

Bailey, C. M., G. Hartfield, G. M. Lackmann, K. Keeter, and S. Sharp, 2003: An objective climatology, classification scheme, and assessment of sensible weather impacts for Appalachian cold-air damming. *Wea. Forecasting*, **18**, 641-661.

Baker, D. G., 1970: A study of high pressure ridges to the east of the Appalachian Mountains. Ph.D. thesis, Massachusetts Institute of Technology, 127 pp.

Baker, A. K., 2009: Convection and Appalachian Cold-Air Damming. Master's thesis, North Carolina State University, 188 pp.

Ballentine, R. J., 1980: A numerical investigation of New England coastal frontogenesis. *Mon. Wea. Rev.*, **108**, 1479-1497.

Bell, G. D., and L. F. Bosart, 1988: Appalachian cold-air damming. *Mon. Wea. Rev.*, **116**,137-161.

Bosart, L. F., C. J. Vaudo, and J. H. Helsdon Jr., 1972: Coastal frontogenesis. *J. Appl. Meteor*., **11**, 1236-1258.

Chu, R., 1994: Algorithms for the Automated Surface Observing System (ASOS). ISL Office Note 94-4, NWS/OSD, 106 pp.

Forbes, G. S., R. A. Anthes, and D. W. Thomson, 1987: Synoptic and mesoscale aspects of an Appalachian ice storm associated with cold-air damming. *Mon. Wea. Rev.,* **115**, 564-591.

Fritsch, J. M., J. Kapolka, and P. A. Hirschberg, 1992: The effects of subcloud-layer diabatic processes on cold air damming. *J. Atmos. Sci.*, **49**, 49-70.

Garreaud, R. D., and J. M. Wallace, 1998: Summertime incursions of midlatitude air into subtropical and tropical South America. *Mon. Wea. Rev*., **126**, 2713-2733.

Green, T. A., Jr., 2006: Cold air damming erosion and associated precipitation in the Southeastern United States. Master's thesis, North Carolina State University, 248 pp.

Grumm R. H., 2015: Mid-Atlantic Ice Storm 4 March 2015. Accessed 22 July 2015. [Available online at http:// cms.met.psu.edu/sref/severe/2015/03Mar2015.pdf]

Hartfield, G., K. Keeter, and P. Badgett, 1996: Spectrum of cold air damming and damming look-alikes. [Available from the Raleigh National Weather Service Office, Raleigh, NC.]

_____, 1998: Cold air damming: An introduction. National Weather Service Eastern Region Training and Evaluation Module 4. [Available online at http://www.erh.noaa.gov/er/hq/ssd/erps/tem/tem4.pdf]

Keeter, K. K., S. Businger, L. G. Lee, and J. S. Waldstreicher, 1995: Winter weather forecasting throughout the eastern United States. Part III: The effects of topography and the variability of winter weather in the Carolinas and Virginia. *Wea. Forecasting*, **10**, 42-60.

Kramer, D., 1997: Real-time mesoscale model evaluation during Appalachian cold air damming. Master's thesis, North Carolina State University, 139 pp.

Lackmann, G. M., 2011: *Midlatitude Synoptic Meteorology: Dynamics, Analysis, and Forecasting*. Amer. Met. Soc., 306-309 pp.

Lackmann, G. M., and W. M. Stanton, 2004: Cold-air damming erosion: Physical mechanisms, synoptic settings, and model representation. Preprints, *20th Conf. on Weather Analysis and Forecasting*, Seattle, WA, Amer. Meteor. Soc., CD-ROM, 18.6.

Langmaid, A. H., and A. J. Riordan, 1998: Surface mesoscale processes during the 1994 Palm Sunday tornado outbreak. *Mon. Wea. Rev.*, **126**, 2117-2132.

Lee, L. G., K. K. Keeter, S. Businger, and A. J. Riordan, 1992: Geography-related forecasting problems in the southeastern United States and a joint North Carolina State University-

National Weather Service effort to improve the understanding and prediction of these events. Preprints, *Symp. on Weather Analysis and Forecasting*, Atlanta, GA, Amer. Meteor. Soc., 166-172.

Mesinger, F., G. DiMego, E. Kalnay, K. Mitchell, P. C. Shafran, W. Ebisuzaki, D. Jović, J. Woollen, E. Rogers, E. H. Berbery, M. B. Ek, Yun Fan, R. Grumbine, W. Higgins, H. Li, Y. Lin, G. Manikin, D. Parrish, W. Shi, 2006: North American Regional Reanalysis. *Bull. Amer. Meteor. Soc*., **87**, 343-360.

NCDC, 2015: Climate at a Glance. Accessed 23 July 2015. [Available online at http://www.ncdc.noaa.gov/cag/]

Rackley, J. A., 2015: Southern Appalachian Cold Air Damming: A Climatology and Simulation of Case Studies. Master's thesis, University of Georgia

Richwien, B. A., 1980: The damming effect of the southern Appalachians. *Natl. Wea. Dig.*, **5** (1), 2-12.

Smith, R. B., 1982: Synoptic observations and the theory of orographically disturbed wind and pressure. *J. Atmos. Sci.*, **39**, 60–70.

Stanton, W., 2003: An analysis of the physical processes and model representation of cold air damming erosion. Master's thesis, North Carolina State University, 207 pp.

Stauffer, D. R., and T. T. Warner, 1987: A numerical study of Appalachian cold-air damming and coastal frontogenesis. *Mon. Wea. Rev.,* **115**, 799-821.

Walter, N. (Ed.), 2001: *Spatial Interpolation*. University of Calgary Press.

Xu, Q., 1990: A theoretical study of cold air damming. *J. Atmos. Sci.*, **47**, 2969–2985.

_____, and S. Gao, 1995: An analytic model of cold air damming and its applications. J. Atmos. Sci., 52, 353-366.

_____, _____, and B. H. Fiedler, 1996: A theoretical study of cold air damming with upstream cold air inflow. J. Atmos. Sci., 53, 312-326.

2.6 Tables and Figures

Table 2.1. Surface stations used to analyze CAD spatial extent and the corresponding number of CAD hours, averaged CAD hours per year, and the average number of affected CAD days per year detected for each station for the 30-yr period.

CAD Spatial Extent Stations			Total				Cold	Warm	CDEN	CDRY	HYBR	WKDR	INST	UNKN
ID	**City**	**State**	Total Hours	Days/ Year	Affected Days/Yr	% of Total	Total Hours	Total Hours	Total Hours	Total Hours	Total Hours	Total Hours	Total Hours	Total Hours
GSP	Greer	SC	19003	26.4	48.7	94.7	13032	5983	3170	5239	4373	4533	851	837
CAE	Columbia	SC	16927	23.5	46.4	84.3	11457	5480	2920	4698	3844	4090	723	652
FLO	Florence	SC	17050	23.7	47.1	85.0	11477	5583	2870	4679	3837	4178	777	709
AHN	Athens	GA	17056	23.7	46.0	85.0	11661	5403	2866	4785	3781	4196	715	713
AGS	Augusta	GA	16341	22.7	45.5	81.4	11013	5338	2849	4609	3568	3998	710	607
ATL	Atlanta	GA	13374	18.6	41.2	66.6	8959	4419	2322	3977	2811	3273	536	455
MCN	Macon	GA	13986	19.4	42.5	69.7	9326	4665	2382	4114	2857	3549	575	509
SAV	Savannah	GA	8249	11.5	34.1	41.1	5203	3047	1422	2453	1555	2145	361	313
RMG	Rome	GA	8172	11.4	34.3	40.7	5119	3054	1459	2274	1775	1992	382	290
CSG	Columbus	GA	13039	18.1	40.5	65.0	8651	4391	2144	3934	2546	3463	507	445
ABY	Albany	GA	11031	15.3	38.2	55.0	7161	3873	1980	3294	2076	2837	490	354
VAD	Valdosta	GA	6999	9.7	31.7	34.9	4225	2777	1244	2050	1367	1796	293	249
TLH	Tallahassee	FL	5522	7.7	28.4	27.5	3400	2122	1051	1551	1021	1488	244	167
ANB	Anniston	AL	12313	17.1	38.9	61.4	8257	4057	2072	3749	2527	3088	478	399
HSV	Huntsville	AL	3961	5.5	24.2	19.7	2362	1598	701	1057	895	1000	196	112
BHM	Birmingham	AL	7548	10.5	31.4	37.6	4552	2998	1328	2195	1563	1971	300	191
MGM	Montgomery	AL	5072	7.0	27.9	25.3	3111	1961	893	1344	1028	1413	216	178
OZR	Ozark	AL	6060	8.4	28.8	30.2	3691	2371	1151	1517	1194	1640	373	185
MSL	Muscle Shoals	AL	2890	4.0	19.1	14.4	1685	1205	520	770	636	751	125	88
TCL	Tuscaloosa	AL	5598	7.8	27.3	27.9	3265	2334	1066	1532	1132	1487	234	147
MOB	Mobile	AL	5192	7.2	25.6	25.9	3272	1921	1088	1307	1007	1332	317	141

Table 2.2. CAD event classifications by percentage of total occurrence, percentage of the strongest 350 events, and the average duration.

Class	% of Total Events	% of Strongest 350 Events	Average Events per Year	Average Duration (h)	Duration Range (h)
CDEN	10.5	22.3	2.5	44.3	25 - 96
CDRY	17.2	34.3	4.0	45.2	25 - 126
HYBR	28.9	32.3	6.8	23.2	6 - 131
WKDR	30.7	18.7	7.2	22.0	6 - 134
INST	6.0	5.0	1.4	22.0	6 - 123
UNKN	6.7	4.0	1.6	19.9	6 - 71

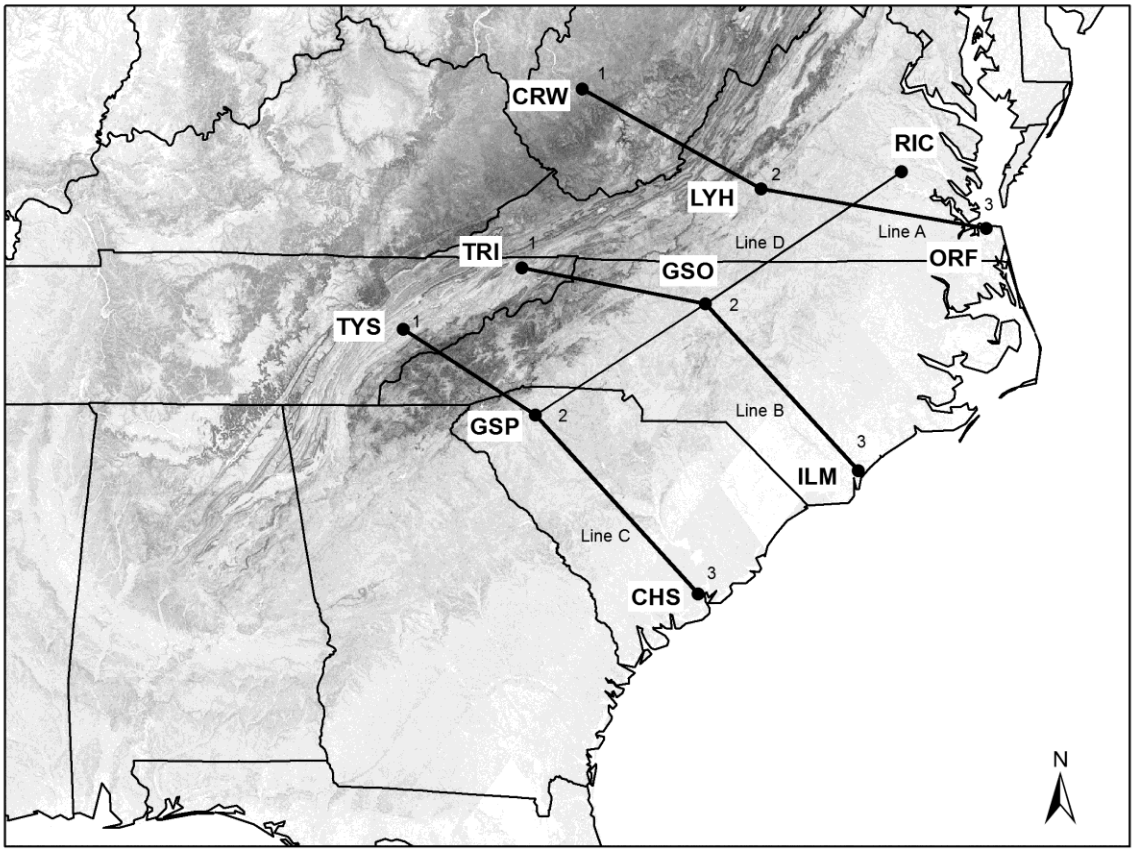

Figure 2.1. The ten surface stations and Laplacian lines constructed for the CAD detection algorithm (modified from Bailey et al. 2003).

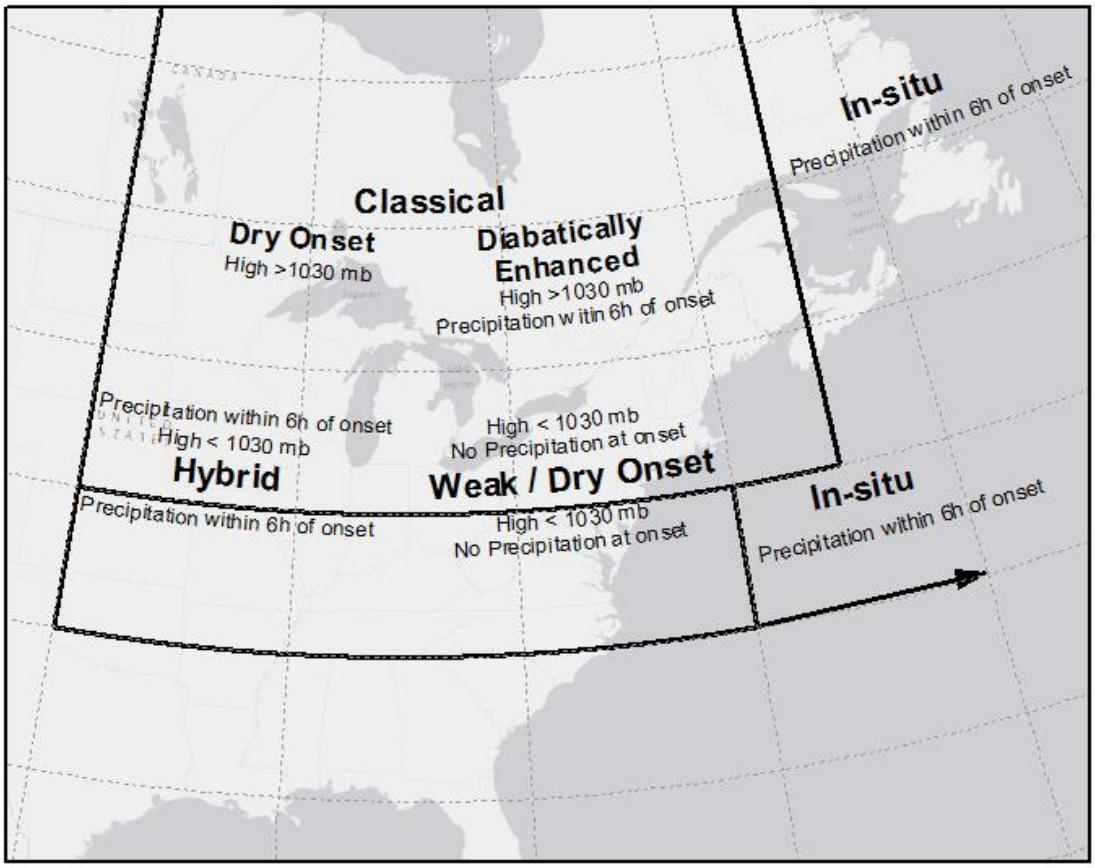

Figure 2.2. Geographical domains applied to the location and intensity of the parent high at CAD onset for use in the CAD classification scheme (modified from Bailey et al. 2003).

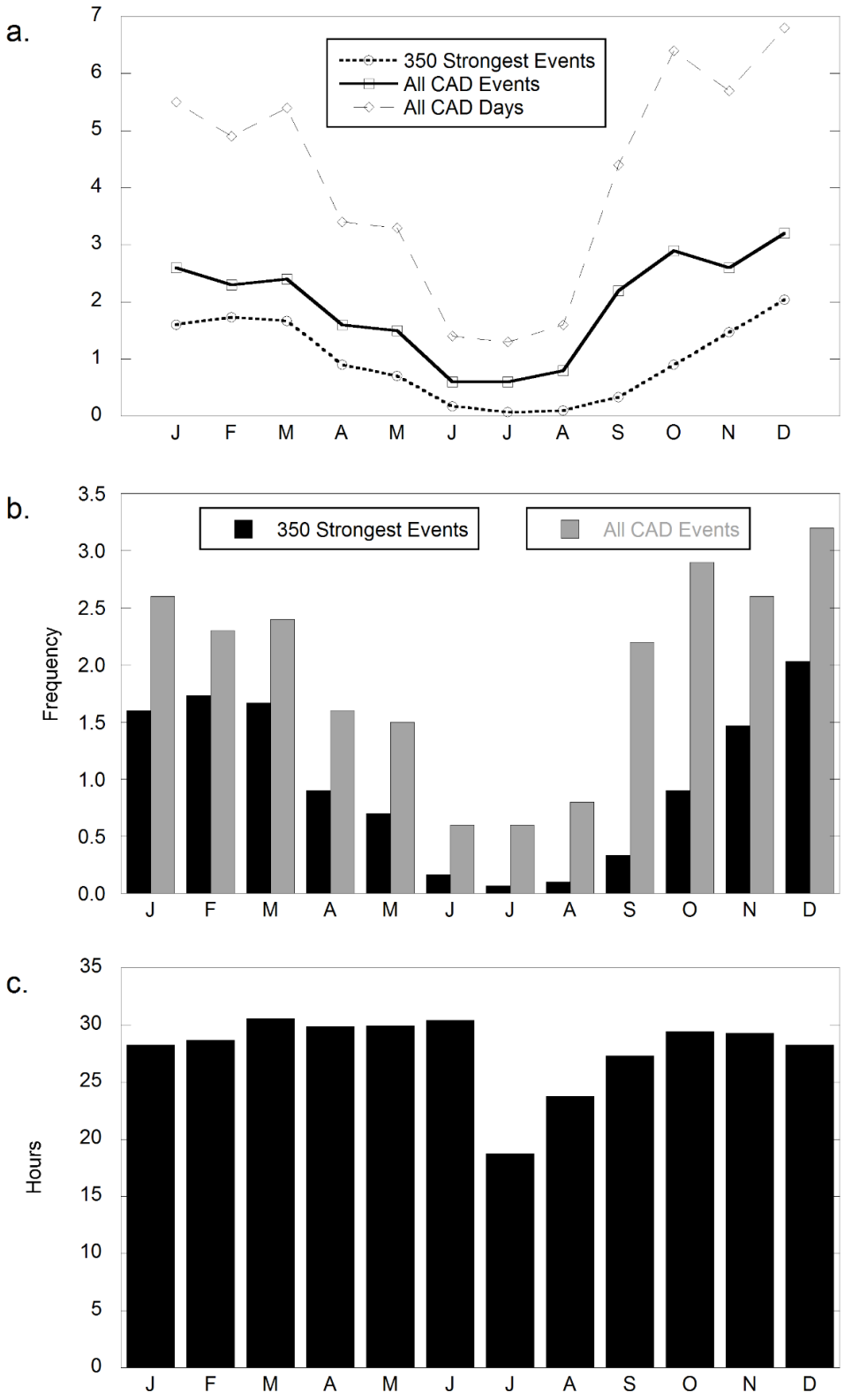

Figure 2.3. a) Monthly average frequency for all CAD days, all CAD events, and the strongest 350 CAD events. b) Monthly frequency of CAD events and strongest 350 CAD events. c) The average duration of events by month.

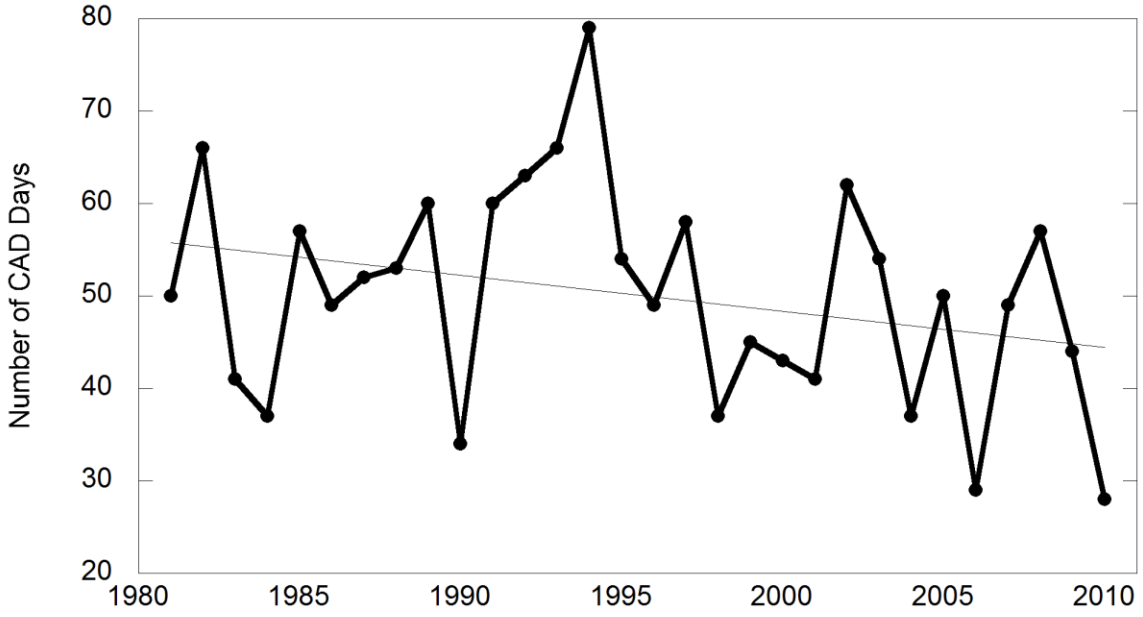

Figure 2.4. Variation in the number of CAD days per year. The data have a statistically insignificant downward trend of 0.39 days per year.

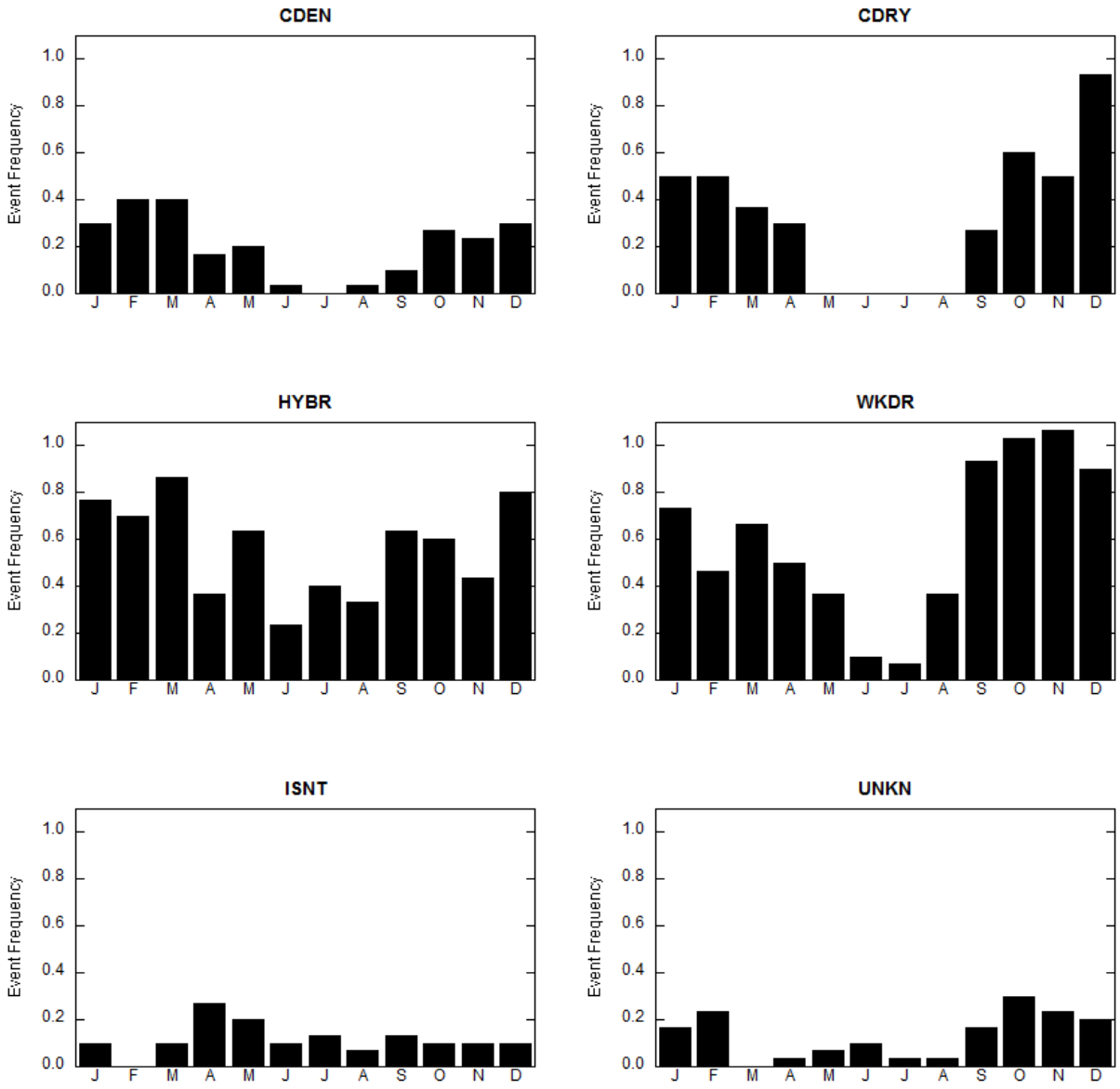

Figure 2.5. The average frequency by month for the different CAD classifications.

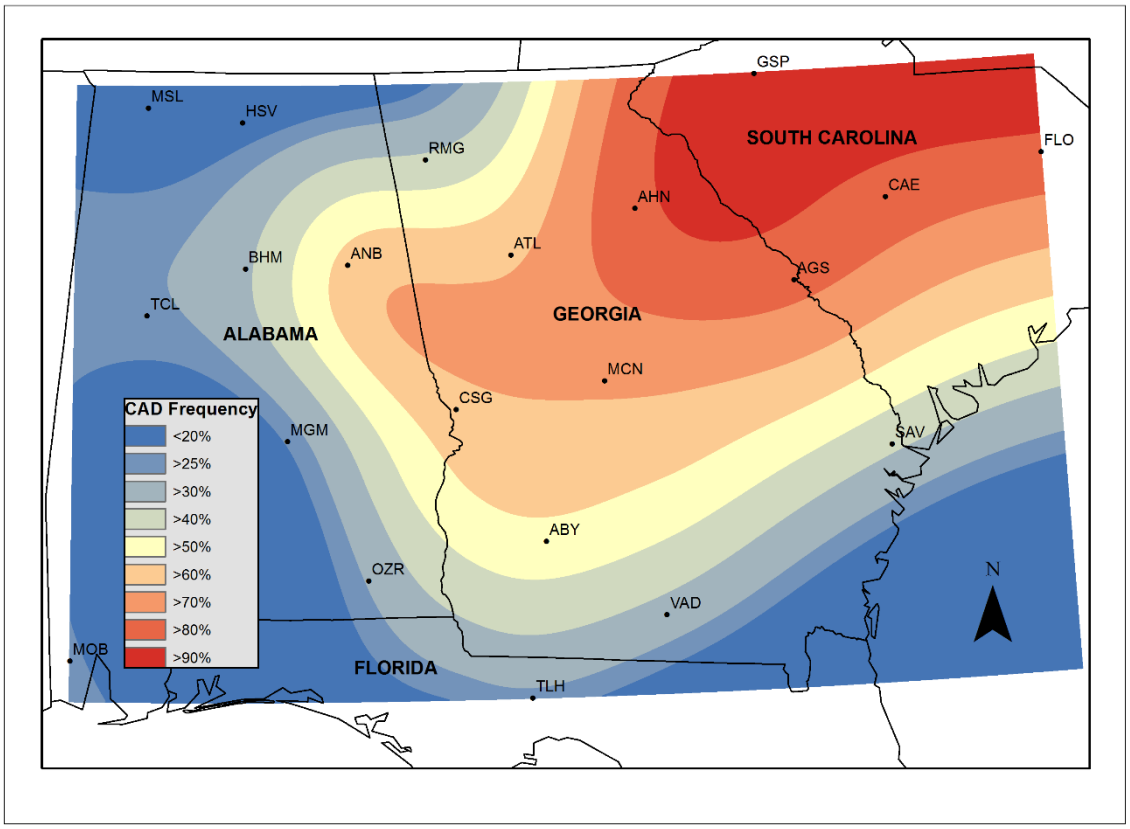

Figure 2.6. Spatial extent and frequency within the southernmost extent of the damming region for all CAD events by percent of total CAD hours.

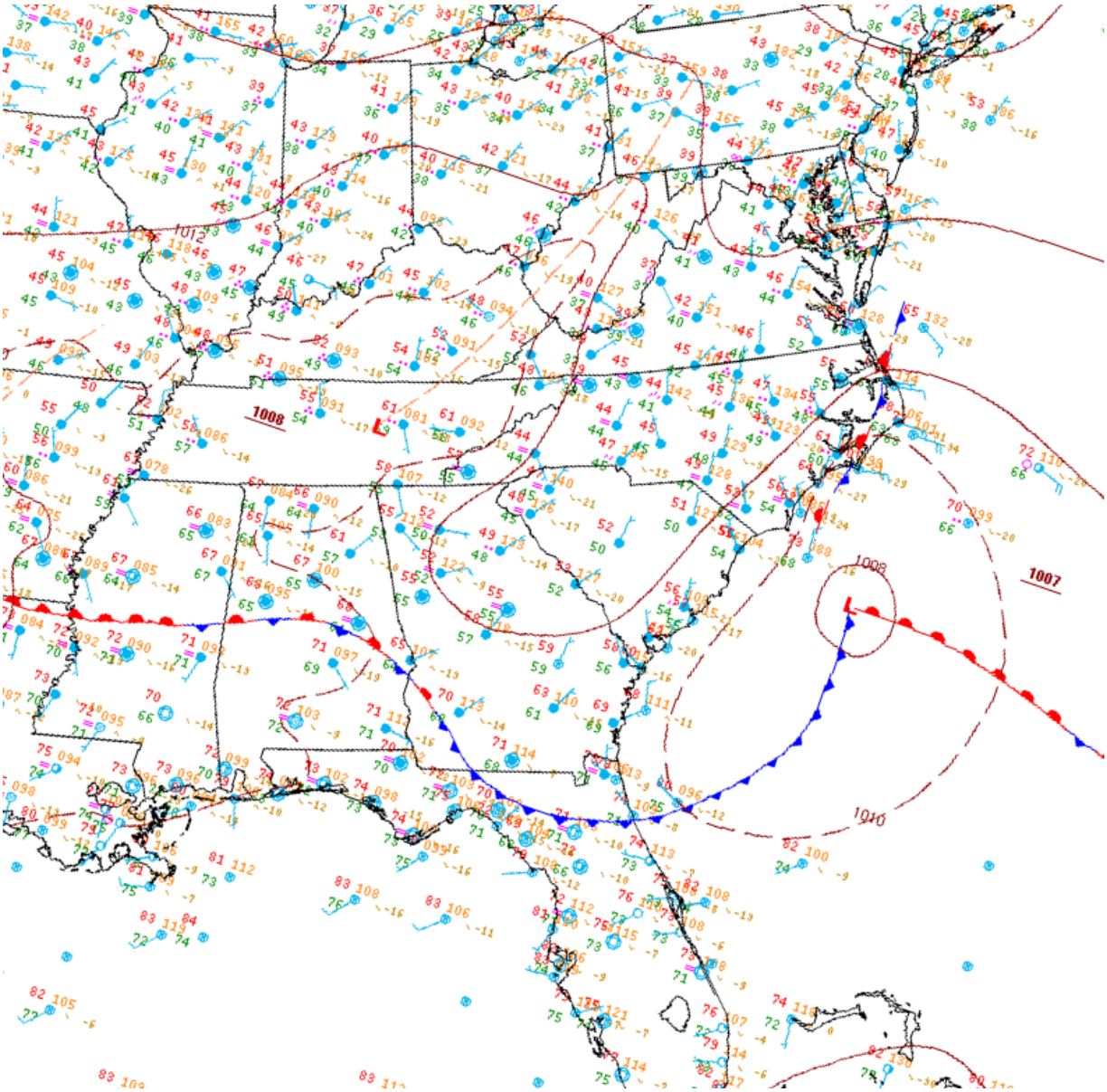

Figure 2.7. WPC surface analysis for 0900 UTC 15 October 2009 showing a cold air dome extending into southern Alabama and northern Florida.

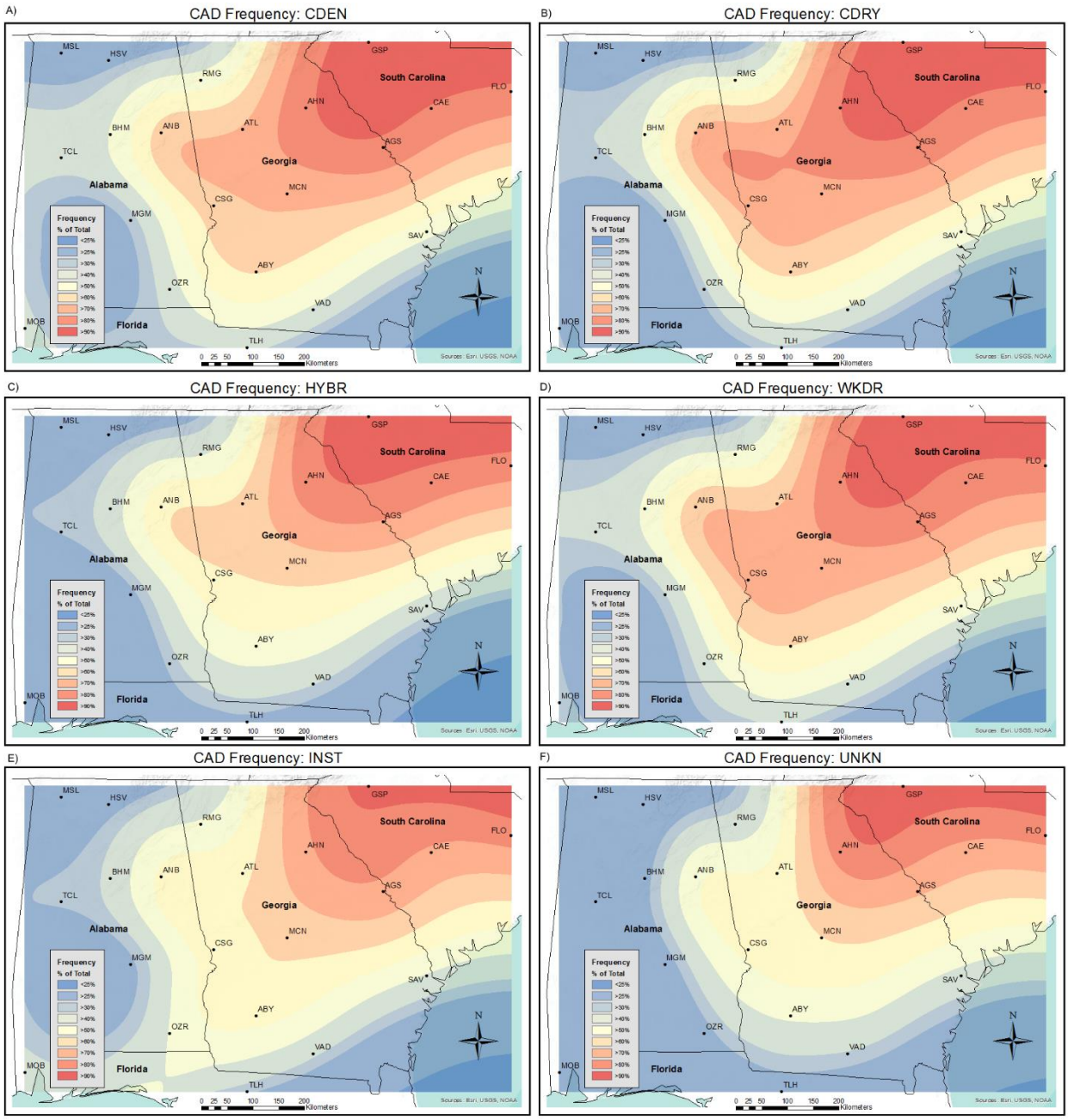

Figure 2.8 a-f. CAD spatial extent and frequency by differing CAD classification. Percentages are out of the total occurrence for each classification as determined by the CAD detection algorithm.

CHAPTER 3

A CASE STUDY OF CONVECTION AND APPALACHIAN COLD AIR DAMMING[2]

[2] Rackley, J.A. and J.A. Knox. To be submitted to *Weather and Forecasting*

Abstract

A case of cold air damming (CAD)-induced wedge front convection (WFC) that occurred on 11 May 2002 in a high instability and low deep layer shear ambient environment was analyzed using high resolution WRF-ARW model simulations. Comparisons a control run and experimental run with flattened terrain, run at 12-km, 4-km, and 1.3-km grid-spacings allowed isolation of the influence of the cold dome and wedge front on explicit convective character and intensity. Results show the cold dome periphery acted to increase low level shear in an environment with sufficient instability and moisture. With CAD in place, enhanced shear, combined with other ingredients, allowed convection to be better organized, have enhanced updraft helicity, and have greater longevity overall. These more intense storms with greater levels of rotation have a higher probability of becoming severe, and thus, may have a greater impact on the public.

Key words: Wedge front convection, cold air damming

3.1 Introduction and Background

Cold air damming (CAD), a result of topographic impacts on synoptic and mesoscale weather patterns, occurs when a shallow, surface-based layer of relatively cold air becomes entrenched against the windward side of a mountain range [Richwien 1980]. While this phenomenon is known to occur in multiple places worldwide [e.g. Dunn 1987; Garreaud and Wallace 1998; Lupo et al. 2001; Chien and Kuo 2006; Schwerdtfeger 1975], the term cold air damming most commonly refers to the phenomenon that occurs on the lee side of the Appalachian Mountains. CAD can often be identified by the characteristic "wedge"-shaped inverted ridge that appears in the sea level pressure field as a shallow dome of cold and stable air becomes established during a CAD event. This cold dome is typically only present below the 850 hPa pressure level [Baker 1970, Bell and Bosart 1988]. As the cross-barrier flow adjusts towards locally modified geostrophy, a low-level, mountain-parallel jet forms that serves to both maintain the cold air dome and drive it farther southward. The cold dome typically extends as far southward as central Georgia, and can occasionally push into central Alabama and northern Florida [Rackley and Knox, in review]. Because of the wedge-shaped inverted ridge that appears during a damming event, the term "wedge" has often been used by operational forecasters in the region to refer to CAD.

While cold season precipitation type forecasts are perhaps the most common CAD-related challenge plaguing operational forecasters [e.g. Keeter et al. 1995], the role of CAD in convective development, especially in the warm season, is a concern among forecasters. Though the interior of the dome acts to stabilize the lower troposphere, the cold air dome's periphery, known as the "wedge front," has been observed to trigger convective development. The wedge front often extends from the southwestern extent of the Appalachians towards the coastline.

Previous studies [e.g. Rackley and Knox, in review] show that the cold dome often dips to the southwest into Georgia and parts of Alabama. Thus, the wedge front is most often seen across these two states, extending eastward towards the coast across South Carolina. The easternmost portion of the front is often referred to as the "coastal front" [e.g., Bosart et al. 1972], and often plays a key role in the erosion process of CAD [e.g. Lackmann and Stanton 2004].

The front itself can behave much like a density current [Jirka and Arita 1987; Nielsen and Neilley 1990] as cold, dense is advected into the area by the mountain-parallel jet. When sufficient moisture and instability are available in the ambient environment, this current can act as a lifting mechanism and trigger wedge front convection (WFC). Convection of this nature may be either surface-based or elevated depending on the presence of convective inhibition and location of initial development. Enhanced convection has been found to increase precipitation totals near the wedge front [e.g. Bosart et al. 1972; Ballentine 1980; Garreaud and Wallace 1997] and in some cases, convection may reach severe intensity [e.g. Businger et al. 1991; Langmaid and Riordan 1998; Baker 2009; Baker and Lackman 2009].

Boundary-layer convergence and baroclinicity associated with a mesoscale feature such as the wedge front is known to alter convective cell motion, intensity, and longevity [Magor 1959; Miller 1972]. The orientation of the boundary to storm motion track has been shown to have an effect on convective behavior and intensity [Maddox et al. 1980; Markowski et al. 1998; Nieuwenhuis 2006]. In addition, baroclinic boundaries may provide horizontal vorticity that can be stretched and tilted into the vertical by a developing updraft [Weisman and Klemp 1982; Klemp and Rotunno 1983; Brady and Szoke 1989; Wakimoto et al. 1998; Rasmussen et al. 2000]. Finally, vertical wind shear introduced at a baroclinic boundary such as the wedge front can significantly affect the convective mode and intensity [e.g., Klemp and Wilhelmson 1978].

Baker and Lackmann [2009] hypothesized that the locally enhanced shear environment of the wedge front could enhance the possibility of severe convection when moisture and instability are sufficient for convective development. Using high resolution numerical models, Baker and Lackmann [2009] simulated and analyzed a case of WFC occurring in a moderate instability and strong deep-layer shear ambient environment, but concluded that the enhanced low-level shear in that particular case failed to compensate for the loss of instability. Their analysis raises additional questions about the effect of the wedge front on convective development in differing ambient environments, particularly and environment with already heightened levels of instability to compensate for the stabilizing effect of the cold dome. The objectives of this research are to clarify and quantify the effects of the CAD cold dome on convection, specifically in a high instability, low shear environment. We hypothesize that the locally enhanced shear within such an environment would act to enhance convection and lead to a higher probability of severe impacts.

3.2 Data, Methods, and Experimental Design

3.2.1 Initial Model Simulations

Initial model simulations (Fig. 3.1) were performed to analyze the impact of the CAD dome on the lower-tropospheric environment. Version 3.5 of the WRF-ARW [Skamarock et al. 2005] model was employed using 12 km horizontal grid spacing, 45 vertical levels, and the Kain-Fritsch convective parameterization scheme to account for sub-gridscale convective processes [Kain and Fritsch 1993]. Additionally, the WSM 6-class microphysics scheme [Hong and Lim 2006], RUC land-surface model [Smirnova et al. 1997, 2000], and YSU boundary layer scheme [Skamarock 2005] were used. Gridded NARR [Mesinger et al. 2006] data were used to initialize the model and serve as 3-hourly boundary conditions throughout the event. The data

spanned 48 hours from 1200 UTC 10 May 2002 (23 hours prior to CAD initialization) to 1200 UTC 12 May 2002 (after the cold dome had begun to erode). Output from the simulations was generated in hourly increments for analysis.

Following the Baker [2009] methodology, a simulation of the event and CAD cold air dome served as the control run. For comparison, a second simulation using the same initial conditions and model parameters, but with terrain flattened to remove the Appalachian Mountains, served as the experimental run. This was accomplished by editing the model terrain height and setting values to zero. Removing the Appalachians effectively eliminated the barrier needed for CAD to form, thus allowing the simulation to run without the influence of a cold dome. In order to account for atmospheric variables in the "underground" areas exposed by the removal of the mountains, the NARR dataset used for model initialization provided interpolated meteorological variables on isobaric levels down to 1000 hPa using the lapse rate for a standard atmosphere. Winds and moisture are held constant below ground within the NARR dataset. Initializing the experimental run 23 hours prior to CAD initialization allowed for a realistic atmospheric evolution without the Appalachians in place. Likewise, the domain used in these simulations was large enough to resolve the parent high as it tracked across the Ohio River Valley, into Canada, and offshore, while also keeping the primary study area (the southeastern U.S. and, more specifically, central Georgia) away from domain boundary influences. An evaluation of the control run was performed to determine if the model correctly reproduced a realistic cold air dome. Finally, the lower-tropospheric environments of both the control and modified-terrain simulations were analyzed and compared to evaluate and isolate the effect of the cold dome in the model.

3.2.2 Convective-Scale Simulations

After an analysis of the general lower-tropospheric environment, additional simulations were performed at higher spatial and temporal resolutions to allow for analysis at the convective scale and isolate the cold dome's influence on explicitly resolved convection. As with the initial model simulations, two WRF-ARW models were constructed using the previously specified model parameters and NARR dataset. However, two nested domains were included within each outer domain with 4-km and 1.3-km horizontal grid spacings to maintain a 3:1 grid spacing ratio between domains. These were run with 1-way nesting (no inter-domain feedback) and used explicit convection instead of a convective parameterization scheme [Molinari and Dudek 1992]. While the 12-km outer domains were again run for 48 hours, the inner domains were initialized "on-the-fly" using initial conditions from the outermost domain at the start of the 24th forecast hour (valid at 1200 UTC 11 May 2002). Output from these domains was generated at 30 minute and 5 minute intervals, respectively. Domain 2 (4-km grid spacing) was centered over the Southeast and included the damming region and WFC study area. Domain 3, the innermost nest (1.3-km grid spacing), was centered over central Georgia to include the WFC study area (Fig. 3.1). The convective scale control run (hereafter referred to as "CAD-CS") retained topography, while the convective scale experimental run (hereafter referred to as "NoCAD-CS") had the mountains removed to simulate the atmosphere without the presence of CAD. The convective scale environment and characteristics of convective development, evolution, and intensity were analyzed and compared for these two simulations to isolate the effect of the cold air dome at convective scales.

3.3 Analysis and Results

3.3.1 Overview of 11 May 2002 WFC Case Study

The 11 May 2002 CAD event was identified as a good candidate for further analysis by Baker [2009] due to the relatively low deep layer shear and high instability ambient environment in which the cold dome and wedge front convection formed. The event lasted for multiple days and was classified as a hybrid CAD event [Bailey et al. 2003]. On 10-11 May 2002, a relatively strong parent surface high pressure system (>1030 hPa) tracked northeastward from the southern Midwest across the Ohio River Valley. Surface analysis indicates that by 1200 UTC 11 May, the center of the parent high had moved into a position just west of Lake Erie, a location appropriate for CAD initiation, and northeasterly flow at the surface can be seen (Fig. 3.2a). The Bailey Algorithm [Bailey et al. 2003] initialized the CAD event one hour prior to this time. By 1500 UTC, CAD was evident in the surface analysis, both as inverted pressure ridging and northeasterly flow. By 1800 UTC, CAD was affecting much of the southeastern U.S. and was in place as far south and west as north Georgia. A wedge front can be identified along a line roughly from Augusta to Milledgeville to Peachtree City to Rome, GA in the 1800 UTC surface analysis (Fig. 3.2b). Fairly zonal flow aloft and a mid-level ridge centered over southern Georgia led to a weakly-sheared environment across the Southeast. An analysis of surface observations, satellite imagery, and base reflectivity (Fig. 3.3) indicate convective initiation in the form of discrete showers within central Georgia along the southern extent of the wedge front by 1800 UTC 11 May 2002.

The cold dome strength was determined to be relatively strong using surface temperature analysis (not shown). A difference in temperature of 14°C from the interior of the dome to the wedge front was found at 1800 UTC. The closed high became elongated and began to shift

offshore by 300 UTC 12 May 2002. By 900 UTC, the high had continued to move offshore, eroding the mountain-parallel jet, and ending the CAD, though a pool of cold air and dense cloud cover remained in place over the damming region. The cold pool and cloud cover would continue eroding throughout the afternoon.

Active WFC was identified for 9 hours across central South Carolina, central Georgia, and east-central Alabama. Previous definitions of WFC [e.g. Baker 2009] require that initial development be within 100 km on either side of the analyzed dome periphery. Weak reflectivity values ($\geq$ 5 dBz to $\leq$ 30 dBz) were identified at 1757 UTC 11 May approximately 10 km east-northeast of Milledgeville, GA. By 1807 UTC, reflectivity values had increased to > 40 dBz, and additional storms were developing across central Georgia. Approximate location of the wedge front was estimated using surface observations, satellite, and observed boundaries within the radar data. While a majority of the WFC developed exterior to the cold dome (i.e. to the south of the wedge front), several cells did form within the dome or formed immediately adjacent to the wedge front and moved into the cold dome. Storms located within the cold dome were assumed to be elevated in nature.

Convection continued to develop along and south of the wedge front across central Georgia, and also began to develop across central South Carolina by 1900 UTC. Convective storms unassociated with the wedge front were identified in the extreme southeast Alabama area. These multicellular storms pushed northwards, interacting with and possibly enhanced by the wedge front at approximately 0100 UTC 12 May before dissipating within the dome's stable air.

WFC initiated or enhanced storms were identified and matched with a total of nine storm reports in the SPC database (Fig. 3.4) mostly across central Georgia using base reflectivity from the KFFC WSR-88D radar. The convection resulted in seven hail reports and two wind reports in

the area from 1945-2200 UTC. Cells maintained a mostly multicellular appearance throughout the event.

The National Weather Service Peachtree City, Georgia (FFC) recognized the potential for severe storms along the wedge front in their early morning Area Forecast Discussion (IEM 2015):

"…HIGH THETA-E AIR POOLING IN EXTREME WEST GA AS WEDGE BOUNDARY APPROACHES. EXPECTING SOME AFTERNOON AND EVENING THUNDERSTORMS THERE...A FEW MAY REACH SEVERE LIMITS..."

The Storm Prediction Center also recognized the threat, and issued a slight risk of severe storms in their 1600 UTC Day 1 Severe Weather Outlook:

"…CONVECTIVE INITIATION IMMINENT AT 16Z S AND W OF FRONTAL ZONE/WEDGE GA WHERE MLCAPES RANGE UPWARDS TO 2500 J/KG. MULTI-CELLULAR STORM MODE EXPECTED GIVEN THE RATHER WEAK SHEAR..HOWEVER WET BULB ZERO LEVELS AND INSTABILITY SUPPORT A FEW SEVERE STORMS. LARGE HAIL EXPECTED TO BE PRIMARY MODE…"

Rapid Update Cycle (RUC) soundings for locations exterior the dome supported this analysis. Model soundings from Charleston, SC (CHS), Tallahassee, FL (TLH), and Jacksonville, FL (JAX) all show moderate surface-based and most-unstable CAPE values and weak deep-layer shear values (Table 3.1).

3.3.2 Initial 12-km Simulations

The 12-km control run was evaluated for realistic representation of the cold air dome. Simulated 2-m temperature, 2-m dewpoint, and 10-m winds (Fig. 3.5) show the evolution of the cold dome as it surges into Georgia (1500 UTC 11 May 2002 – 0000 UTC 12 May 2002). At 1500 UTC, the simulated cold dome had progressed across much of northern Georgia and into the metro Atlanta area. Though potential temperatures within the dome increased somewhat with solar heating by 1800 UTC, the cold dome continued to surge to the south and east as evidenced by the 10-m wind field. By 0100 UTC 12 May 2002, the simulated cold dome had reached its maximum extent across northern Georgia.

Output from the control run was compared to the real event analysis to evaluate differences in the real and simulated cold domes. The simulated 2-m temperature (°C) and 2-m potential temperature (K) were plotted for 1800 UTC 11 May 2002 and compared to the surface temperature analysis for the same time (Fig. 3.6). Temperatures between the two were very similar, though the core of the simulated damming region appeared to be 1-2°C cooler than observed in the surface analysis. Interestingly, the NARR 2-m temperatures were not as accurate for this time and tended to be several degrees too warm within the damming region. As observed in previous CAD WRF experiments [e.g., Baker 2009], the eastern periphery of the cold dome eroded and retreated inland too quickly in the model. The southernmost extent of the cold dome was also not as far south as observed in the real case. This was similarly observed by Baker [2009], who noted that differences may result from the shallow mixing implemented in the YSU boundary layer scheme. Beyond these differences, the model did adequately simulate the CAD setup, timing, location, and strength. Thus, the simulation was concluded to serve as a sufficient control.

Before comparative analyses could be conducted, the modified-terrain run was analyzed to determine if CAD development was successfully inhibited. To accomplish this, the 2-m potential temperature fields for the control and modified-terrain runs were compared and analyzed for signs of a cold dome for the duration of the real event. Figure 3.7a shows 2-m potential temperatures and 10-m wind barbs for 2100 UTC 11 May 2002, near the peak of the real and simulated CAD events. By comparison, the modified-terrain run exhibited no sign of a cold air dome or cold air advection within the damming region (Fig. 3.7b). Instead, much of the region saw offshore, southeasterly flow consistent with the large-scale synoptic regime.

Successfully simulating the CAD event within the control run and eliminating CAD development within the modified-terrain run allow for a comparative analysis between the two runs and the opportunity to isolate the direct influence of the cold dome on the lower-tropospheric convective environment.

Simulated convective precipitation was analyzed for the period from 1700 UTC 11 May 2002 – 0300 UTC 12 May 2002, the active period of wedge front convection. The 10-hr accumulated convective precipitation with overlain 2-m potential temperature for the two runs are shown in Figure 3.8. Precipitation totals from the control run indicate simulated convective precipitation in areas along and exterior to the wedge front and area of maximum baroclinicity from northwestern Georgia to central Georgia and central South Carolina. Maximum accumulation values are located exterior the simulated cold dome in southeast Georgia and south-central South Carolina. The modified-terrain run shows similar accumulation amounts, but shifted towards west-central South Carolina. This suggests that convection would be present without CAD presence, but within a slightly different area.

A comparison of dew point temperatures between the two model simulations also highlights the substantially decreased moisture content (5 to 10°C lower) within the core of the damming region versus the same area for the modified-terrain run. Even areas exterior to the cold dome, including central and southern Georgia, saw dew point temperatures nearly 5°C lower. However, locations immediately exterior the wedge front in central South Carolina exhibited no marked decrease in dew points versus the modified-terrain run, likely because of this area's close proximity to the coast.

The development of a mountain-parallel jet of cold, northeasterly flow along the eastern slopes of the Appalachians by 1000 UTC 11 May 2002 (Fig. 3.9), acted to enhance frontogenesis and convergence along and near the cold dome periphery before and during WFC initiation (Fig. 3.10). An area of convergence also developed across central South Carolina as the local sea breeze pushed inland towards the expanding dome of cold air.

SBCAPE and 0-3 km SRH were analyzed to assess the cold dome's influence on the simulated lower-tropospheric instability and vertical wind shear (Fig. 3.11a). As expected, the cold dome was analyzed to be in a location of limited SBCAPE with a strong gradient to moderate SBCAPE values (> 2000 J/kg) near the periphery of the dome. Values of SRH were relatively low exterior to the dome, but increased substantially to values capable of producing rotating convection within the dome.

Though the modified-terrain run showed increased SBCAPE values over north Georgia and northwest South Carolina (i.e. areas within the cold dome in the control run), the east-central Georgia and central Carolina regions (immediately south of the wedge front in the control run) showed lower SBCAPE values than in the control run (Fig. 3.11b). Simulated SRH values were at a minimum throughout the region.

Deep-layer (0-6 km) vertical wind shear values were low (< 30 kts) for both the control and modified-terrain runs (Fig. 3.12a,b). Areas within the cold dome did experience slightly higher deep-layer shear values in the control versus the modified-terrain run due to the increase in low-level shear, though these heightened values were marginal at best.

While these results demonstrate the ability of CAD to alter the lower tropospheric convective environment and show that the region near the wedge front may serve as a lifting mechanism capable of triggering convective development, the specific influence of the wedge front on convection cannot be determined with coarse 12-km grid spacing and parameterized convection. For this reason, nested 4-km and 1.3-km domains were used to explicitly resolve convection and isolate the actual influence of the cold dome on convective character and intensity. These convective-scale simulations are reviewed in the following section.

3.3.3 Convective-Scale Simulations

Additional simulations were run for the event using higher spatial and temporal resolutions in order to explicitly resolve processes at the convective scale. These convective-scale simulations allowed for analysis of the specific location and evolution of convection along the wedge front. Comparison between the convective-scale control run (CAD-CS) and the convective-scale experimental run (NoCAD-CS) with flattened terrain allowed for isolation of the cold dome's influence on explicitly simulated convection.

Simulated composite reflectivity, 10-m streamlines, and 2-m theta were analyzed within the CAD-CS inner nests (4-km and 1.3-km grid spacing) to determine the timing and location of initial precipitation and the later convective development associated with the wedge front. Precipitation began to develop within the damming region, specifically western North Carolina

and northwestern South Carolina, as early as 1300 UTC 11 May. This area of precipitation continued to develop and spread to the southeast.

Two distinct occurrences of initial convective development or "ICD" (an increase in simulated reflectivity values to ≥ 35 dBZ, as specified previously) were observed within the simulation. The first began a precipitation at 1450 UTC along the Georgia/South Carolina border. ICD for this region occurred immediately south of the wedge front (i.e. within the warm sector) an hour later at 1600 UTC (Fig. 3.13a). After this ICD, discrete cells began to merge into multicellular clusters, and convection continued to develop to the west along the wedge front. A majority of these cells were surface-based as they developed outside of the cold dome. However, several cells did develop within the dome and appeared to be elevated. These storms remained mostly stationary until 1730 UTC when the simulated cold dome convection began to slowly propagate farther to the south.

The second case of ICD occurred along the wedge front across central and west-central Georgia. Areas of precipitation began to develop along the wedge front by 1845 UTC. ICD was observed at 1900 UTC at several locations along the wedge front (Fig. 3.13b). Unlike much of the convection to the east, these cells were elevated and developed inside the cold dome, propagating slowly to the northeast. Storms also developed across east-central Georgia, approximately 50-100 km south of the analyzed wedge front. This convection also propagated to the northeast. As storms pushed into the cold dome, they became elevated and eventually dissipated. By 0300 UTC, most areas of convection across the region had dissipated.

Conversely, the NoCAD-CS run exhibited precipitation in the area at 1630 UTC, nearly two hours later than in the CAD-CS run. Initial convective development occurred soon after at 1700 UTC when convection began approximately 50 km west of the Georgia/South Carolina

border (Fig. 3.14). This area of ICD is in roughly the same area as ICD within the CAD-CS run, but displaced slightly to the northwest. Without the presence of CAD, convection generally remained more discrete and exhibited less overall coverage area than was observed in the CAD-CS run. Individual storms also had a lessened longevity, tending to dissipate in under an hour. By 0000 UTC 12 May, coverage area of storms across north and central Georgia was significantly reduced, and storms remaining after 0200 UTC were associated with westward-moving sea breeze front.

Output from the NoCAD-CS run was analyzed for evidence of a low-level source of lift that might act as a trigger for convective development. Although a broad area of surface confluence was analyzed over north Georgia during the morning hours of 11 May, the surface flow evolved into southerly winds by the afternoon hours, and no surface boundary could be determined.

Convection in the NoCAD-CS run developed in an area of noticeable higher instability, while ICD in the CAD-CS run developed along the strong gradient in SB-CAPE from 0-2500 J/kg. Conversely, both areas of convection developed in relatively low deep-layer shear. Determining convective intensity differences between the two model simulations is key to isolating CAD's effect on convection. Intensity was quantified using simulated updraft helicity and vertical velocity (Kain et al. 2008). Multiple individual cells from each simulation were analyzed for updraft helicity and updraft speed throughout their life cycle (not shown). Simulated convection in the CAD-CS run, especially those storms that developed during the first case of ICD, exhibited much higher updraft helicity than NoCAD-CS simulated convection in similar locations. High helicity values (> 500 m^2/s^2 in some cases) indicated rotating updrafts present

within the CAD-CS run. However, updraft speeds were similarly moderate (> 10 m/s) for both simulations.

3.4 Summary and Conclusions

Simulations at 12-km, 4-km, and 1.3-km grid-spacings were run and analyzed to isolate the influence of the cold dome and wedge front on explicit convective character and intensity. While convection within the two runs developed in roughly the same location across north and central Georgia, the experimental run and NoCAD-CS runs exhibited convection farther to the north. Convection in the CAD-CS model tended to better organize into multicellular clusters, while convection in the NoCAD-CS model tended to remain discrete and single-cellular. Individual storm updraft helicity was also greatly enhanced within the CAD-CS run versus the No-CAD run, and storms tended to have greater longevity on average with a cold dome present. These findings emphasize that heightened levels of low-level vertical shear with the cold dome present were able to overcome lower instability values when instability values exterior the dome are moderate to high. Increased low-level shear along the wedge front allowed storms to develop in a multicellular mode, increasing their longevity and intensity as measured with updraft helicity. These more intense storms with greater rotation have a higher probability of becoming severe. Thus, forecasters should be aware of the increased possibility for severe convection when CAD events form in low shear, high CAPE environments.

3.5 References

Bailey, C. M., G. Hartfield, G. M. Lackmann, K. Keeter, and S. Sharp, 2003: An objective climatology, classification scheme, and assessment of sensible weather impacts for Appalachian cold-air damming. *Wea. Forecasting*, **18**, 641-661.

Baker, D. G., 1970: A study of high pressure ridges to the east of the Appalachian Mountains. Ph.D. thesis, Massachusetts Institute of Technology, 127 pp.

Baker, A. K., 2009: Convection and Appalachian Cold-Air Damming. Master's thesis, North Carolina State University, 188 pp.

Ballentine, R. J., 1980: A numerical investigation of New England coastal frontogenesis. *Mon. Wea. Rev.*, **108**, 1479-1497.

Bell, G. D., and L. F. Bosart, 1988: Appalachian cold-air damming. *Mon. Wea. Rev.*, **116**,137-161.

Bosart, L. F., C. J. Vaudo, and J. H. Helsdon Jr., 1972: Coastal frontogenesis. *J. Appl. Meteor*., **11**, 1236-1258.

Brady, R. H., and E. J. Szoke, 1989: Case study of a nonmesocyclone tornado development in northeast Colorado: Similarities to waterspout formation. *Mon. Wea. Rev.*, **117**, 843-856.

Businger, S., W. H. Bauman, and G. F. Watson, 1991: The development of the piedmont front and associated outbreak of severe weather on 13 March 1986. *Mon. Wea. Rev.*, **119**, 2224-2251.

Chien, F. C., and Y. H. Kuo, 2006: Topographic effects on a wintertime cold front in Taiwan. *Mon. Wea. Rev.,* **124**, 3297-3316.

Dunn, L., 1987: Cold air damming by the Front Range of the Colorado Rockies and its relationship to locally heavy snows. *Wea. Forecasting*, **2**, 177-189.

Garreaud, R. D., and J. M. Wallace, 1998: Summertime incursions of midlatitude air into subtropical and tropical South America. *Mon. Wea. Rev*., **126**, 2713-2733.

Hong, S.-Y., and J.-O. Lim, 2006: The WRF single-moment 6-class microphysics scheme (WSM6). *J. Korean Meteor. Soc.*, **42**, 129-151.

IEM, 2014: Iowa Environmental Mesonet NWS Text Product Finder. Accessed 2 April 2014. [Available online at https://mesonet.agron.iastate.edu/wx/afos/]

Jirka, G. H., and M. Arita, 1987: Density currents or density wedges: Boundary-layer influence and control methods. *J. Fluid Mech.*, **177**, 187-206.

Kain, J. S., and J. M. Fritsch, 1993: Convective parameterization for mesoscale models: The Kain-Fritsch scheme. *The Representation of Cumulus Convection in Numerical Models, Meteor. Monogr.*, No. 46, Amer. Meteor. Soc., 165-170.

Kain, J. S., and Coauthors, 2008: Some practical considerations regarding horizontal resolution in the first generation of operational convection-allowing NWP. *Wea. Forecasting*, **23**, 931–952.

Keeter, K. K., S. Businger, L. G. Lee, and J. S. Waldstreicher, 1995: Winter weather forecasting throughout the eastern United States. Part III: The effects of topography and the variability of winter weather in the Carolinas and Virginia. *Wea. Forecasting*, **10**, 42-60.

Klemp, J. B., and R. Rotunno, 1983: A study of the tornadic region within a supercell thunderstorm. *J. Atmos. Sci.*, **40**, 359-377.

_____, and R. B. Wilhelmson, 1978: Simulations of right- and left-moving storms produced through storm splitting. *J. Atmos. Sci.*, **35**, 1097-1110.

Lackmann, G. M., and W. M. Stanton, 2004: Cold-air damming erosion: Physical mechanisms, synoptic settings, and model representation. Preprints, *20th Conf. on Weather Analysis and Forecasting*, Seattle, WA, Amer. Meteor. Soc., CD-ROM, 18.6.

Langmaid, A. H., and A. J. Riordan, 1998: Surface mesoscale processes during the 1994 Palm Sunday tornado outbreak. *Mon. Wea. Rev.*, **126**, 2117-2132.

Lupo, A. R., J. J. Nocera, L. F. Bosart, E. G. Hoffman, and D. J. Knight, 2001: South American cold surges: Types, composites, and case studies. *Mon. Wea. Rev*., **129**, 1021-1041.

Maddox, R. A., L. R. Hoxit, and C. F. Chappell, 1980: A study of tornadic thunderstorm interactions with thermal boundaries. *Mon. Wea. Rev.*, **108**, 322-336.

Magor, B. W., 1959: Meso-analysis: Some operational analysis techniques utilized in tornado forecasting. *Bull. Amer. Meteor. Soc.*, **40**, 499-511.

Markowski, P. M., E. N. Rasmussen, and J. M. Straka, 1998: The occurrence of tornadoes in supercells interacting with boundaries during VORTEX-95. *Wea. Forecasting*, **13**, 852-859.

Mesinger, F., G. DiMego, E. Kalnay, K. Mitchell, P. C. Shafran, W. Ebisuzaki, D. Jović, J. Woollen, E. Rogers, E. H. Berbery, M. B. Ek, Yun Fan, R. Grumbine, W. Higgins, H. Li, Y. Lin, G. Manikin, D. Parrish, W. Shi, 2006: North American Regional Reanalysis. *Bull. Amer. Meteor. Soc*., **87**, 343-360.

Miller, R. C., 1972: Notes on analysis and severe storm forecasting procedures of the Air Force Global Weather Central. Tech. Rep. 200 (revised), AWS, USAF, 181 pp.

Molinari, J. and M. Dudek, 1992: Cumulus parameterization in mesoscale numerical models: A critical review. *Mon. Wea. Rev.*, **120**, 326-344.

Nielsen, J. W., and P. P. Neilley, 1990: The vertical structure of New England coastal fronts. *Mon. Wea. Rev.*, **118**, 1793-1807.

Nieuwenhuis, B. P., 2006: A study of severe thunderstorm interaction with thermal boundaries: Collision angle and stability. Master's thesis, North Carolina State University, 50 pp.

_____, and J. A. Knox, 2015: A Climatology of Southern Appalachian Cold Air Damming. *Wea. Forecassting.*, [in review].

Rasmussen, E. N., S. Richardson, J. M. Straka, P. M. Markowski, and D. O. Blanchard, 2000: The association of significant tornadoes with a baroclinic boundary on 2 June 1995. *Mon. Wea. Rev.*, **128**, 174-191.

Richwien, B. A., 1980: The damming effect of the southern Appalachians. *Natl. Wea. Dig.*, **5** (1), 2-12.

Schwerdtfeger, W., 1975: The effect of the Antarctic peninsula on the temperature regime of the Weddell Sea. *Mon. Wea. Rev.*, **103**, 45-51.

Skamarock, W. C., J. B. Klemp, J. Dudhia, D. O. Gill, D. M. Barker, W. Wang, and J. G. Powers, 2005: A description of the Advanced Research WRF version 2. NCAR Tech. Note NCAR/TN-468+STR, 88 pp.

Smirnova, T.G., J.M. Brown, and S.G. Benjamin, 1997: Performance of different soil model configurations in simulating ground surface temperature and surface fluxes. *Mon. Wea. Rev.*, **125**, 1870-1884.

Smirnova, T.G., J.M. Brown, S.G. Benjamin, and D. Kim, 2000: Parameterization of cold season processes in the MAPS land-surface scheme. *J. Geoph. Res*, **105** (D3), 4077-4086.

Wakimoto, R. M., and C. Liu, and H. Cai, 1998: The Garden City, Kansas, storm during VORTEX 95. Part I: Overview of the storm's life cycle and mesocyclogenesis. *Mon. Wea. Rev.*, **126**, 372-392.

Weisman, M. L., and J. B. Klemp, 1982: The dependence of numerically simulated convective storms on vertical wind shear and buoyancy. *Mon. Wea. Rev.*, **110**, 504-520.

3.6 Tables and Figures

Table 3.1. Values of surface-based CAPE an CIN, most-unstable CAPE and CIN, and deep-layer shear from RUC model soundings at Charleston, South Carolina (CHS), Tallahassee, Florida (TLH), and Jacksonville, Florida (JAX).

	SBCAPE	**SBCIN**	**MUCAPE**	**MUCIN**	**DL SHEAR**
MHX	70	-66	104	-53	40
CHS	3970	0	3970	0	30
TLH	2428	0	3040	0	20
JAX	3040	0	2428	0	15
Average	2377	-17	2386	-13	26

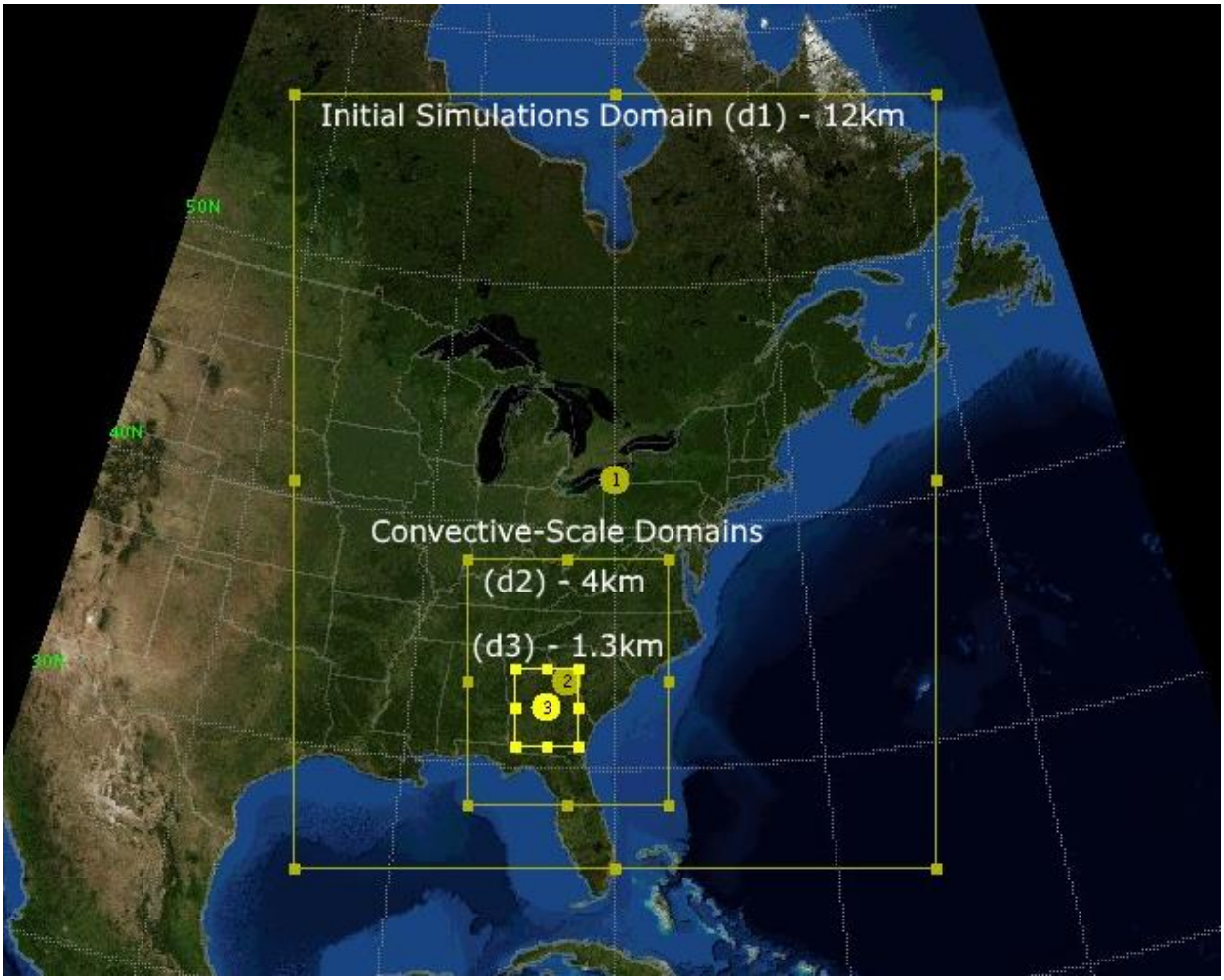

Figure 3.1. A map of model domains showing the large parent domain used for 12-km grid spacing simulations and the inner nests, d2, and d3, run at 4-km and 1.3-km grid spacings.

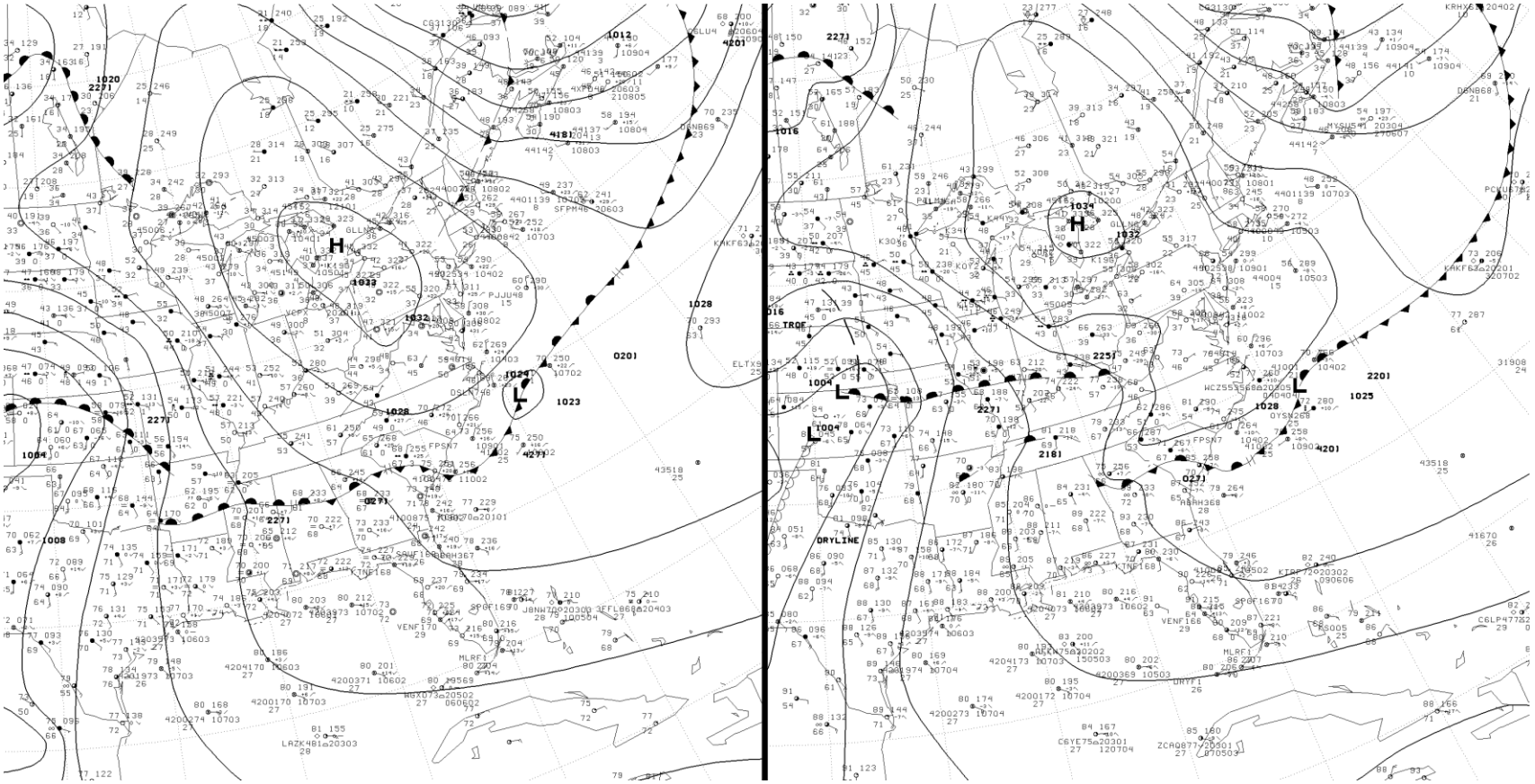

Figure 3.2. HPC surface analysis for a) 1200 UTC and b) 1800 UTC 11 May 2002.

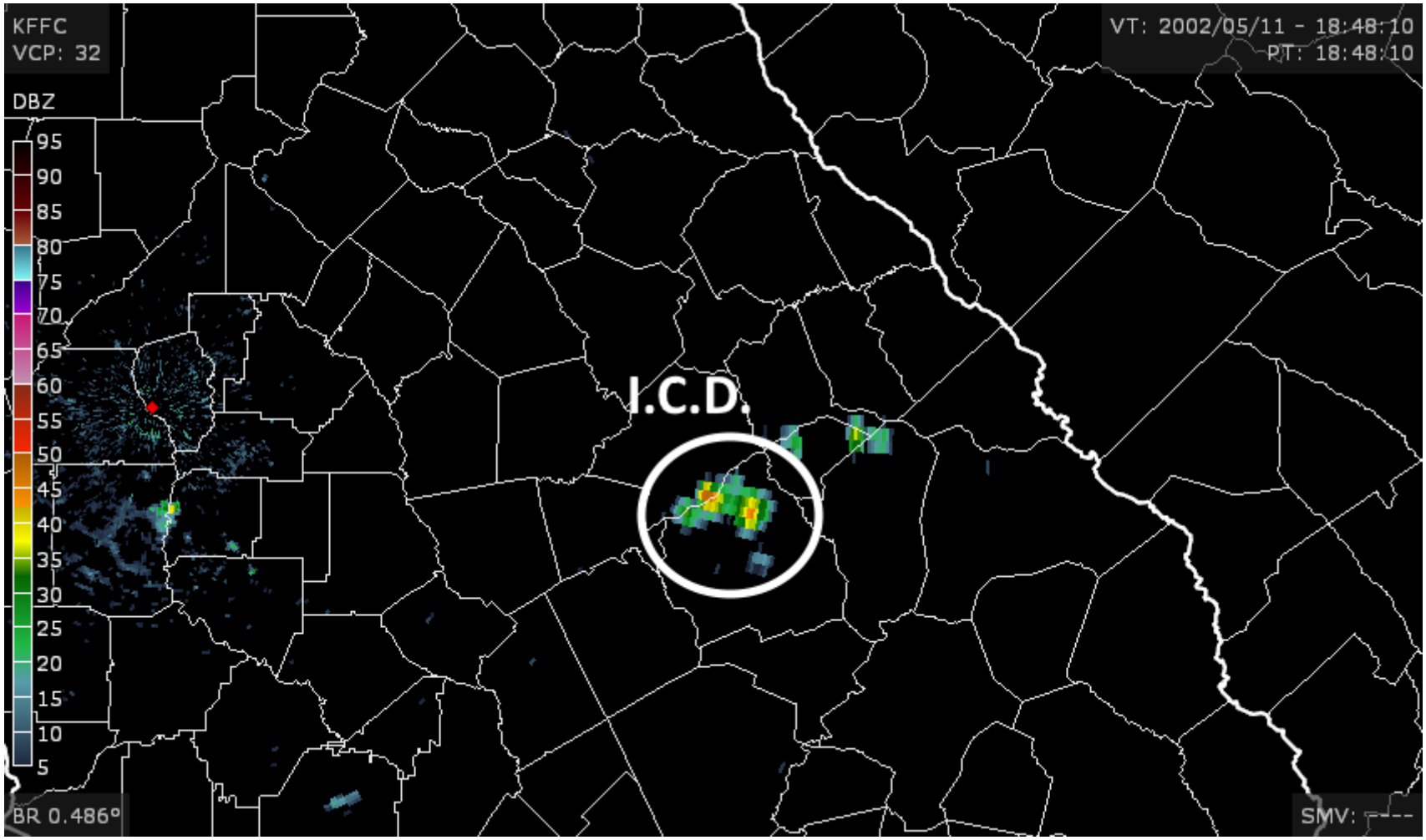

Figure 3.3. WSR-88D reflectivity from the KFFC Peachtree City, GA radar at initial convective development (1848 UTC 11 May 2002).

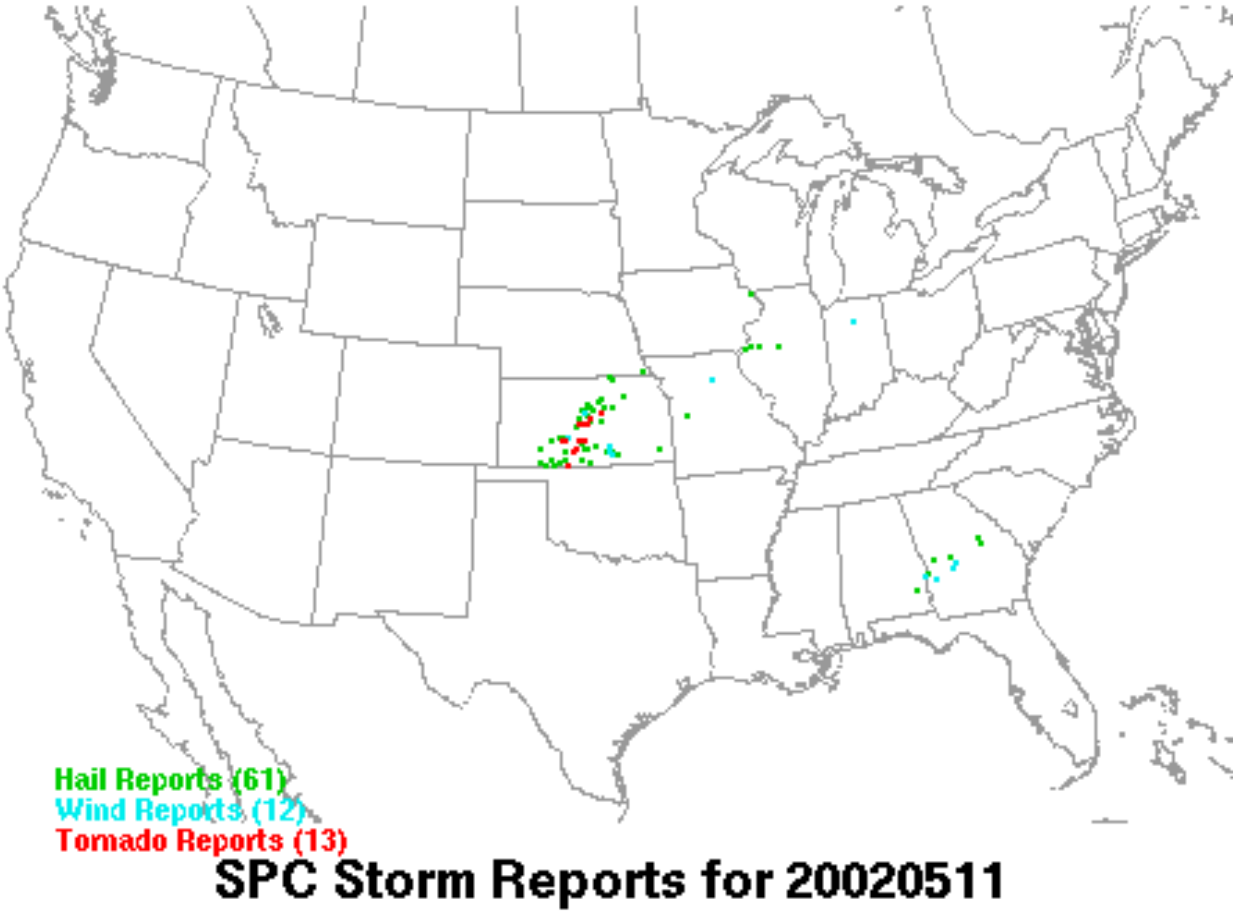

Figure 3.4. Storm Prediction Center storm reports for 11 May 2002.

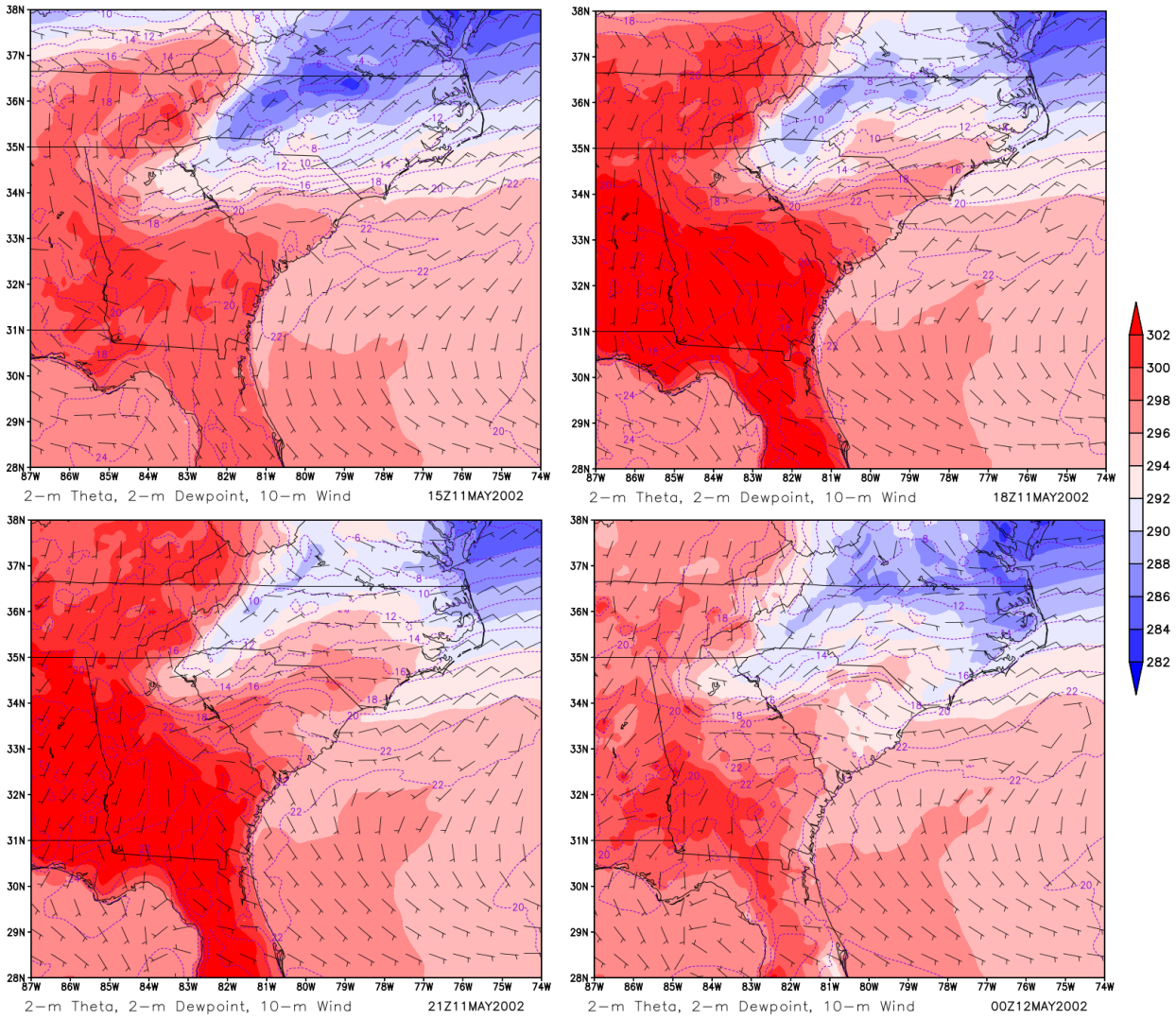

Figure 3.5. Simulated 2-m potential temperature (shaded, K), 2-m dewpoint (dashed, °C), and 10-m winds (barbs, knts) for a) 1500 UTC, b) 1800 UTC, c) 2100 UTC 11 May 2002, and d) 0000 UTC 12 May 2002.

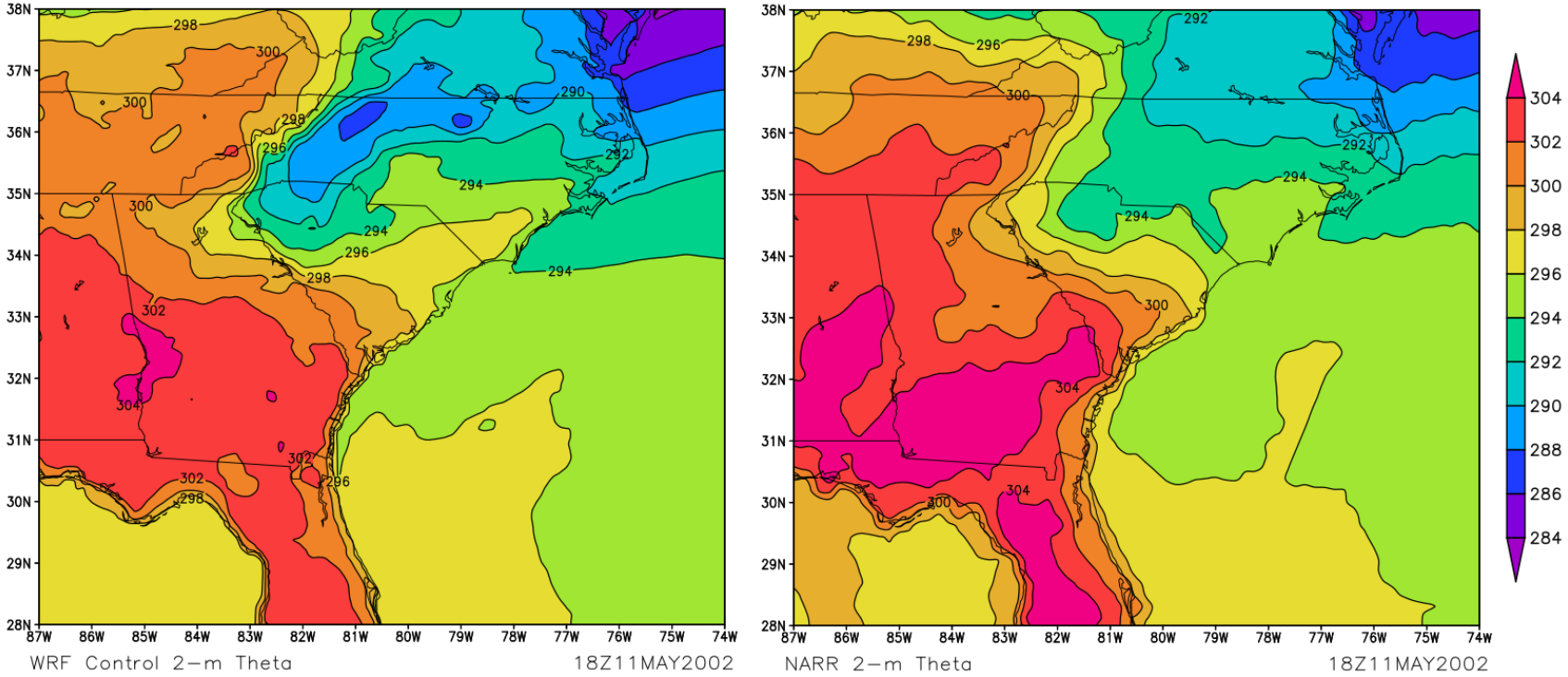

Figure 3.6. Simulated 2-m potential temperature (contours, K) at 1800 UTC 11 May 2002 for a) the control run and b) surface observations.

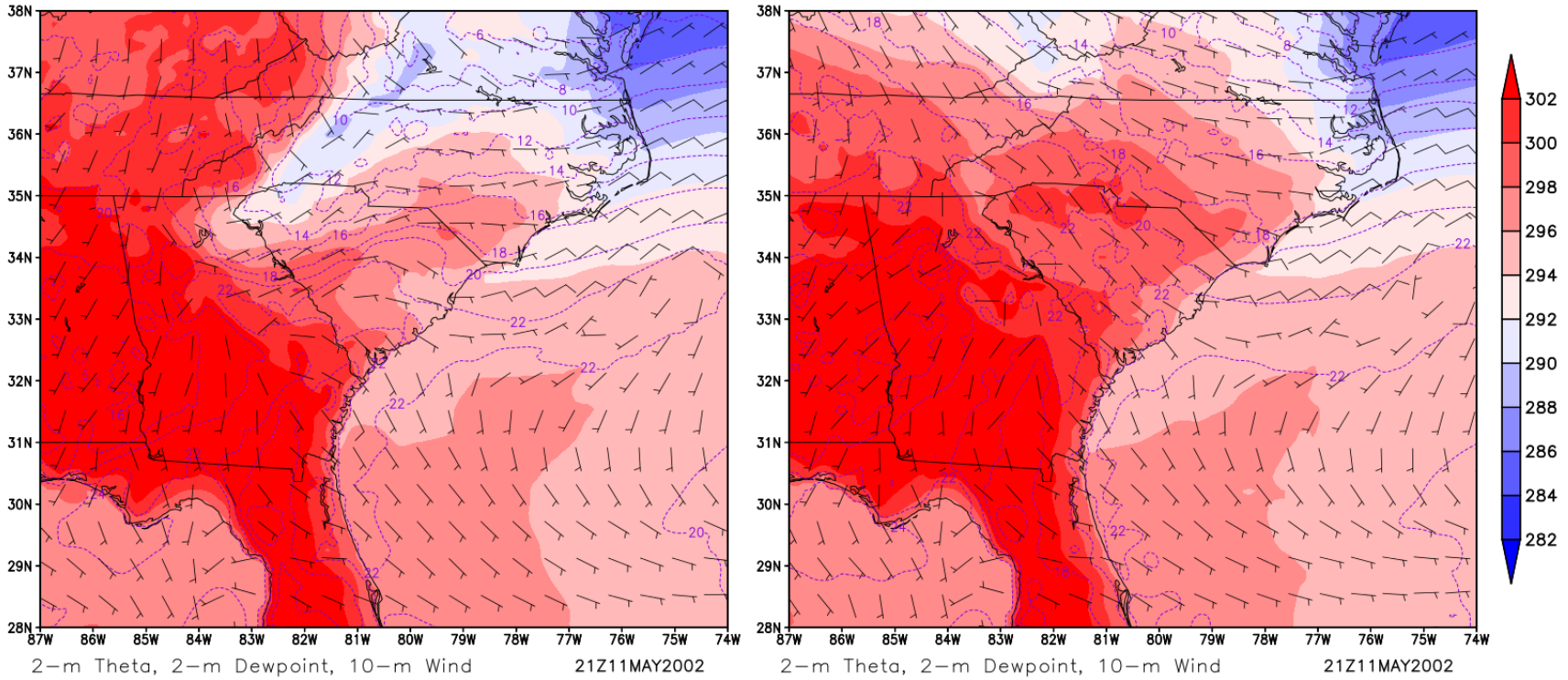

Figure 3.7. Simulated 2-m potential temperature (shaded, K), 2-m dewpoint (dashed, °C), and 10-m winds (barbs, knts) for a) the control run, and b) the experimental run at 2100 UTC 11 May 2002, near the peak of the real and simulated CAD events.

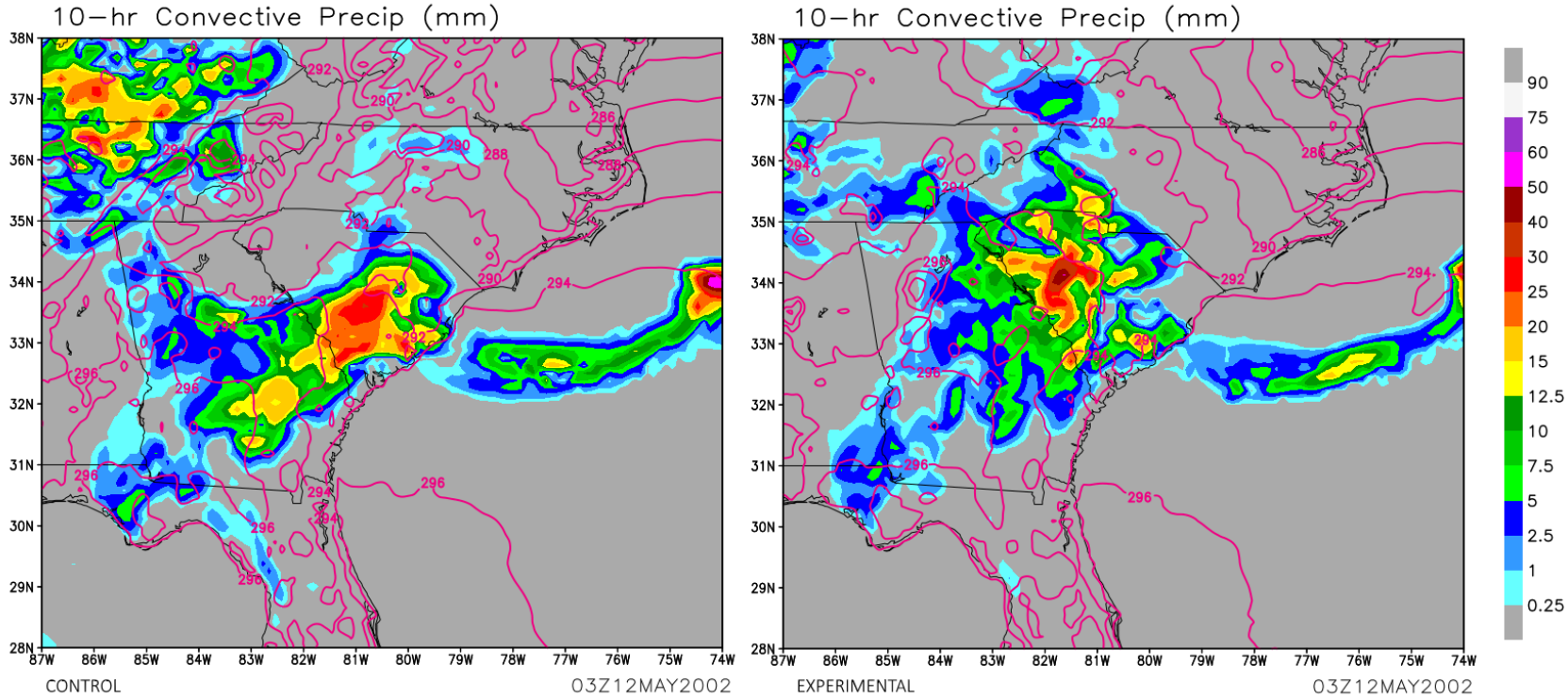

Figure 3.8. The 10-hr accumulated convective precipitation valid at 0300 UTC 12 May 2002 with overlain 2-m potential temperature.

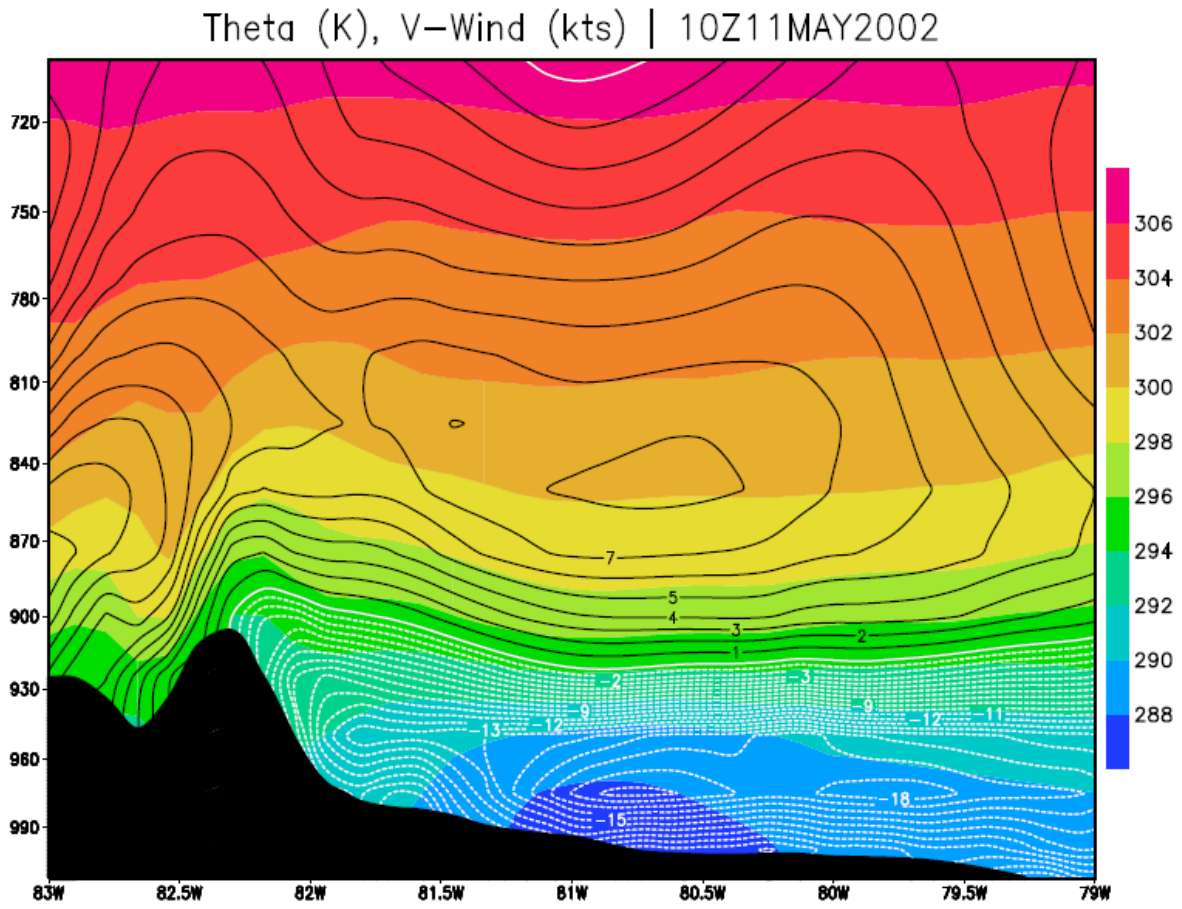

Figure 3.9. A cross section of theta (shaded, K) and the v-component of wind into (black) and out of (white, dashed) the page at 1000 UTC 11 May 2002.

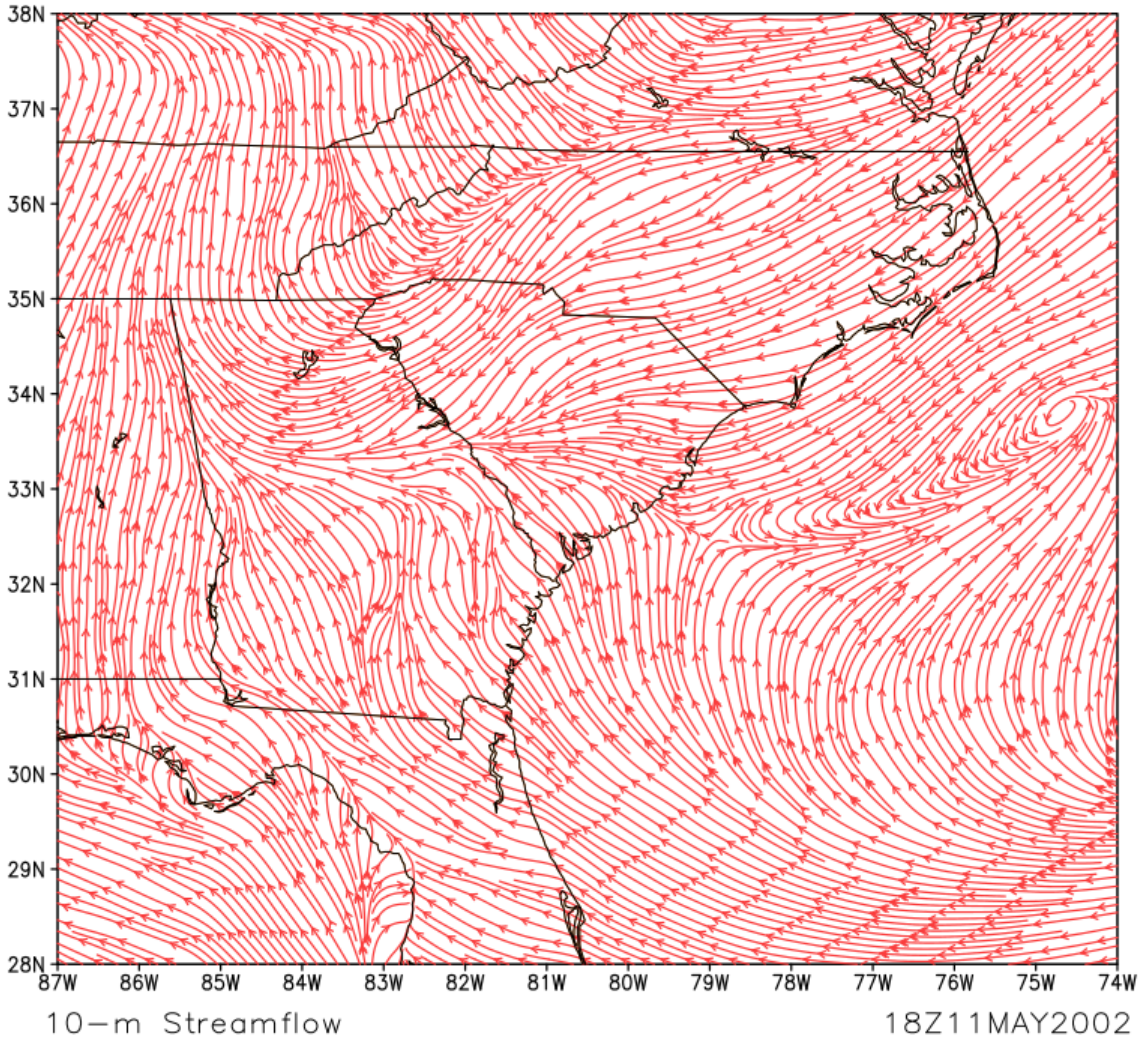

Figure 3.10. 10-m stream analysis for 1800 UTC 11 May 2002, highlighting surface convergence at the wedge front.

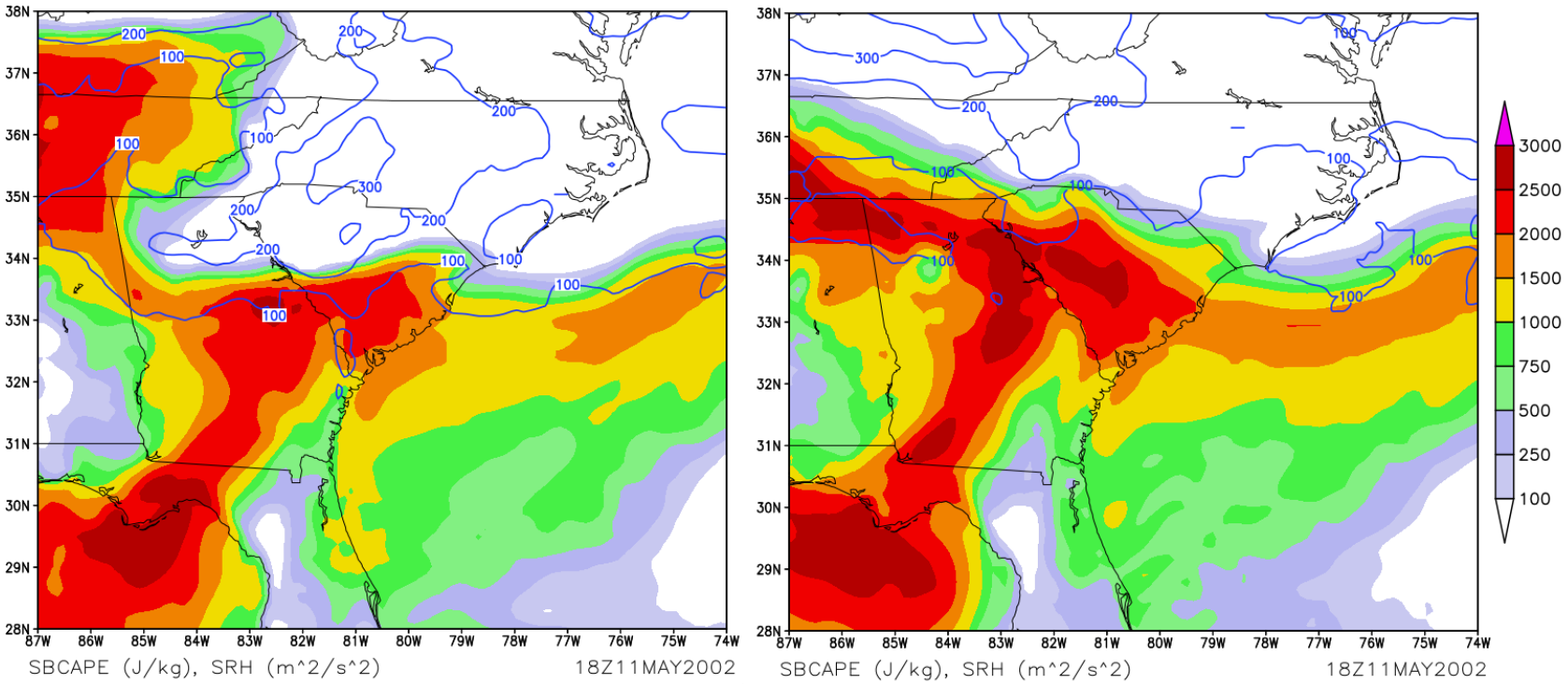

Figure 3.11. SBCAPE and 0-3 km SRH at 1800 UTC 11 May 2002 for the a) control run and b) experimental run.

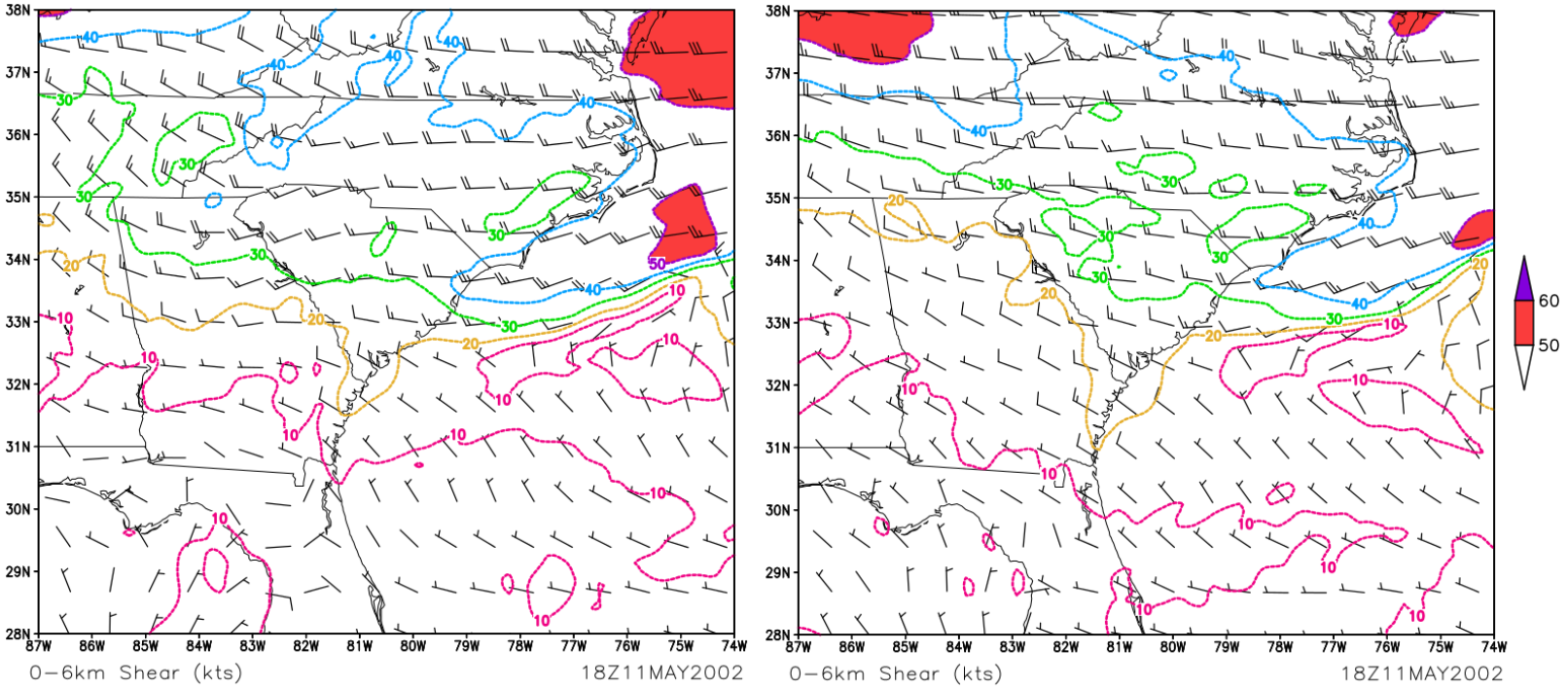

Figure 3.12. Deep-layer (0-6km) vertical shear at 1800 UTC 11 May 2002 for the a) control run and b) experimental run.

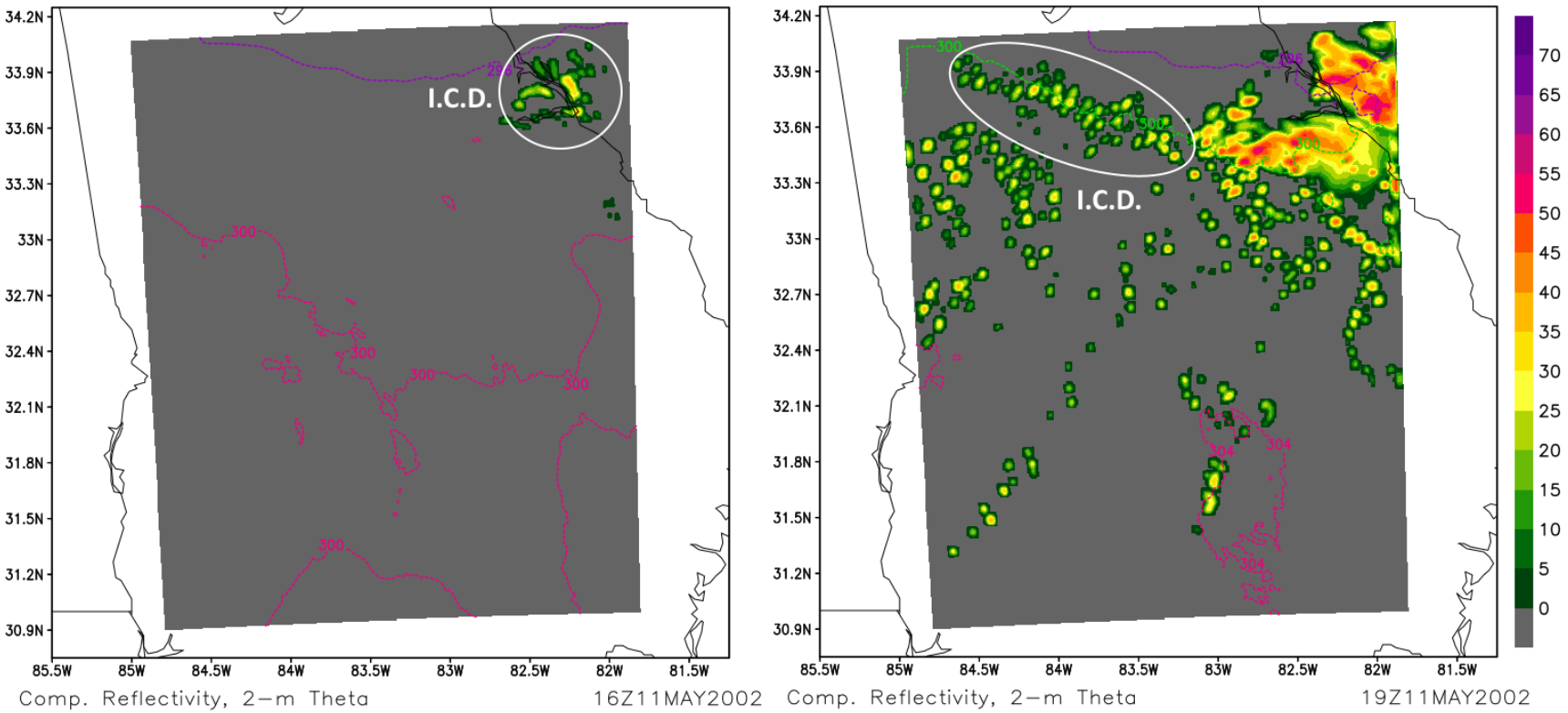

Figure 3.13. Simulated reflectivity from the CAD-CS simulation for initial convective development at a) 1600 UTC and b) 1900 UTC 11 May 2002.

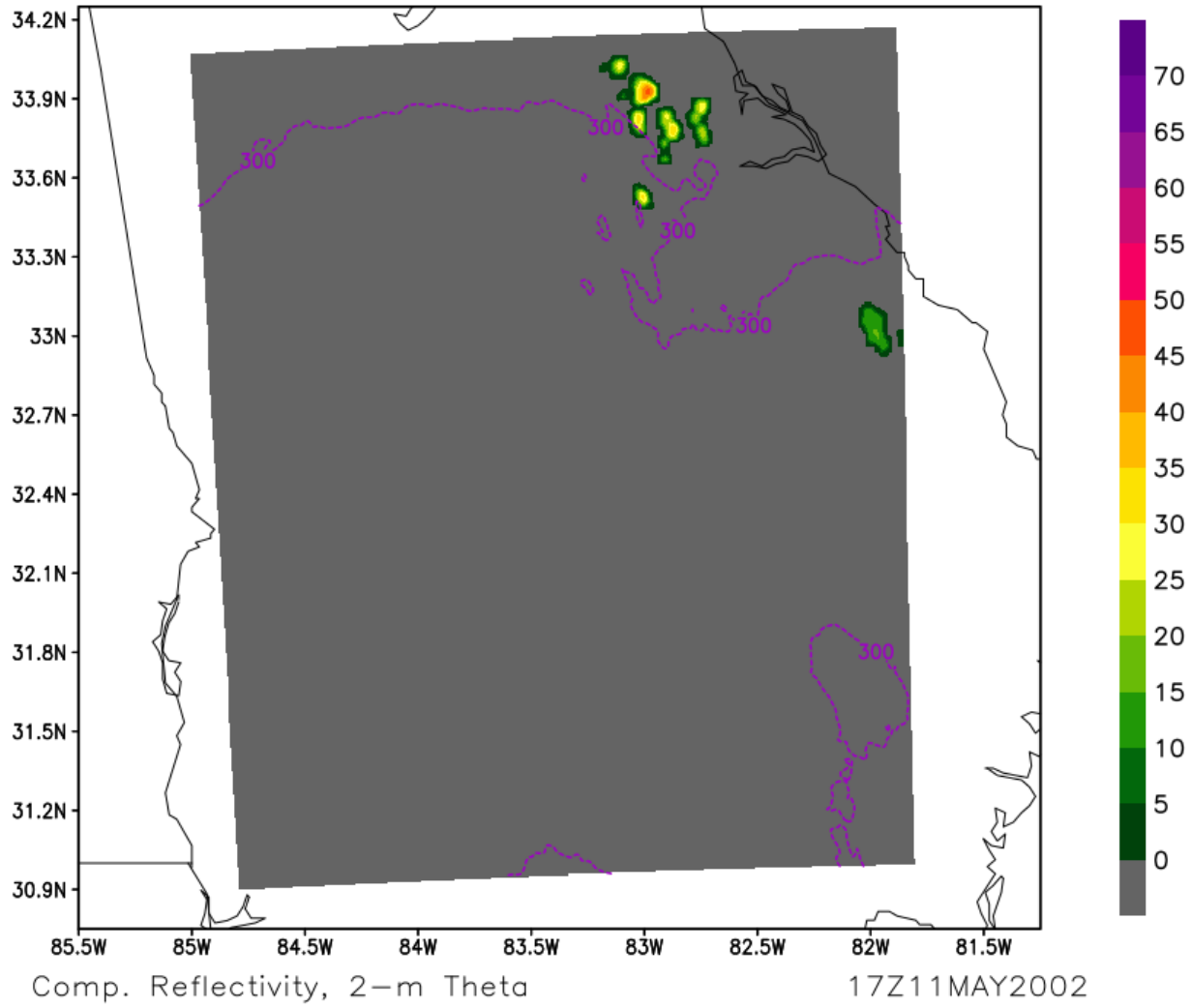

Figure 3.14. Simulated reflectivity from the NoCAD-CS simulation for initial convective development at 1700 UTC 11 May 2002.

CHAPTER 4

A CASE STUDY OF POORLY FORECAST POST-CAD EROSION PRECIPITATION[3]

[3] Rackley, J.A. and J.A. Knox. To be submitted to Weather and Forecasting

Abstract

A case of unforecast precipitation over Georgia occurring immediately after a cold air damming (CAD) event was analyzed using observations and WRF-ARW high resolution modeling. Following previous studies, a control run and modified terrain experimental run were used in order to isolate CAD's effect on the environment. Initial hypotheses linking the widespread stratiform precipitation to the CAD erosion process failed to be substantiated. Although it was confirmed that CAD did not play a direct role in the event, results pose further questions regarding the failure of high resolution model simulations to adequately resolve the precipitation.

Key words: unforecast precipitation, cold air damming, modeling

4.1 Introduction and Background

Cold air damming (CAD) is a commonly occurring phenomenon along the eastern slopes of the Appalachian Mountains. CAD occurs when a shallow, surface-based layer of relatively cold air becomes entrenched against the windward side of a mountain range [Richwien 1980]. In the southeastern U.S., CAD generally occurs when a strong surface anticyclonic system (typically 1030 hPa central pressure or higher), referred to as the "parent high" [Bailey et al. 2003], is situated to the north of the Appalachians (most favorably north of 40° N). Cross barrier flow, driven by the parent high, loses westward momentum and converges near the mountain barrier [Smith 1982]. As Coriolis forcing weakens, the flow turns towards the south and accelerates in response to the unbalanced pressure gradient force. Geostrophic adjustment occurs as increased Coriolis in the toward-mountain direction becomes balanced by the increased pressure gradient force resulting from accumulation of mass and orographic ascent along the slopes. This orographically modified geostrophic balance helps to form a low-level mountain-parallel jet that serves to maintain and extend the cold dome [Baker 1970; Richwien 1980; Bell and Bosart 1988; Xu 1990; Xu and Gao 1995]. Diabatic processes (i.e. clouds and precipitation) can also play an important, though usually secondary, role in cold air dome maintenance through evaporational cooling and solar sheltering [Forbes et al. 1987; Bell and Bosart 1988; Lee et al. 1992; Fritsch et al. 1992; Langmaid and Riordan 1998; Bailey et al. 2003].

The shallow dome of cold and stable air that becomes established along the eastern slopes of the Appalachians during a CAD event is often identified by the characteristic "U"- or "wedge"- shaped inverted ridge that appears in the sea level pressure [Baker 1970; Bell and Bosart 1988]. This "wedge" signature has led to the use of the term by operational forecasters in the region. CAD can also be observed in the near-surface temperature field, where the difference

in temperature between the damming region and coast can exceed 20°C during strong CAD events [Bell and Bosart 1988].

Even with increased forecast accuracy and further knowledge of CAD events over the past four decades, CAD remains a well-known challenge to operational forecasters in the southeastern U.S. [Baker 1970; Bell and Bosart 1988; Hartfield 1998]. The cold dome's presence has a substantial impact on the region's sensible weather, including temperature, sky cover, and precipitation. In particular, CAD can significantly affect precipitation type forecasting during the cold season [e.g. Forbes et al. 1987; Keeter et al. 1995] and has been known to trigger convection along the cold dome periphery, or "wedge front," during the warm season [Bosart et al. 1972; Ballentine 1980; Garreaud and Wallace 1997; Baker 2009]. While modern mesoscale numerical models have significantly improved forecasting capabilities of CAD events in the past two decades, today's numerical models still have a tendency to underestimate CAD impacts and duration, often eroding the cold air domes prematurely [Forbes et al 1987; Stauffer and Warner 1987; Bell and Bosart 1988; Keeter et al. 1995; Kramer 1997; Stanton 2003; Lackmann and Stanton 2004; Green 2006]. Even modern rapidly updating, high-resolution mesoscale models such as the High Resolution Rapid Refresh show a tendency to underestimate effects of solar sheltering and erode the cold air dome too quickly [Grumm 2015].

The mechanisms and processes involved in CAD erosion were first studied in depth by Stanton [2003]. Through examination of observational data, five mechanisms primarily responsible for CAD erosion were determined: (i.) differential thermal advection, (ii.) solar heating, (iii.) lower-tropospheric divergence, (iv.) shear-induced mixing (entrainment) across the top of the cold dome, and (v.) the advance of the coastal/warm front that often marks the eastern/southern terminus of the CAD cold dome. Stanton [2003] identified four distinct synoptic

patterns that are characteristically associated with erosion of the cold dome: (i.) coastal cyclone, (ii.) cold-frontal passage, (iii.) residual cold pool, and (iv.) northwestern low. Green [2006] expanded this research, focusing on specific precipitation patterns associated with different erosion scenarios.

This study will examine the synoptic and mesoscale environment surrounding the evolution of a coastal low erosion event that occurred prior to a poorly forecast rainfall across north Georgia on 17 October 2009. The utilization of multiple observations and high-resolution modeling will yield a better understanding of how the cold dome eroded and what interactions a residual cold pool continued to have on the damming region. It is hypothesized that poorly forecast precipitation formed in an area of increased surface convergence, shear, and lift due to the remnants of a cold air dome interacting with the synoptic environment. Analysis of model simulations of real-case scenarios will help to cast light on poor operational numerical weather prediction performance leading up to the event. Likely, forecast models prematurely eroded the cold air dome and associated cloud cover, neglecting to properly forecast interactions between the residual cold pool and the synoptic environment. Simulations using the modern WRF-ARW model at high resolutions may also produce better results than were seen in operational model output from 2009, to some extent signifying model forecasting capabilities. Analysis of this case may also provide a better overall understanding of interactions between CAD erosion and the synoptic environment.

4.2 Data, Methods, and Experimental Design

Initial model simulations (Fig. 4.1) were performed to analyze the impact of the CAD dome on the lower-tropospheric environment. Version 3.5 of the WRF-ARW [Skamarock 2005] model was employed using 12-km horizontal grid spacing, 45 vertical levels, and the Kain-

Fritsch convective parameterization scheme to account for sub-gridscale convective processes [Kain and Fritsch 1993]. Additionally, the WSM 6-class microphysics scheme [Hong and Lim 2006], RUC land-surface model [Smirnova et al. 1997, 2000], and YSU boundary layer scheme [Skamarock 2005] were used. Gridded NARR [Mesinger et al. 2006] data were used to initialize the model and serve as 3-hourly boundary conditions throughout the event. The data spanned 156 hours from 0000 UTC 12 October 2009 to 1200 UTC 18 October 2009. Output from the simulations was generated in hourly increments for analysis.

Following previous methodologies [e.g. Baker 2009], two simulations were run in order to isolate CAD's influence on the environment. Following the Baker [2009] methodology, a simulation of the event and CAD cold air dome served as the control run. For comparison, a second simulation using the same initial conditions and model parameters, but with terrain flattened to remove the Appalachian Mountains, served as the experimental run. This was accomplished by editing the model terrain height and setting values to zero. Removing the Appalachians effectively eliminated the barrier needed for CAD to form, thus allowing the simulation to run without the influence of a cold dome. In order to account for atmospheric variables in the "underground" areas exposed by the removal of the mountains, the NARR dataset used for model initialization provided interpolated meteorological variables on isobaric levels down to 1000 hPa using the lapse rate for a standard atmosphere. Winds and moisture are held constant below ground within the NARR dataset.

Initializing the experimental run prior to CAD setup allowed for a realistic atmospheric evolution throughout the entire event even without the Appalachians in place. Likewise, the domain used in these simulations was large enough to resolve both parent highs as they tracked to the east, while also keeping the primary study area (the southeastern U.S. and, more

specifically, northeast Georgia) away from domain boundary influences. An evaluation of the control run was performed to determine if the model correctly reproduced a realistic cold air dome. Finally, the lower-tropospheric environments of both the control and modified-terrain simulations were analyzed and compared to evaluate and isolate the effect of the cold dome in the model.

Additional nested domains were run within the 12-km parent domains at higher spatial and temporal resolutions to allow for analysis at the convective scale and to better resolve mesoscale features. Two nested domains were included within each outer domain with 4-km and 1.3-km horizontal grid spacings to maintain a 3:1 grid spacing ratio between domains. These were run with 1-way nesting (no inter-domain feedback) and used explicit convection instead of a convective parameterization scheme [Molinari and Dudek 1992]. The inner domains were initialized "on-the-fly" using initial conditions from the outermost domain at the start of the 96th and 126th forecast hour (valid at 1200 UTC 15 and 1800 UTC 16 May 2009). Output from these domains was generated at 30 minute and 5 minute intervals, respectively. Domain 2 (4-km grid spacing) was centered over the Southeast and included the damming region and WFC study area. Domain 3, the innermost nest (1.3-km grid spacing), was centered over the core of the damming region (Fig. 4.1). The convective scale control run (hereafter referred to as "CAD-CS") retained topography, while the convective scale experimental run (hereafter referred to as "NoCAD-CS") had the mountains removed to simulate the atmosphere without the presence of CAD. The convective scale environment and characteristics of convective development, evolution, and intensity were analyzed and compared for these two simulations to isolate the effect of the cold air dome at convective scales.

An analysis of this CAD event's development and evolution will be conducted using archived surface observations and charts, upper air soundings, GOES satellite imagery, and WRF-ARW simulations to determine the role of CAD in the development of poorly forecast precipitation and to gain a better understanding of the erosion processes in this particular event.

4.3 Case Study of CAD Erosion 12-17 October 2009

A series of closely consecutive CAD events occurring during the week of 12 October 2009 was chosen for study because of an area of poorly forecast precipitation that developed across parts of North Carolina, South Carolina and northern Georgia after the CAD erosion process. The entire study consists of an initial CAD event, quick erosion through a frontal passage, a second CAD setup, and ultimately the erosion of the second cold dome.

The hybrid CAD event was identified by the Bailey Algorithm [Bailey et al. 2003] at 1200 UTC 12 October 2009 as a 1031 hPa parent high over New York ridged down the Appalachians. By 0600 UTC the following day, the event met its demise and the parent high pushed offshore into the Atlantic as a coastal low off the coast of North Carolina and a cold front pushing through the damming region helped to erode the cold dome. Although previously thought to be an elongated erosion process, the Bailey Algorithm initialized a new CAD event, this time classified as a classical-diabatically enhanced event, at 0900 UTC 14 October as a large, elongated 1033 hPa high shifted northwest of the Great Lakes. By 1200 UTC 14 October, a wedge front could be analyzed across Georgia. The cold dome continued to strengthen into 15 October as another low began to develop off the Georgia/South Carolina coast. By 1900 UTC, cyclonic flow about the coastal low had disrupted northeasterly flow across North Carolina, South Carolina, and Georgia, ending the CAD even by the Bailey Algorithm. However, as the low tracked to the northeast, the damming region once again fell into northeasterly flow by 0900

UTC 16 October. This flow pattern was eventually supported by the large-scale synoptic regime as an area of high pressure developed over the central US. Dense cloud cover and the remnants of a surface boundary remained over the damming region at this time, unlike what was indicated as traditional coastal low erosion by Stanton [2003]. Synoptic interaction with the residual cold pool and northeasterly flow is hypothesized to be responsible for poorly forecast precipitation in the North Carolina, South Carolina, and northeast Georgia region beginning around 1000 UTC on 17 October 2009 (Fig. 4.2). Poor numerical weather forecasts of this precipitation event surprised forecasters at the National Weather Service Weather Forecast Office in Peachtree City, GA and forced them to update the forecast grids with precipitation probabilities after the poorly forecast rainfall was observed for multiple hours:

"AREA FORECAST DISCUSSION...UPDATED
NATIONAL WEATHER SERVICE PEACHTREE CITY GA
745 AM EDT SAT OCT 17 2009
.UPDATE...
AHN HAS BEEN REPORTING -RA FOR THE PAST FEW HOURS AND RADAR SHOWING SPRINKLES IN NE HALL COUNTY. HAVE DECIDED TO GO AHEAD AND ADD AREA OF SPRINKLES THROUGH 00Z TO ENCOMPASS MOST AREAS NORTH OF LGC-OPN-AGC THROUGH 00Z. NO OTHER CHANGES BEING MADE AT THIS TIME."

An analysis of this CAD event's development and evolution will be conducted using archived surface observations and charts, upper air soundings, GOES satellite imagery, and WRF-ARW simulations to determine the role of CAD in the development of poorly forecast precipitation and to gain a better understanding of the erosion processes in this particular event.

4.4 Results

The 12-km control run was initially evaluated for realistic representation and evolution of the cold air dome. Simulated 2-m potential temperature, 2-m dewpoint, and 10-m winds (Fig. 4.3) show the evolution of the cold dome throughout the event. Other model fields such as 500 hPa heights, 200 hPa wind speeds, and sea level pressure (not shown) were analyzed and compared to real event analysis. The control run did an excellent job at simulating the CAD event, though it is noted that the model did not deepen the second coastal low enough.

Before comparative analyses could be conducted, the modified-terrain run was analyzed to determine if CAD development was successfully inhibited. To accomplish this, the 2-m potential temperature fields for the control and modified-terrain runs were compared and analyzed for signs of a cold dome for the duration of the real event. The modified-terrain run exhibited no sign of a cold air dome or cold air advection within the damming region. Instead, much of the region saw offshore, easterly flow or northwesterly flow as the cold front approached the Southeast.

While previous studies have successfully used an experimental WRF-ARW run with terrain removed, in this case, the experimental run did not produce favorable results. Analysis of the pressure field shows large fluctuations and non-natural evolution of the system. Banding patterns in the simulated reflectivity throughout the event (e.g. Fig. 4.4) also indicate the likelihood of improper feedbacks and unrealistic gravity waves within the model. This may be due to the longer nature of this case study (i.e. errors tend to grow) or a result of the more complex synoptic and mesoscale setup of this event. The model did manage to capture both coastal lows, however, though they were not deep enough. Without use of the experimental runs, isolation of CAD or terrain effects on the event was not possible.

After rejecting the validity of the experimental runs, full attention was turned to the control runs. The 12-km control run was analyzed for the poorly forecast precipitation event that occurred on 17 October 2009. Unfortunately, the model was not able to reproduce this precipitation (Fig. 4.5). The convective scale control simulations were also analyzed for evidence of the poorly forecast precipitation on 17 October. Surprisingly, neither the 4-km nor the 1.3-km runs sufficiently resolved this feature. This may highlight the need for higher vertical resolutions to better forecast such an event.

Even though the model was not able to specifically resolve the poorly forecast precipitation, further attempts were made to link the CAD erosion process or lingering cold pool with conditions conducive to forming an area of stratiform precipitation. An hour-by-hour analysis with vertical cross sections of theta and v-wind revealed that the remaining cold pool had fully eroded by 0300 UTC 17 October, prior to the precipitation event. Low-level cold air advection from the northwest on 17 October removed any chance for a lingering cold pool in the damming region. Without a cold pool or other lingering effects of CAD in place immediately before and during the unforecast precipitation, CAD's role in the event becomes increasingly doubtful. Further synoptic analysis may reveal a connection between the precipitation and a shortwave that pushed through a deepening trough over the eastern U.S. on 17 October (Fig. 4.6).

4.5 Conclusions and Future Work

While the poorly forecast precipitation over north Georgia was not specifically related to CAD, this event is a fascinating example of modern mesoscale models inability to properly simulate a fairly large area of stratiform rain. Even running WRF-ARW at higher resolutions than today's operational mesoscale models could not properly forecast the precipitation. An investigation into

why these models failed even at high horizontal resolutions could lead to future enhancements to mesoscale models or a better understanding of the behavior of model physics and boundary layer schemes in similar cases. Future work may involve model sensitivity testing with the WRF-ARW to determine why the model forecast failed and which model physics and other parameters, if any, improve verification for this setup.

4.6 References

Bailey, C. M., G. Hartfield, G. M. Lackmann, K. Keeter, and S. Sharp, 2003: An objective climatology, classification scheme, and assessment of sensible weather impacts for Appalachian cold-air damming. *Wea. Forecasting*, **18**, 641-661.

Baker, D. G., 1970: A study of high pressure ridges to the east of the Appalachian Mountains. Ph.D. thesis, Massachusetts Institute of Technology, 127 pp.

Baker, A. K., 2009: Convection and Appalachian Cold-Air Damming. Master's thesis, North Carolina State University, 188 pp.

Ballentine, R. J., 1980: A numerical investigation of New England coastal frontogenesis. *Mon. Wea. Rev.*, **108**, 1479-1497.

Bell, G. D., and L. F. Bosart, 1988: Appalachian cold-air damming. *Mon. Wea. Rev.*, **116**,137-161.

Forbes, G. S., R. A. Anthes, and D. W. Thomson, 1987: Synoptic and mesoscale aspects of an Appalachian ice storm associated with cold-air damming. *Mon. Wea. Rev.,* **115**, 564-591.

Fritsch, J. M., J. Kapolka, and P. A. Hirschberg, 1992: The effects of subcloud-layer diabatic processes on cold air damming. *J. Atmos. Sci.*, **49**, 49-70.

Garreaud, R. D., and J. M. Wallace, 1998: Summertime incursions of midlatitude air into subtropical and tropical South America. *Mon. Wea. Rev*., **126**, 2713-2733.

Green, T. A., Jr., 2006: Cold air damming erosion and associated precipitation in the Southeastern United States. Master's thesis, North Carolina State University, 248 pp.

Grumm R. H., 2015: Mid-Atlantic Ice Storm 4 March 2015. Accessed 22 July 2015. [Available online at http:// cms.met.psu.edu/sref/severe/2015/03Mar2015.pdf]

Hartfield, G., 1998: Cold air damming: An introduction. National Weather Service Eastern Region Training and Evaluation Module 4. [Available online at http://www.erh.noaa.gov/er/hq/ssd/erps/tem/tem4.pdf]

Hong, S.-Y., and J.-O. Lim, 2006: The WRF single-moment 6-class microphysics scheme (WSM6). *J. Korean Meteor. Soc.*, **42**, 129-151.

Kain, J. S., and J. M. Fritsch, 1993: Convective parameterization for mesoscale models: The Kain-Fritsch scheme. *The Representation of Cumulus Convection in Numerical Models, Meteor. Monogr.*, No. 46, Amer. Meteor. Soc., 165-170.

Keeter, K. K., S. Businger, L. G. Lee, and J. S. Waldstreicher, 1995: Winter weather forecasting throughout the eastern United States. Part III: The effects of topography and the variability of winter weather in the Carolinas and Virginia. *Wea. Forecasting*, **10**, 42-60.

Kramer, D., 1997: Real-time mesoscale model evaluation during Appalachian cold air damming. Master's thesis, North Carolina State University, 139 pp.

Lackmann, G. M., and W. M. Stanton, 2004: Cold-air damming erosion: Physical mechanisms, synoptic settings, and model representation. Preprints, *20th Conf. on Weather Analysis and Forecasting*, Seattle, WA, Amer. Meteor. Soc., CD-ROM, 18.6.

Langmaid, A. H., and A. J. Riordan, 1998: Surface mesoscale processes during the 1994 Palm Sunday tornado outbreak. *Mon. Wea. Rev.*, **126**, 2117-2132.

Lee, L. G., K. K. Keeter, S. Businger, and A. J. Riordan, 1992: Geography-related forecasting problems in the southeastern United States and a joint North Carolina State University-National Weather Service effort to improve the understanding and prediction of these events. Preprints, *Symp. on Weather Analysis and Forecasting*, Atlanta, GA, Amer. Meteor. Soc., 166-172.

Mesinger, F., G. DiMego, E. Kalnay, K. Mitchell, P. C. Shafran, W. Ebisuzaki, D. Jović, J. Woollen, E. Rogers, E. H. Berbery, M. B. Ek, Yun Fan, R. Grumbine, W. Higgins, H. Li, Y. Lin, G. Manikin, D. Parrish, W. Shi, 2006: North American Regional Reanalysis. *Bull. Amer. Meteor. Soc*., **87**, 343-360.

Molinari, J. and M. Dudek, 1992: Cumulus parameterization in mesoscale numerical models: A critical review. *Mon. Wea. Rev.,* **120**, 326-344.

Richwien, B. A., 1980: The damming effect of the southern Appalachians. *Natl. Wea. Dig.*, **5** (1), 2-12.

Skamarock, W. C., J. B. Klemp, J. Dudhia, D. O. Gill, D. M. Barker, W. Wang, and J. G. Powers, 2005: A description of the Advanced Research WRF version 2. NCAR Tech. Note NCAR/TN-468+STR, 88 pp.

Smirnova, T.G., J.M. Brown, and S.G. Benjamin, 1997: Performance of different soil model configurations in simulating ground surface temperature and surface fluxes. *Mon. Wea. Rev.,* **125**, 1870-1884.

Smirnova, T.G., J.M. Brown, S.G. Benjamin, and D. Kim, 2000: Parameterization of cold season processes in the MAPS land-surface scheme. *J. Geoph. Res*, **105** (D3), 4077-4086.

Smith, R. B., 1982: Synoptic observations and the theory of orographically disturbed wind and pressure. *J. Atmos. Sci.*, **39**, 60–70.

Stanton, W., 2003: An analysis of the physical processes and model representation of cold air damming erosion. Master's thesis, North Carolina State University, 207 pp.

Stauffer, D. R., and T. T. Warner, 1987: A numerical study of Appalachian cold-air damming and coastal frontogenesis. *Mon. Wea. Rev.,* **115**, 799-821.

Xu, Q., 1990: A theoretical study of cold air damming. *J. Atmos. Sci.*, **47**, 2969–2985.

_____, and S. Gao, 1995: An analytic model of cold air damming and its applications. J. Atmos. Sci., 52, 353-366.

_____, _____, and B. H. Fiedler, 1996: A theoretical study of cold air damming with upstream cold air inflow. J. Atmos. Sci., 53, 312-326.

4.7 Figures

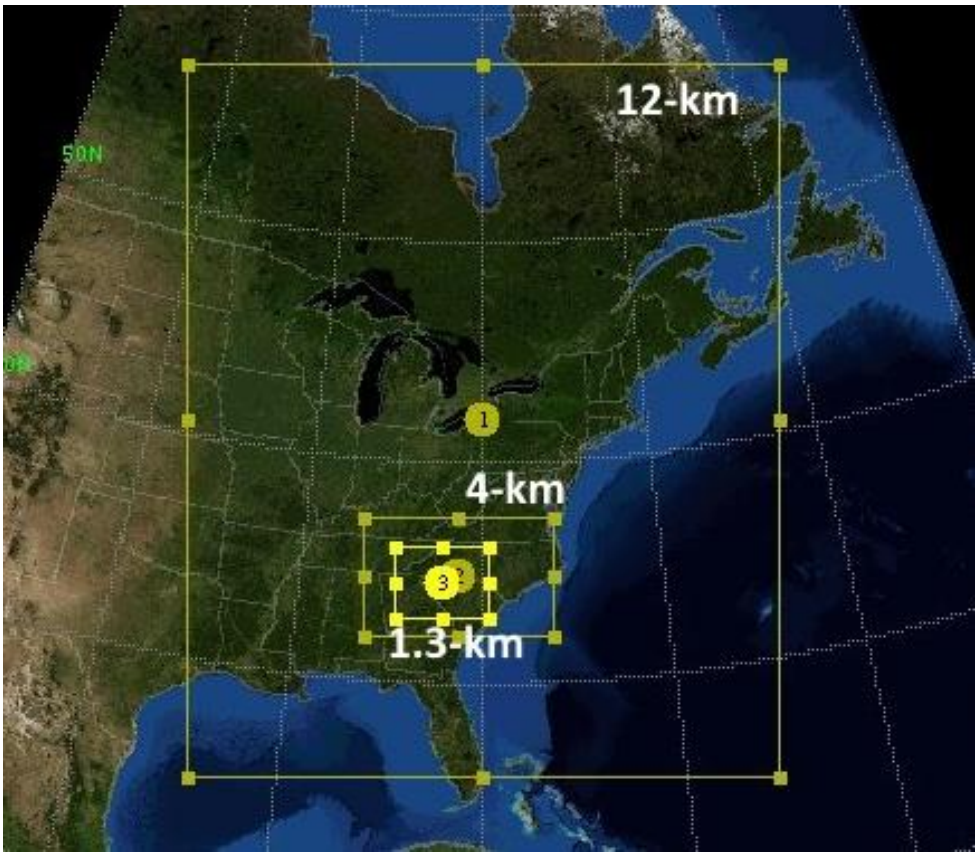

Figure 4.1. A map of model domains showing the large parent domain used for 12-km grid spacing simulations and the inner nests, d2, and d3, run at 4-km and 1.3-km grid spacings.

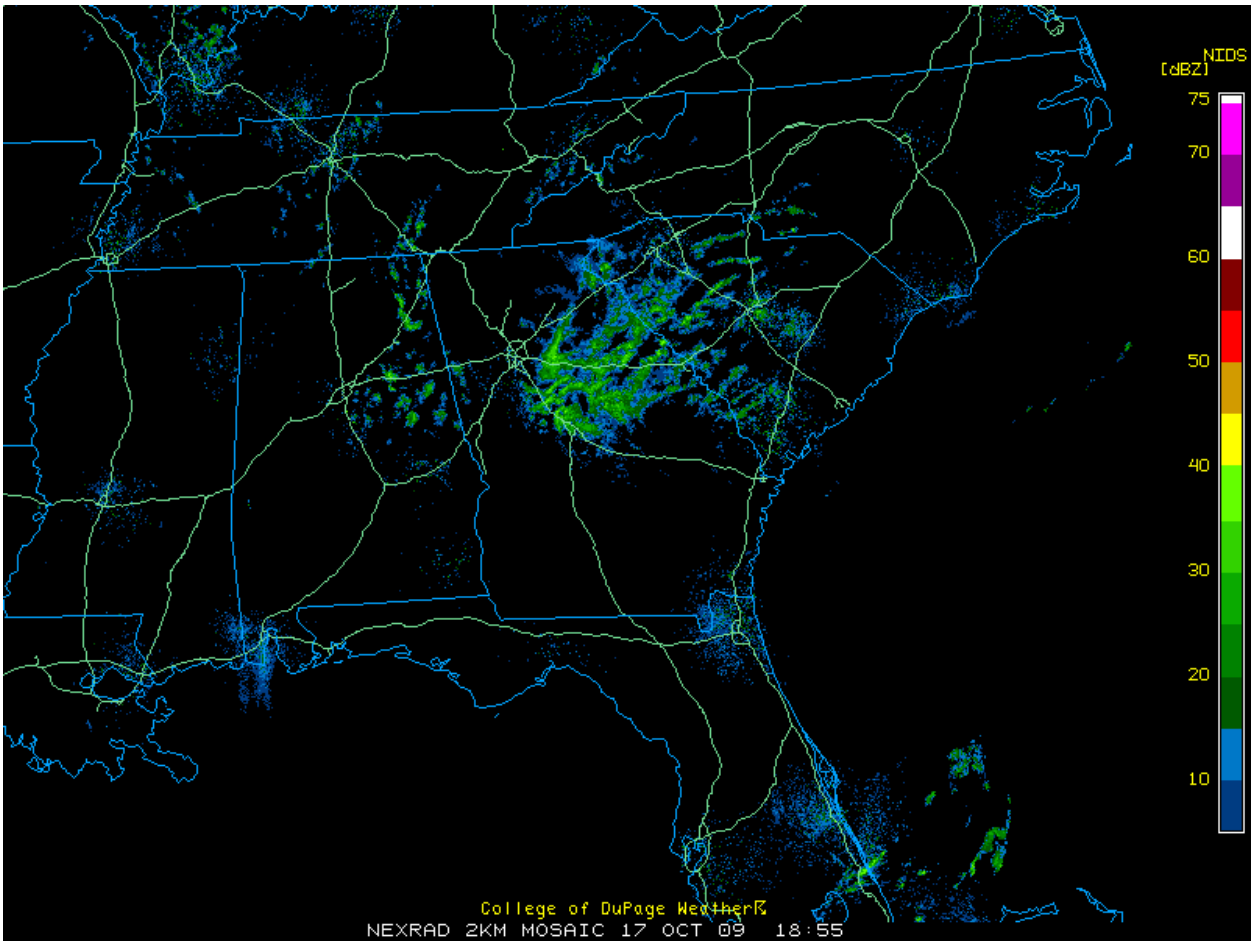

Figure 4.2. A regional radar mosaic for the Southeast showing an area of stratiform rain across northeast Georgia at 1855 UTC 17 October 2009.

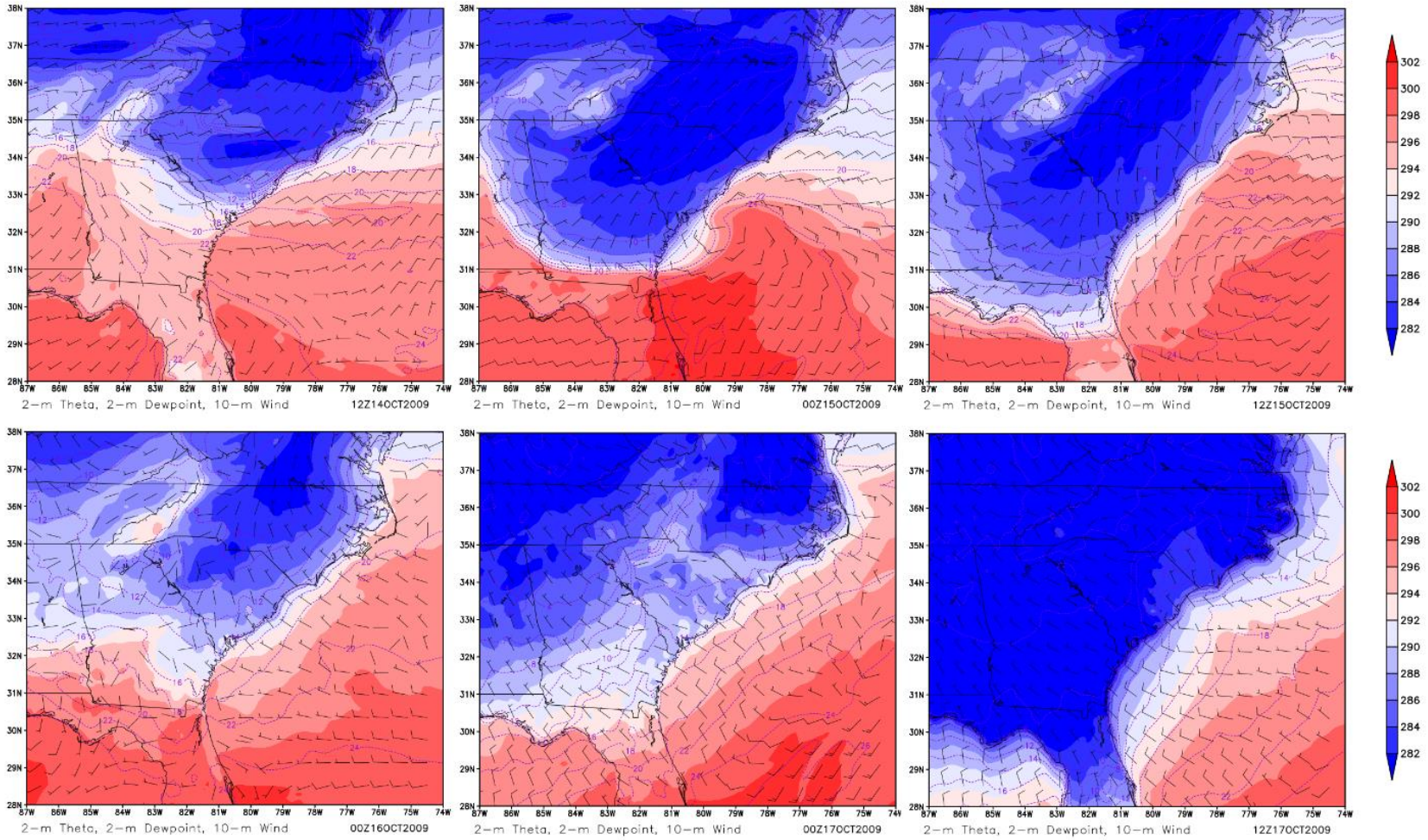

Figure 4.3. Simulated 2-m potential temperature (shaded, K), 2-m dewpoint (dashed, °C), and 10-m winds (barbs, knts) for a) 1200 UTC 14 October, b) 0000 UTC 15 October, c) 1200 UTC 15 October, d) 0000 UTC 16 October, e) 0000 UTC 17 October, and f) 1200 UTC 17 October 2009.

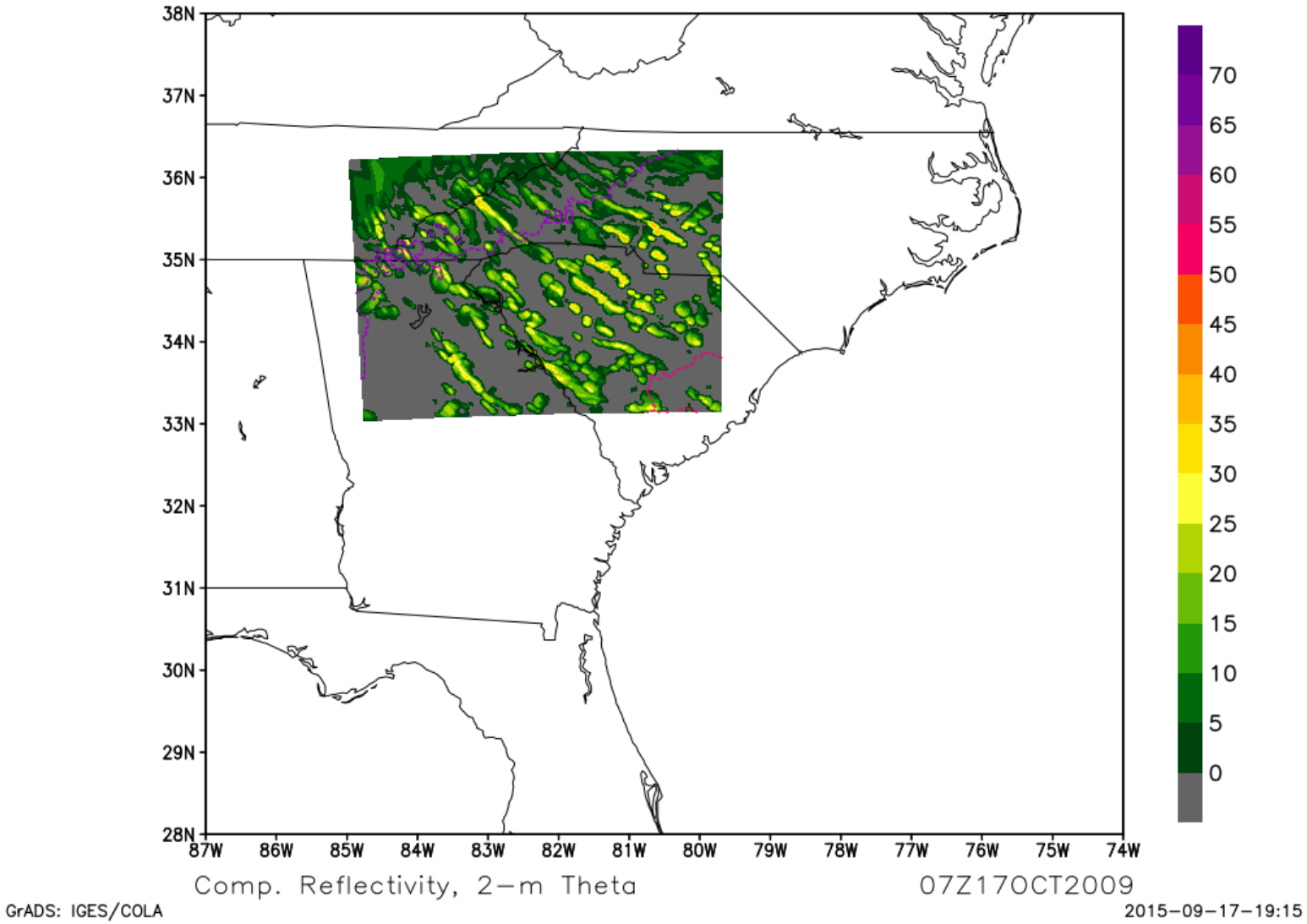

Figure 4.4. The 1.3-km No-CAD domain for 700 UTC 17 October 2009 showing bands of precipitation.

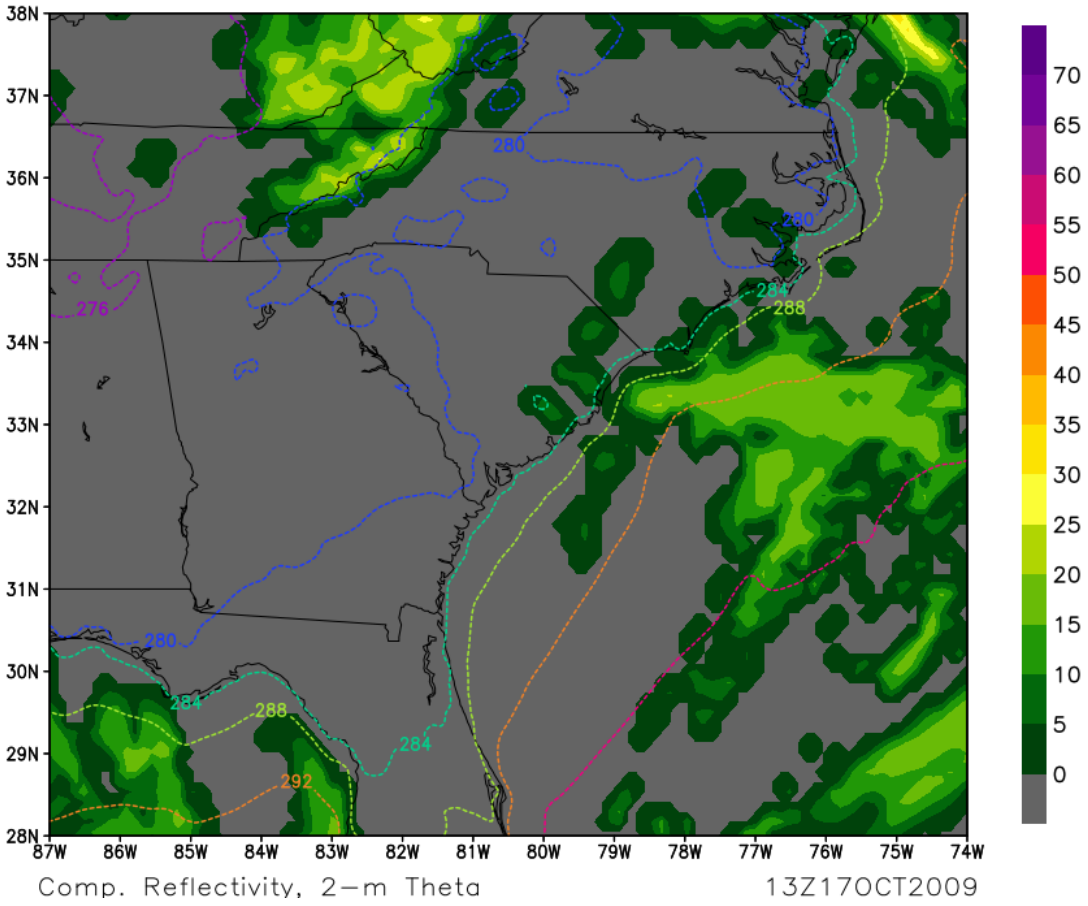

Figure 4.5. Simulated composite reflectivity for the 12-km control run at 1300 UTC 17 October 2009 showed no precipitation in the area that experience unforecast rain.

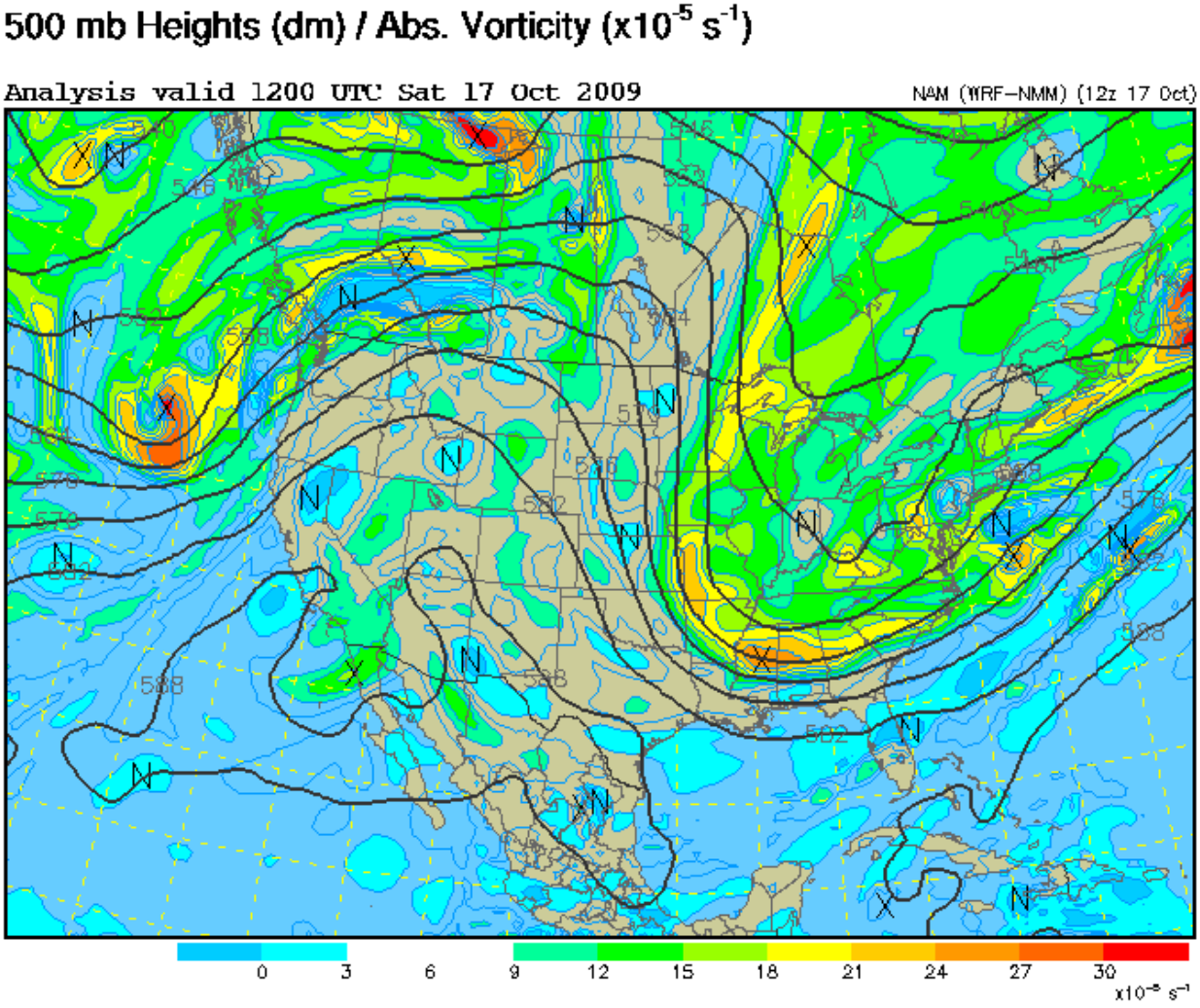

Figure 4.6. 500 hPa heights and absolute vorticity for 1200 UTC 17 October 2009.

CHAPTER 5

CONCLUSIONS

This thesis has addressed the following questions. First, will results of a longer term CAD climatology differ significantly from previous climatologies, and can the previously unstudied frequency and spatial pattern of CAD impacts in the southern extent of the damming region be determined? Second, can the effects of the CAD cold dome on convection, specifically in a high-instability, low-shear environment, be clarified and quantified? And finally, what role did CAD play in an event of unforecast precipitation over north Georgia?

Chapter 2 of this thesis objectively classifies cold air damming along the southern Appalachians and maps its spatial extent within the southernmost damming region (i.e. SC, GA, AL, and FL) for a 30-yr period. While climatologies of cold air damming have been constructed in the past, this study is the first to both objectively classify events and do so over a long period. In addition, analysis of the spatial extent of the cold dome across the southernmost damming region has not been performed previously. The purposes of this research are to assess the application of the Bailey et al. [2003] objective detection and classification schemes to longer time periods and to assess the frequency and extent to which the cold dome pushes into its southern reaches.

On average, CAD was detected by the algorithm on more than 50 days, or more than 7 weeks, per year. Fifty days per year is non-trivial for a phenomenon with the potential to significantly impact forecasts of sensible weather. As found in previous studies, detected CAD is much more frequent during the cold season than in the warm season. This can increase the

potential for difficult winter weather forecasts with the threat of dangerous icy precipitation. However, the results also demonstrate that strong CAD events can occur during the spring and summer months when the cold dome periphery is likely to trigger or enhance convection.

Maps of cold dome spatial extent reveal the surprisingly high frequency with which the cold dome pushes into portions of Florida and Alabama. Forecasters with CAD experience know that CAD can push as far west as Birmingham or as far south as Tallahassee; this study provides a quantitative measure of that assessment. The maps also indicate two potential trajectories once the dome pushes into central Georgia. A west-northwesterly path turns towards Anniston, Alabama, and north of the Birmingham, Alabama area. Its counterpart, the southwesterly trajectory, continues pushing into southwest Georgia and Florida. Cold-season events seemed to favor the west-northwesterly track, as did the stronger CAD categories. These findings may provide forecasters with a quick estimate of where and how far the cold dome will push given the synoptic conditions.

Work from chapters 3 and 4 utilized the WRF-ARW to simulate events with CAD and with the CAD cold dome removed. In the first modeling study, simulations at 12-km, 4-km, and 1.3-km grid-spacings were run and analyzed to isolate the influence of the cold dome and wedge front on explicit convective character and intensity. While convection within the two runs developed in roughly the same location across north and central Georgia, the experimental run and NoCAD-CS runs exhibited convection farther to the north. Convection in the CAD-CS model tended to better organize into multicellular clusters, while convection in the NoCAD-CS model tended to remain discrete and single-cellular. Individual storm updraft helicity was also greatly enhanced within the CAD-CS run versus the No-CAD run, and storms tended to have greater longevity on average with a cold dome present. These findings emphasize that heightened

levels of low-level vertical shear with the cold dome present were able to overcome lower instability values when instability values exterior the dome are moderate to high. Increased low-level shear along the wedge front allowed storms to develop in a multicellular mode, increasing their longevity and intensity as measured with updraft helicity. These more intense storms with greater rotation have a higher probability of becoming severe. Thus, forecasters should be aware of the increased possibility for severe convection when CAD events form in low shear, high CAPE environments.

Due to modeling issues and issues with the case itself, the final modeling study did not produce expected results. First, the poorly forecast precipitation over north Georgia was found to not be related to CAD, as previously thought. However, this event is a fascinating example of modern mesoscale models inability to properly simulate a fairly large area of stratiform rain. Even running WRF-ARW at higher resolutions than today's operational mesoscale models could not properly forecast the precipitation. An investigation into why these models failed even at high horizontal resolutions could lead to future enhancements to mesoscale models or a better understanding of the behavior of model physics and boundary layer schemes in similar cases. Future work may involve model sensitivity testing with the WRF-ARW to determine why the model forecast failed and which model physics and other parameters, if any, improve verification for this setup.

REFERENCES

Bailey, C. M., G. Hartfield, G. M. Lackmann, K. Keeter, and S. Sharp, 2003: An objective climatology, classification scheme, and assessment of sensible weather impacts for Appalachian cold-air damming. *Wea. Forecasting*, **18**, 641-661.

Baker, D. G., 1970: A study of high pressure ridges to the east of the Appalachian Mountains. Ph.D. thesis, Massachusetts Institute of Technology, 127 pp.

Baker, A. K., 2009: Convection and Appalachian Cold-Air Damming. Master's thesis, North Carolina State University, 188 pp.

_____, and G. M. Lackmann, 2009: Convection and Appalachian cold-air damming. Extended Abstract, 23rd Conf. on Weather Analysis and Forecasting/19th Conference on Numerical Weather Prediction, Omaha, NE, Amer. Meteor. Soc., online, 7B.4.

Ballentine, R. J., 1980: A numerical investigation of New England coastal frontogenesis. *Mon. Wea. Rev.*, **108**, 1479-1497.

Bell, G. D., and L. F. Bosart, 1988: Appalachian cold-air damming. *Mon. Wea. Rev.*, **116**,137-161.

Bosart, L. F., C. J. Vaudo, and J. H. Helsdon Jr., 1972: Coastal frontogenesis. *J. Appl. Meteor*., **11**, 1236-1258.

Brady, R. H., and E. J. Szoke, 1989: Case study of a nonmesocyclone tornado development in northeast Colorado: Similarities to waterspout formation. *Mon. Wea. Rev.*, **117**, 843-856.

Businger, S., W. H. Bauman, and G. F. Watson, 1991: The development of the piedmont front and associated outbreak of severe weather on 13 March 1986. *Mon. Wea. Rev.*, **119**, 2224-2251.

Changnon, S. A., T. R. Karl, 2003: Temporal and Spatial Variations of Freezing Rain in the Contiguous United States: 1948–2000. *J. Appl. Meteor*., 42, 1302–1315.

Chien, F. C., and Y. H. Kuo, 2006: Topographic effects on a wintertime cold front in Taiwan. *Mon. Wea. Rev.*, **124**, 3297-3316.

Chu, R., 1994: Algorithms for the Automated Surface Observing System (ASOS). ISL Office Note 94-4, NWS/OSD, 106 pp.

Dunn, L., 1987: Cold air damming by the Front Range of the Colorado Rockies and its relationship to locally heavy snows. *Wea. Forecasting*, **2**, 177-189.

Forbes, G. S., R. A. Anthes, and D. W. Thomson, 1987: Synoptic and mesoscale aspects of an Appalachian ice storm associated with cold-air damming. *Mon. Wea. Rev.*, **115**, 564-591.

Fritsch, J. M., J. Kapolka, and P. A. Hirschberg, 1992: The effects of subcloud-layer diabatic processes on cold air damming. *J. Atmos. Sci.*, **49**, 49-70.

Garreaud, R. D., and J. M. Wallace, 1998: Summertime incursions of midlatitude air into subtropical and tropical South America. *Mon. Wea. Rev*., **126**, 2713-2733.

Green, T. A., Jr., 2006: Cold air damming erosion and associated precipitation in the Southeastern United States. Master's thesis, North Carolina State University, 248 pp.

Grumm R. H., 2015: Mid-Atlantic Ice Storm 4 March 2015. Accessed 22 July 2015. [Available online at http:// cms.met.psu.edu/sref/severe/2015/03Mar2015.pdf]

Hartfield, G., K. Keeter, and P. Badgett, 1996: Spectrum of cold air damming and damming look-alikes. [Available from the Raleigh National Weather Service Office, Raleigh, NC.]

_____, 1998: Cold air damming: An introduction. National Weather Service Eastern Region Training and Evaluation Module 4. [Available online at http://www.erh.noaa.gov/er/hq/ssd/erps/tem/tem4.pdf]

Hong, S.-Y., and J.-O. Lim, 2006: The WRF single-moment 6-class microphysics scheme (WSM6). *J. Korean Meteor. Soc.*, **42**, 129-151.

IEM, 2014: Iowa Environmental Mesonet NWS Text Product Finder. Accessed 2 April 2014. [Available online at https://mesonet.agron.iastate.edu/wx/afos/]

Jirka, G. H., and M. Arita, 1987: Density currents or density wedges: Boundary-layer influence and control methods. *J. Fluid Mech.*, **177**, 187-206.

Kain, J. S., and J. M. Fritsch, 1993: Convective parameterization for mesoscale models: The Kain-Fritsch scheme. *The Representation of Cumulus Convection in Numerical Models, Meteor. Monogr.*, No. 46, Amer. Meteor. Soc., 165-170.

Kain, J. S., and Coauthors, 2008: Some practical considerations regarding horizontal resolution in the first generation of operational convection-allowing NWP. *Wea. Forecasting*, **23**, 931–952.

Keeter, K. K., S. Businger, L. G. Lee, and J. S. Waldstreicher, 1995: Winter weather forecasting throughout the eastern United States. Part III: The effects of topography and the variability of winter weather in the Carolinas and Virginia. *Wea. Forecasting*, **10**, 42-60.

Klemp, J. B., and R. Rotunno, 1983: A study of the tornadic region within a supercell thunderstorm. *J. Atmos. Sci.*, **40**, 359-377.

_____, and R. B. Wilhelmson, 1978: Simulations of right- and left-moving storms produced through storm splitting. *J. Atmos. Sci.*, **35**, 1097-1110.

Kramer, D., 1997: Real-time mesoscale model evaluation during Appalachian cold air damming. Master's thesis, North Carolina State University, 139 pp.

Lackmann, G. M., 2011: *Midlatitude Synoptic Meteorology: Dynamics, Analysis, and Forecasting*. Amer. Met. Soc., 306-309 pp.

Lackmann, G. M., and W. M. Stanton, 2004: Cold-air damming erosion: Physical mechanisms, synoptic settings, and model representation. Preprints, *20th Conf. on Weather Analysis and Forecasting*, Seattle, WA, Amer. Meteor. Soc., CD-ROM, 18.6.

Langmaid, A. H., and A. J. Riordan, 1998: Surface mesoscale processes during the 1994 Palm Sunday tornado outbreak. *Mon. Wea. Rev.*, **126**, 2117-2132.

Lee, L. G., K. K. Keeter, S. Businger, and A. J. Riordan, 1992: Geography-related forecasting problems in the southeastern United States and a joint North Carolina State University-National Weather Service effort to improve the understanding and prediction of these events. Preprints, *Symp. on Weather Analysis and Forecasting*, Atlanta, GA, Amer. Meteor. Soc., 166-172.

Lupo, A. R., J. J. Nocera, L. F. Bosart, E. G. Hoffman, and D. J. Knight, 2001: South American cold surges: Types, composites, and case studies. *Mon. Wea. Rev*., **129**, 1021-1041.

Maddox, R. A., L. R. Hoxit, and C. F. Chappell, 1980: A study of tornadic thunderstorm interactions with thermal boundaries. *Mon. Wea. Rev.*, **108**, 322-336.

Magor, B. W., 1959: Meso-analysis: Some operational analysis techniques utilized in tornado forecasting. *Bull. Amer. Meteor. Soc.*, **40**, 499-511.

Manins, P. C., and B. L. Sawford, 1982: Mesoscale observations of upstream blocking. *Quart. J. Roy. Meteor. Soc.*, **108**, 427-434.

Markowski, P. M., E. N. Rasmussen, and J. M. Straka, 1998: The occurrence of tornadoes in supercells interacting with boundaries during VORTEX-95. *Wea.*

Forecasting, **13**, 852-859.

Mesinger, F., G. DiMego, E. Kalnay, K. Mitchell, P. C. Shafran, W. Ebisuzaki, D. Jović, J. Woollen, E. Rogers, E. H. Berbery, M. B. Ek, Yun Fan, R. Grumbine, W. Higgins, H. Li,

Y. Lin, G. Manikin, D. Parrish, W. Shi, 2006: North American Regional Reanalysis. *Bull. Amer. Meteor. Soc.*, **87**, 343-360.

Miller, R. C., 1972: Notes on analysis and severe storm forecasting procedures of the Air Force Global Weather Central. Tech. Rep. 200 (revised), AWS, USAF, 181 pp.

Molinari, J. and M. Dudek, 1992: Cumulus parameterization in mesoscale numerical models: A critical review. *Mon. Wea. Rev.*, **120**, 326-344.

NCDC, 2015: Climate at a Glance. Accessed 23 July 2015. [Available online at http://www.ncdc.noaa.gov/cag/]

Nielsen, J. W., and P. P. Neilley, 1990: The vertical structure of New England coastal fronts. *Mon. Wea. Rev.*, **118**, 1793-1807.

Nieuwenhuis, B. P., 2006: A study of severe thunderstorm interaction with thermal boundaries: Collision angle and stability. Master's thesis, North Carolina State University, 50 pp.

Rackley, J. A., 2015: Southern Appalachian Cold Air Damming: A Climatology and Simulation of Case Studies. Master's thesis, University of Georgia

_____, and J. A. Knox, 2015: A climatology of Southern Appalachian cold air damming. *Wea. Forecassting.*, [in review].

Rasmussen, E. N., S. Richardson, J. M. Straka, P. M. Markowski, and D. O. Blanchard, 2000: The association of significant tornadoes with a baroclinic boundary on 2 June 1995. *Mon. Wea. Rev.*, **128**, 174-191.

Richwien, B. A., 1980: The damming effect of the southern Appalachians. *Natl. Wea. Dig.*, **5** (1), 2-12.

Schwerdtfeger, W., 1975: The effect of the Antarctic peninsula on the temperature regime of the Weddell Sea. *Mon. Wea. Rev.*, **103**, 45-51.

Skamarock, W. C., J. B. Klemp, J. Dudhia, D. O. Gill, D. M. Barker, W. Wang, and J. G. Powers, 2005: A description of the Advanced Research WRF version 2. NCAR Tech. Note NCAR/TN-468+STR, 88 pp.

Smirnova, T.G., J.M. Brown, and S.G. Benjamin, 1997: Performance of different soil model configurations in simulating ground surface temperature and surface fluxes. *Mon. Wea. Rev.*, **125**, 1870-1884.

Smirnova, T.G., J.M. Brown, S.G. Benjamin, and D. Kim, 2000: Parameterization of cold season processes in the MAPS land-surface scheme. *J. Geoph. Res*, **105** (D3), 4077-4086.

Smith, R. B., 1982: Synoptic observations and the theory of orographically disturbed wind and pressure. *J. Atmos. Sci.*, **39**, 60–70.

Stanton, W., 2003: An analysis of the physical processes and model representation of cold air damming erosion. Master's thesis, North Carolina State University, 207 pp.

Stauffer, D. R., and T. T. Warner, 1987: A numerical study of Appalachian cold-air damming and coastal frontogenesis. *Mon. Wea. Rev.*, **115**, 799-821.

Walter, N. (Ed.), 2001: *Spatial Interpolation*. University of Calgary Press.

Wakimoto, R. M., and C. Liu, and H. Cai, 1998: The Garden City, Kansas, storm during VORTEX 95. Part I: Overview of the storm's life cycle and mesocyclogenesis. *Mon. Wea. Rev.*, **126**, 372-392.

Weisman, M. L., and J. B. Klemp, 1982: The dependence of numerically simulated convective storms on vertical wind shear and buoyancy. *Mon. Wea. Rev.*, **110**, 504-520.

Xu, Q., 1990: A theoretical study of cold air damming. *J. Atmos. Sci.*, **47**, 2969–2985.

_____, and S. Gao, 1995: An analytic model of cold air damming and its applications. J. Atmos. Sci., **52**, 353-366.

_____, _____, and B. H. Fiedler, 1996: A theoretical study of cold air damming with upstream cold air inflow. J. Atmos. Sci., **53**, 312-326.